ROLE OF SELF-ORGANIZED SURFACTANT SYSTEMS IN ORGANIC REACTIONS, NANOPARTICLES AND MOLECULAR SIEVES SYNTHESIS

A THESIS

SUBMITTED TO THE

UNIVERSITY OF PUNE

FOR THE DEGREE OF

DOCTOR OF PHILOSOPHY

IN CHEMISTRY

BY

RAMDAS BHAGVAN KHOMANE

M.Sc. (CHEMISTRY)

CHEMICAL ENGINEERING DIVISION

NATIONAL CHEMICAL LABORATORY

PUNE 411 008

FEBRUARY 2002

DEDICATED TO MY PARENTS

CERTIFICATE

Certified that the work incorporated in the thesis **"Role of Self-Organized Surfactant Systems in Organic Reactions, Nanoparticles and Molecular Sieves Synthesis"** submitted by ***Mr. Ramdas Bhagvan Khomane***, for the degree of Doctor of Philosophy, was carried out by the candidate under my supervision in the Chemical Engineering Division, National Chemical Laboratory, Pune, India. Such materials as has been obtained from other sources has been duly acknowledged in the thesis.

Date: February 26, 2002

Dr. B. D. Kulkarni
Research Guide

DECLARATION

I hereby declare that the thesis entitled **"Role of Self-Organized Surfactant Systems in Organic Reactions, Nanoparticles and Molecular Sieves Synthesis."** Submitted for Ph. D. degree to the University of Poona (Pune) has been carried out at National Chemical Laboratory, under the supervision of Dr. B. D. Kulkarni. The work is original and has not been submitted in part or fully by me for any degree or diploma to this or any other University.

Date: February 26, 2002

Chemical Engineering Division
National Chemical Laboratory
Pune 411 008

Ramdas B. Khomane

ACKNOWLEDGEMENT

I would like to express my deep sense of gratitude to Dr. B. D. Kulkarni, my research advisor, Deputy Director & Head, Chemical Engineering Division, National Chemical Laboratory, for his guidance, encouragement, advice and the freedom of work he provided all throughout my research work without which I would not have completed this thesis successfully.

I am grateful to my parents and my wife Archana for their love, unfailing support, patience and encouragement during the course of my research carrier.

I am grateful to Dr. V. Ravikumar, Dr. S. S. Tambe, Dr. V. K. Jayraman, Dr. N. K. Yadav and Dr. A. N. Gokarn for their help during the study.

I am also grateful to Dr. Sainker, Dr. Mandle, Dr. Badbade, Dr. (Ms) Pavasker, Dr. Gopinathan, Dr. Jadker and Dr. Shah for their help during sample analysis.

I am especially thankful to my senior colleague Dr. Abhijeet Manna for his valuable suggestions.

I am also grateful to Mr. B. G. Poman, Mr. T. S. Kamble, Mr. B. K. Kedari, Mr. Bhalerao, Mr. Banerjee and Mr. Pingale for their help during the study.

I am grateful to all my friends Shelokar, Nandi, Perbhane, Ghosh, Sankpal, Cheema, Lonari, Potdar, Anand, Ahedi for their good wishes.

Finally I would like to thank Dr. Paul Ratnasamy, Director, National Chemical Laboratory, for allowing me to submit my work in the form of a thesis for the award of Ph.D. degree. The financial support in the form of research fellowship by C.S.I.R, New Delhi, is duly acknowledged.

Ramdas B Khomane

TABLE OF CONTENT

LIST OF FIGURES

CHAPTER 1

GENERAL INTRODUCTION

This chapter gives a brief introduction and background literature on micelles and microemulsions, along with their technological applications to cover chemical reactions, nanoparticles and molecular sieves synthesis.

1.1 PREFACE

This chapter presents brief overview of the self-organized surfactant systems and discusses the various investigations carried out under micellar / microemulsion conditions. In 1894, first Emil Fisher has introduced the superamolecular interactions. Since then, there has been a growing interest in the research on organized surfactant assemblies that include micelles and microemulsions, vesicles, self-assembled monolayer and supramolecular hosts such as zeolites. Among them micelles and microemulsions exhibit a wide unusual properties, such as high interfacial area, low viscosity, high solubilizing capacity etc., which can offer the high potential for numerous applications in industries dealing with catalysts, pharmaceuticals, biotechnology, tertiary oil recovery etc.

1.2 SURFACE ACTIVE AGENTS (SURFACTANTS)

A surfactant[1,2] molecule has a hydrophilic and hydrophobic regions. The hydrophilic region of the molecule is called the head group and it is generally depicted as a circle. The hydrophobic region of the molecule is called the tail and consists of one or more hydrocarbon

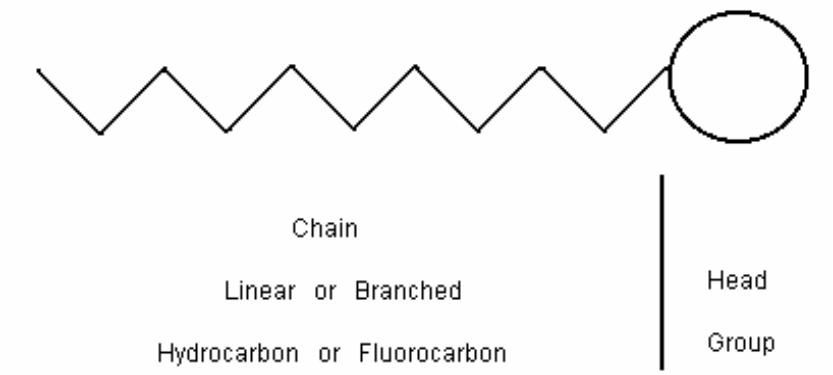

Figure 1.1: Schematic diagram of surface active molecule.

chains, usually with 6-22 carbon atoms. Chains may be linear or branched. The tail may be depicted either as a straight line or a wavy tail. Figure 1.1 illustrates the schematic diagram of a typical surface active molecule. Surfactant molecules are also called amphiphiles from the greek words "amphi" and "philo" which means both and loving respectively. This dual nature is responsible for the phenomenon of surface activity, and of micellization and solubilization.[3] They can get adsorbed on to surfaces and interfaces of the dispersed and

continuous phase and bring about a change in the interfacial energy.[4-7] Based on the head group-charge, surfactants are divided into four categories i) cationic[8], ii) zwitterionic[9], iii) nonionic[10] and, iv) anionic[11]. In aqueous solution, the anionic surfactant dissociates giving an anion carrying the amphiphilic properties and an inactive cation (e.g. Na^+ or K^+). In aqueous solutions, cationic surfactants are ionized in a cation carrying the amphiphic properties, and an inactive anion, such as Cl^- or Br^-. The cationic group is most often a quarternary ammonium group. Nonionic surfactants as the name implies do not give ions in solution. The hydrophilic part of their molecule contains polar groups such as ether, alcohol, carbonyl or amino groups. Amphoteric surfactants are ionic surfactants containing positive and negative charges on the same molecule. Table 1.1 lists the representative class of surfactants.

In several important applications, ionic surfactants are used in conjunction with a co-surfactant such as a medium chain-length alcohol. The co-surfactant is an uncharged entity and its adsorption is not impeded by the electric field. It therefore provides the additional lowering of interfacial tension necessary for microemulsion formation. Cosurfactants are usually alcohols or amines ranging from C_4 to C_{10} and helps in the formation and stabilization of micelles/microemulsions. In many cases it also acts as a organic solvent. The co-surfactant provides a "dilution effect" in addition to that of the surfactant and causes a further decrease of the interfacial tension. If salt is added to the solution, the surface potential is partly neutralized. This decreases coulombic repulsion between adjacent head groups and allows the formation of larger micelle.

1.3 MICELLAR STRUCTURE AND PROPERTIES

The characteristic concentration of surface active agents (surfactants) in solution above which the appearance and development of micelles brings about sudden variation in the relation between the concentration and certain physico-chemical properties of the solution is (such as the surface tension) known as critical micellization concentration (CMC).[12,13] A schematic two-dimensional representation with different regions of micelle/ microdroplet is shown in figure 1.2. Electrical charge on the micelle is neutralized by counterions in the electrical double layer around it. The first layer immediately adjacent to its surface is called the Stern Layer.[14] In this layer the counterions are adsorbed so strongly that there is no thermal agitation and they migrate together with the colloidal micelle in an electrical field. According to the most widely accepted model, head groups of surfactant molecules also

Table 1.1: Different type of surfactants with their examples

Type	Chemical name	Molecular formula	Abbreviations
Anionic	Sodium dodecylsulfate	$C_{12}H_{25}OSO_3Na$	SDS
	Sodium p-dodecylbenzenesulfonate	p-$C_{12}H_{25}(C_6H_4)SO_3Na$	SDBS
	Sodium bis(2-ethylhexyl) sulfosuccinate	$C_{20}H_{37}O_7SNa$	AOT
Cationic	Cetyltrimethylammonium bromide	$C_{16}H_{33}N(CH_3)_3Br$	CTAB
	Didodecyldimethylammonium bromide	$(C_{12}H_{25})_2N(CH_3)_2Br$	DDAB
	Dodecytrimethylammonium bromide	$C_{16}H_{33}PyBr$	DTAB
	Cetylpyredenium bromide monohydrate	$C_{21}H_{38}BrN.H_2O$	HDPB
Zwitter ionic	Tetradecyldimethylamine	$C_{14}H_{29}$-N^+ $(CH_3)_2O^-$	TDMAD
	Hexadecylsulfo betaine	$C_{16}H_{33}$-$N^+Me_2(CH2)_3SO_3^-$	SB3-16
	N-Dodecyl-N,N-diemethyl glycine	$CH_3(CH_2)_{11}N^+(CH_3)_2COO^-$	-
Non-ionic	Polyoxyethylene (23)-dodecyl ether	4-(C_9H_{19})-C_6H_4O-$(CH_2CH_2O)_4$-CH_2CH_2OH	Igepal C0-520
	Sorbitan monolaurate	$C_{11}H_{23}CO$-OCH_2CHOH-(C_4H_5O)-$(OH)_2$	Span 20
	Polyoxyethylene (23)-dodecyl ether	$CH_3(CH_2)_{11}(OCH_2CH_2)_n$ OH N~23	Brij-35
	1-(1,1-Dimethyl-3,3-dimethyl-butane)4-polyoxyethylene (9.5)	$(CH_3)_3CCH_2C(CH_3)_2$-(C_6H_4)-$(C_2H_4O)_{9.5}OH$	TritonX-100

situate in this layer. The remainder of the double layer is called the diffuse (Gouy-Chapman) layer since the ions are diffused into the bulk solution as a consequence of the thermal motion. The decrease in counterion concentration with the distance from the micellar surface has an exponential form.[15-18] The core radius is about the length of the fully extended alkyl chain of the amphiphile. The core is believed to consist of two regions, namely the inner and outer core. The outer core contains approximately the first four methylene groups. There is also another defned region within micelles called palisade layer (mantle) which includes the head groups and the first few methylene groups. On the basis of Hartley model, the overall volume of a micelle is approximately twice that of Stern Layer.[19-21] Hydrophobic core of the micelles have diameters of about 10-30A. The charged coat of ionic micelles, called the stern layer is usually 60-90% neutralized by counterions in aqueous surfactant solutions without added salt.

Above the CMC the concentration of singly dispersed surfactant molecules is virtually constant and the surfactant is at essentially its optimum of activity for many

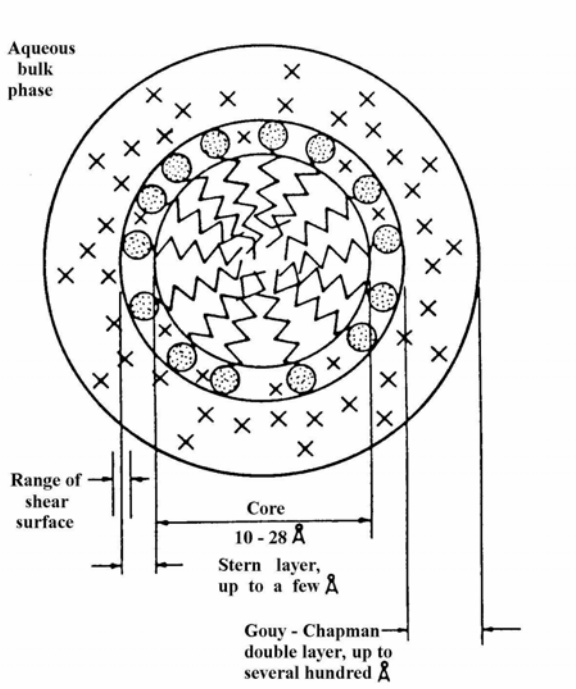

Figure 1.2: A two dimensional schematic representation of the regions of a spherical micelle. The head group (O), the hydrocarbon chain (/\/\) and counterions (X) are schematically indicated to denote their relative locations.

applications. CMC values for commonly used surfactants range from about 10^{-4} - 10^{-2}M. The value of CMC is dependant on a large number of parameters. Usually the more surface active the amphiphilic monomer, the higher is the tendency for micellization and, hence, the lower

the CMC of the micelle produced. Addition of salt to the solution usually decreases the CMC.

1.4 MICROEMULSIONS

It is well known that water and oil do not mix. However, two immiscible liquids one polar such as water, glycols or diethyl formamide and non-polar hydrocarbon can be converted into an optically transparent and thermodynamically stable emulsion by adding an amphiphile. This solution is termed as micelle/microemulsion.[22-25] The term "microemulsion" was introduced by J. H. Schulman in 1958. The main difference between micellar solution and microemulsion is in their sizes; micelles are smaller (≤ 10 nm) than microemulsion droplets (≤ 100 nm) and usually microemulsion includes an extra component, the co-surfactant. The solubilization capacity of microemulsions is generally much higher than that of micellar solutions.[26] A microemulsion consists of two phases (i) dispersed phase (the phase broken into fine droplets) and (ii) continuous phase (the liquid surrounding the droplets). Depending on the proportion of components and the hydrophilic-lipophilic balance (HLB) value of the surfactant used, the formation of microdroplets can be in the form of oil-swollen micelles dispersed in water as oil-in-water (o/w) microemulsion (Figure 1.3b & Figure 1.4a) or water swollen micelles dispersed in oil as for water-in-oil (w/o) microemulsion (Figure 1.3f & Figure 1.4b), also called reverse microemulsion. The w/o and o/w types are inverted form of one type to the other and can be achieved by adding excess of one phase or by changing the emulsifier. In the intermediate phase region between w/o and o/w microemulsions, there may exist bicontinuous microemulsions whose immiscible phases are inter connected randomly in the form of sponge-like microstructures (Figure 1.4c). Usually bicontinuous phases are viscous-gels (semi-solids). The viscoelastic gel stage (adjacent to the w/o microemulsion) comprises of an hexagonal array of water cylinders and lamellar phase (Figure 1.3e & Figure 1.4d) of swollen bimolecular leaflets (adjacent to the o/w microemulsion). The phase of the gel stage is also called liquid crystalline or myelinic stage (Figure 1.3d,e). Bicontinuous microemulsions have both oil and water as continuous phases with surfactant residing at extended oil-water interfaces (Figure 1.3f).

In addition to the single-phase microemulsions, multiphase microemulsion-containing systems, namely Winsor systems, are also important.[27] A Winsor I (W I) system

consists of an o/w microemulsion which is in equilibrium with an excess oil phase, while a Winsor II (W II) system is a w/o microemulsion which is in equilibrium with an excess aqueous phase. The Winsor III (W III) system is a bicontinuous microemulsion, which co-exists with oil and water phases containing low concentrations of droplets (w/o and o/w respectively) while a macroscopically single phase microemulsion is denoted as Winsor IV (W IV) system (Figure 1.4e,f,g).

1.5 PHASE DIAGRAM AND MICROEMULSIONS

A phase may be defined as a region of component space homogeneously filled with matter. Any phase diagram is the compact graphical representation of phase boundaries of any feasible system (uni- or multicomponent). A ternary mixture of water (W), oil (O) and surfactant (S) has four independent thermodynamic variables namely pressure, temperature, and two composition variables. Out of these variables, effect of pressure is small compared to that of temperature. Assuming, that pressure is constant at atmospheric level, the phase diagram of a ternary system may then be represented in an upright prism with the Gibbs triangle as base and temperature (T) as the ordinate (Figure 1.5). The composition variables are conveniently expressed in mass fraction of oil (α) in the mixture of water and oil, α (= O/ (W+O)), and that for amphiphile (γ) in the mixture of all three components, γ (= S/(W+O+S)), both expressed in weight percent (wt %). Each point in the phase prism is then unambiguously expressed by a set of co-ordinate (α, γ, and T) which represents the composition of a particular system.[29-31] An isothermal phase equilibrium of a ternary system can be described with the cross-section of the phase prism (triangular phase diagram) as schematically shown in Figure 1.4. These diagrams are helpful in various ways, like knowing the extent of solubilization, presence of multiphases etc., corresponding to any particular composition chosen.

A very convenient method for preparation of a microemulsion and construction of planer triangular phase diagram is the titration procedure. A surfactant is dissolved in aqueous (or organic) medium and is titrated with organic (or aqueous) phase. The transition points (turbid and transparent) are noted. The single-phased, optically transparent domains correspond to the microemulsions whereas turbid zones are for multiphase systems. Repeating the same procedure for different concentration of surfactant solution, almost all transition points can be noted. Thus, a triangular phase diagram can easily be drawn.

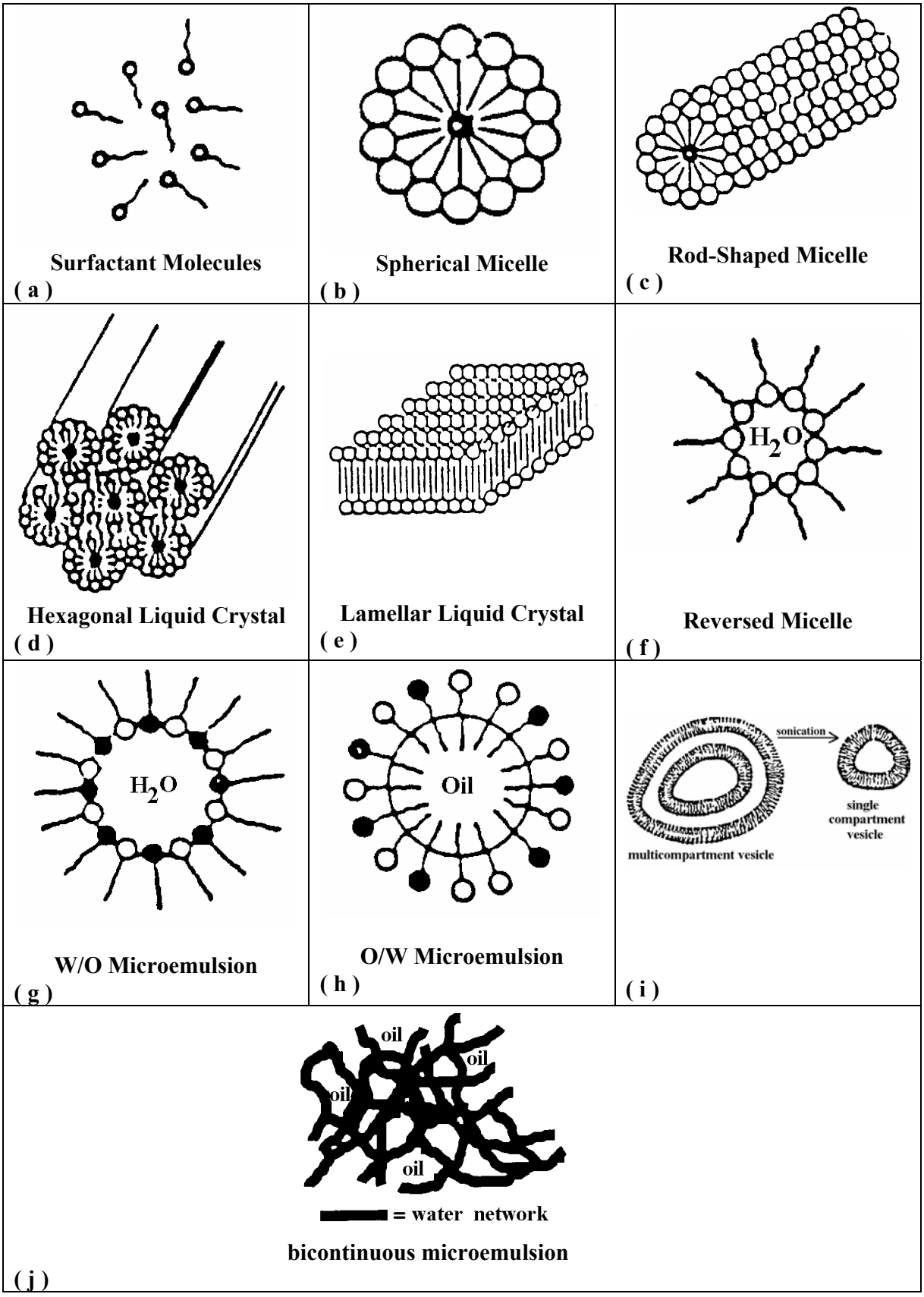

Figure 1.3: Schematic representation of organized colloidal aggregates that may form in aqueous solution of surfactant depending on the concentration.

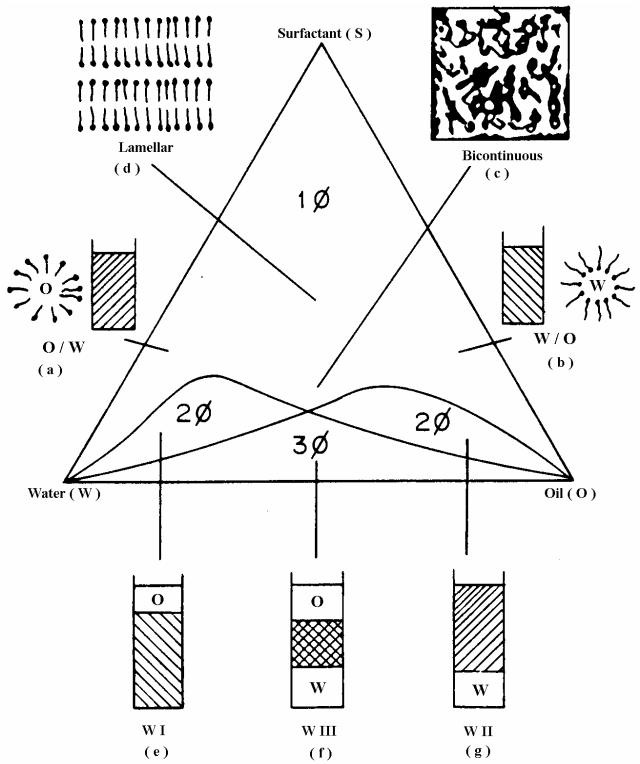

Figure 1.4: Illustration of some phase equilibria encountered in multicomponent systems, where O = oil phase, W = aqueous phase, 2ϕ = two phase (W I & W II), 3ϕ = three phase.

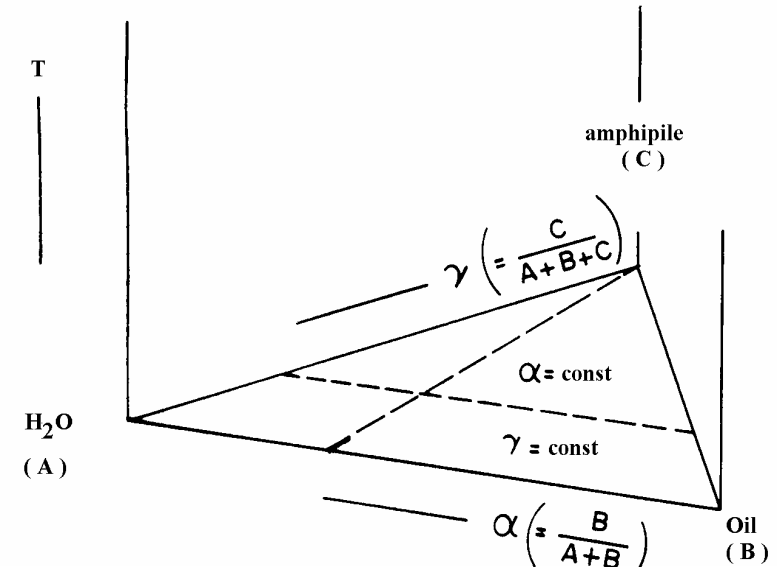

Figure 1.5 : Phase prism with the Gibbs phase triangle as base (ABC) and the temperature axis (T) as ordinate.

Any mixture of three components, A, B, and C, can be represented using properties of an equilateral triangle (ternary diagrams, Figure 1.6). The relative amounts of A, B and C are expressed in percentage of the selected parameter, such as: A% + B% + C% = 100%.--1.1

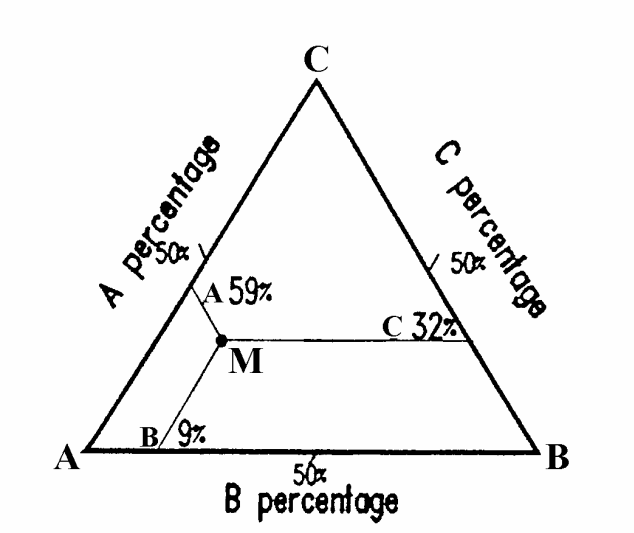

Figure 1.6: The ternary phase diagram representation. Point M represents the liquid composition with 59% of A, 9% of B and 32% of C (total 100%) The percentage can be mass, volume or mole percentages.

Only two percentages are independent, the third one we can be obtained by the eq. 1.1. Figure 1.6 shows that how the given mixture can be plotted. Point M is obtained at the crossing of the respective percentage values of A, B and C. Some microemulsions made with four components. In this case, eq. 1.1 can not be used, unless a pseudo-component is defined, such as a given ratio of surfactant to alcoholic cosurfactant. This active mixture is considered as a third component and is placed at the C apex.

1.6 THERMODYNAMIC FREE ENERGY, INTERFACIAL TENSION AND VISCOSITY

Spontaneous formation of a stable dispersion with decrease of the free energy can only be expected if the interfacial tension is so low (nearly zero[3]) that the remaining free energy of the interface can be overcompensated by the entropy of dispersion of the

droplets in the medium.[32-35] It is known that amphiphiles generally reduce the interfacial tension

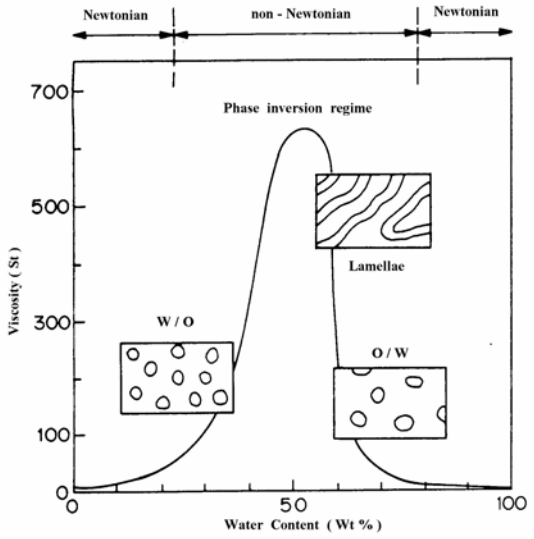

Figure 1.7: represents a relationship of viscosity vs. water content in microemulsion.

between oil and water (nearly 50 mN m^{-1}) considerably. In most cases, C.M.C. is reached before the interfacial tension is close to zero. Addition of a second surfactant of a completely different nature then lowers the interfacial tension further and at times, even transiently negative values, may be reached. Thus, formation of micelles/ microemulsions are spontaneous processes. The viscosity of both o/w and w/o microemulsion systems are generally low and behave as Newtonian fluids, whereas mesophase structured lamellar phases (bicontinuous) are highly viscous and behave as non-Newtonian fluids.[36]

1.7 MICELLAR SOLUBILIZATION AND FACTORS AFFECTING SOLUBILIZATION

One of the most important processes leading to micellar effects on reactions is the solubilization of substrates in to the surfactant micelles.[4,37-40] It is possible to solubilize water insoluble substances or to increase the solubilities of slightly soluble ones in aqueous micellar solutions. They penetrate towards the hydrocarbon-like cores of the micelles. The pathways and the rates of the reactions in micellar systems depend to a great extent on how deep the solubilized species are located within the micelle.[41-43] The solubilized molecules

interact with the polar head groups of a micelle and penetrate towards the core. They reside in the inner core,[44-45] outer core,[46-47] palisade layer[48-50] or between the polar head groups.[51-52]

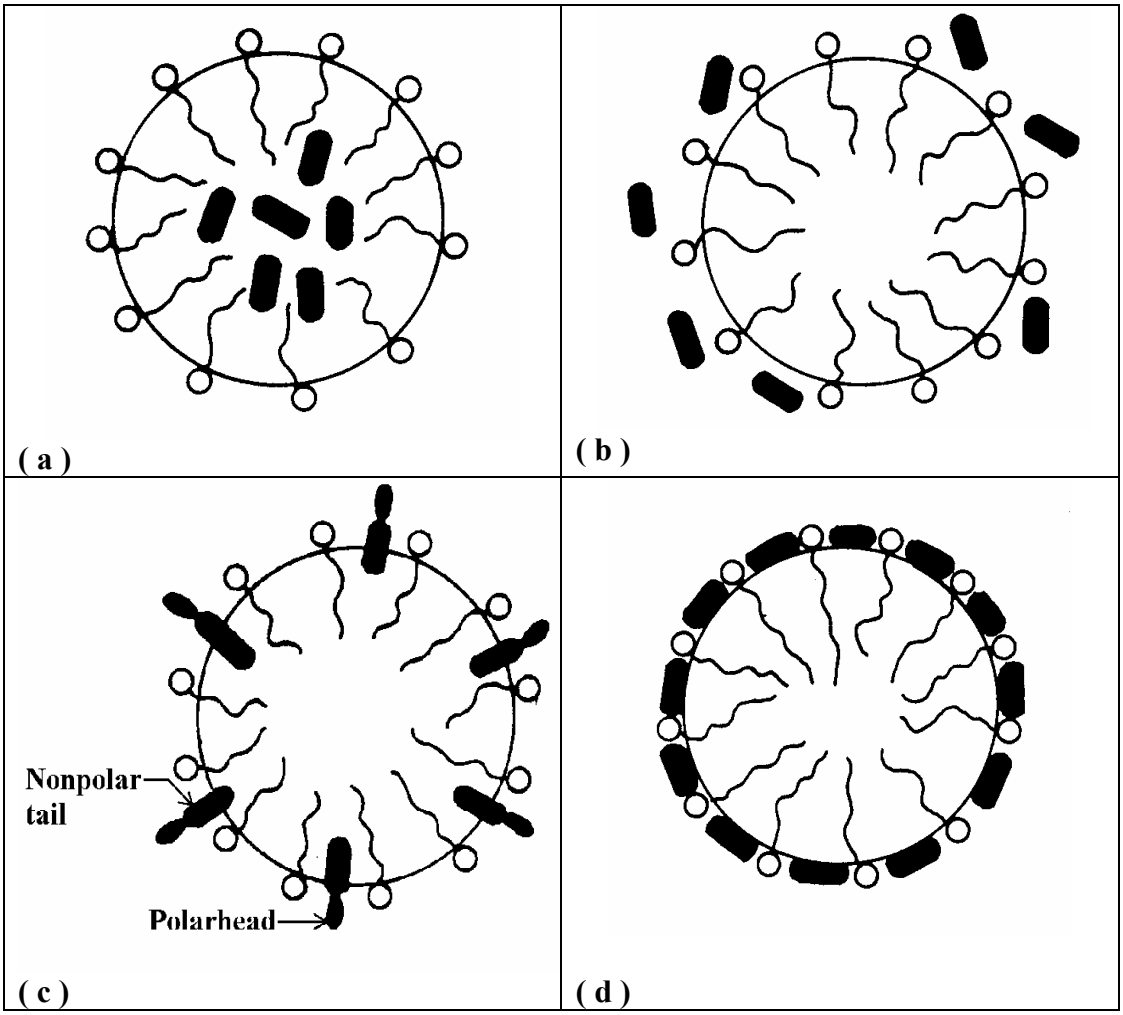

Figure 1.8: Schematic representation of the four possible solubilization sites in surfactant aggregates organized: (a) micelle interior, (b) outer hydrophilic region, (c) oriented in the micellar surface, (d) adsorbed in the interface.

Sometimes micellar effect can also be obsorved as a result of the solubilization of substrates as counterions, i.e., without solubilization , with the substrates not hydrophobic enough to be solubilized in the micellar interior.[53] This depends on different factors affecting the solubilization such as, (i) concentration of the surfactant and co-surfactant; generally above C.M.C., the solubility increases with the surfactant and co-surfactant concentrations, (ii) structure and chain length of the surfactant; if the solubilization occurs in the hydrophobic portion of the surfactant, this will increase with increase in the size of that group, (iii) nature

and structure of the solubilizate: molecular size, shape and structure, polarity and polarizability, chain branching, (iv) temperature: in most cases solubilization increases with increase in temperature, (v) nature of the counter ion; in general the solubility increases with increase in size and charge of counter ions, (vi) electrolyte; addition of electrolytes to ionic surfactants usually causes an increase in the C.M.C. and hence an increase in the solubilization capacity. The solubilization capacity of micellar systems, generally follow the order: nonionics > cationics > anionics for the amphiphiles with same hydrophobic moiety. It is also noted that micelle formation is a dynamic equilibrium process, and hence solubilization process is also called as dynamic solubilization. Schematic view of the four different types of solubilization are shown in Figure 1.8. The micellar interaction is not static or rigid and consequently a solubilized substrate is relatively mobile. Few studies also indicate that the solubilization is, on the average, uniformly distributed in the micellar interior.

1.8 MOLECULAR INTERACTIONS AND SURFACTANT ADSORPTION

The interactions between molecules can be sorted following an increasing polarity order as: van der Waals forces, hydrogen bonding interaction, and electrostatic forces.[54-57]

The van der Waals forces cover a variety of short distance range interactions, whose intensity decreases with the sixth power of the distance between two molecules. They include the London or dispersion forces between nonpolar molecules, the Debye forces between the permanent dipole of the molecule and induced dipole of another molecule and the Keesom forces or dipole-dipole interactions between two polar molecules. The order of magnitude of van der Waals forces is 2kJ/mol for polar and moderately polar molecules, and less than 1kj/mol for nonpolar molecules.

A hydrogen bond is the strong attraction between the hydrogen atom covalently bonded to an electronegative atom, and another electronegative atom. Only N, O nad F are sufficiently electronegative to take part in hydrogen bonding in neutral molecules. The strength of the hydrogen bond is about ten fold higher than any van der Waals forces. It is about 20 kJ/mole for the O-H-O. Ion-ion interactions are long distance range forces, decreasing with the square of the distance between two ions. The ion-ion interaction strength is tenfold higher than the hydrogen bonding force, in the 200kJ/mol range. They are very important in the comprehension of the micelle formation of ionic surfactants.

The notion of hydrophobic interaction was well developed by Tanford. When a nonpolar solute is dissolved in water, some hydrogen bonds are disrupted. The solute tends to locally distort the water structure and to restrict the motion of the water molecules. Thus, a large entropy increase in the water molecule is associated with the removal of the nonpolar solute from aqueous solution. This entropy increase is responsible for the surface activity and micelle formation of surfactant molecules.

Surfactant Adsorption: The amphiphilic character of surfactant molecules explains their trend to adsorb at any interface. Two phases of different polarity are separated by an interface. This

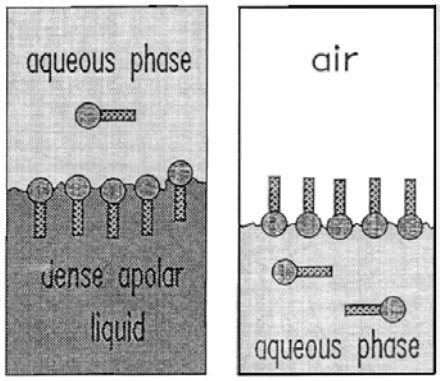

Figure 1.9: Surfactant adsorption at (a) liquid-liquid, and (b) air-water interfaces.

polarity difference attracts surfactant molecules because this can minimise the entropy change by putting their polar part in the more polar phase and their nonpolar part in less polar phase.

1.9 CHARACTERIZATION TECHNIQUES FOR MICROEMULSIONS

Microemulsions have been characterized by various techniques such as (i) Phase diagrams; the boundaries of different phase regions can be found, (ii) Polarization microscope; helps to determine whether phases are anisotropic or not, (iii) Interfacial tension; Dynamic light scattering; determines the diffusion coefficients and radius of microdroplets, (iv) Small angle X-ray scattering; information about particle shape and size, (v) Small angle neutron scattering; information about droplet core and surfactant layer, (vi) NMR spectroscopy; measures diffusion coefficients and mobility of various components, (vii) Interfacial Tension; low interfacial tension is the typical characteristic of microemulsions which helps to determine the area per surfactant or co-surfactant and the radius of droplets, (viii) Viscosity; helps to determine the structure and flow properties, (ix) Electrical

conductivity; helps to determine whether the microemulsion is w/o or bicontinuous or o/w type, (x) Classical light scattering; informs the identity of droplets, particle size and interaction between particles, and (xi) Electronmicroscopy.[58-62]

1.10 APPLICATION OF MICELLES AND MICROEMULSIONS

There has been a revolution in the last two decades in the utilization of microemulsion systems in a variety of chemical and industrial processes. A brief account of processes and applications is presented here in order to demonstrate their significance and potential.

1.10.1 TERTIARY OIL RECOVERY

The most spectacular application of microemulsion is found in the tertiary oil recovery due to low interfacial tension and good wetting properties. Roughly 20 % of the otherwise unrecoverable underground oil can be obtained by the enhanced oil recovery process. The oil remains trapped in the capillary of the rocks of the reservoir because of high interfacial tension (about 20-25 mN/m) between the crude oil and reservoir brine. If the interfacial tension can be reduced to around 10^{-3} mN/M, a substantial fraction of the residual oil in the porous media in which it is trapped can be mobilized. Low interfacial viscosity of the system is also advantageous. Usually an aqueous or a microemulsion slug of petroleum surfactant is injected in to the reservoir and is followed by polymer solution (for mobility control) and excess water. The injected slugs are generally miscible with the reservoir oil and produce a microemulsion of a new composition which mobilizes the residual oil.[63,64]

1.10.2 MICROEMULSIONS AS FUELS

One of the direct advantages of microemulsion-based fuels is the presence of water in a stable microemulsion and they are successfully used to reduce soot formation. When the water is vaporized during the combustion, this will lower the heat released and the combustion temperature. As a direct consequence, the emission rate of gases like nitrogen oxides (NO_x) and carbon monoxide will decrease. The presence of water is also supposed to cause improved fuel atomization, minimization of particulate emission and sooting, and improved fuel economy in terms of price and miles/volume of the fuel. Another interesting

feature of microemulsion-based fuel is their capacity to increase the octane number of diesel oils. Octane number improvers includes formamide, glycols, urea etc.[65,66]

1.10.3 PHARMACEUTICALS AND COSMETICS

Thermodynamic stability, higher degree of homogeneity and solubilization capacity give rise to the various applications of microemulsions (particularly gel or liquid crystalline phases) in pharmaceuticals and cosmetics. The easy formation, remarkable environment independent stability, excellent solubilization capacity, etc. favour microemulsions to be a better proposition over other compartmentalized systems. For example, the solubilization of strongly hydrophobic fluoroalkanes are used as short-time blood plasma substitutes to maintain a patient's oxygen supply. Oinments and creams also use emulsions and microemulsions to improve healing conditions of wounds, treatment of skin disease as well as to slow down the aging process of the skin. These systems are mostly gel phased (semisolid) emulsions or microemulsions under ambient conditions and are transformed to the liquid state when sheared during the application on the skins.[67-73] Microemulsions are promising delivery systems[74-77] to allow sustained or controlled drug release for precutaneous, peroral, topical, transdermal and parenteral administration.

1.10.4 LUBRICANTS AND CUTTING OILS

Microemulsion or reverse micellar solution are in use as lubricants, cutting oils and corrosion inhibitors for several decades. These liquids are usually reverse micellar solutions of certain compositions where surfactant shows two effects (a) corrosion inhibition by the formation of self-assembled monolayer (SAM) on the surfaces and (b) the increased water content (compared to pure oils) leads to high heat capacity which helps to cool down the engine. In microemulsions, water with much higher thermal conductivity, imparts higher heat capacity to the system. Such formulation can be used in cutting oil; the oil lubricates the cutting surface, and the water helps to remove the frictional heat generated during the cutting process.[78-80]

1.10.5 WASHING AND SEPARATIONS

The removal of contaminants from solid surfaces or tissue capillaries (particularly non-ionic surfactants) is significantly improved by the extremely low interfacial tensions in

microemulsion systems. Surfactant-based separation techniques are becoming increasingly important in industrial applications. These techniques generally require much less energy than traditional methods and have the added advantage that many of the surfactants used are eco-friendly and less toxic. Industrial wastewater streams frequently contain high concentrations of heavy metal cations.[81-84] An anionic or nonionic surfactant is injected into the wastewater stream coming from an industrial process. The final surfactant concentration should be well above C.M.C. of the surfactant. The stern layers of the micelles have higher-charge density and high absolute electric potential; therefore, the multivalent metal cations electrostatically adsorb or bind to it. The stream is subsequently forced through an ultrafiltration membrane with pore size smaller than micellar size (associated metal cations). The filtrate stream will have very low concentration of both metal and surfactant. Soil remediation via soil washing is also based on a separation technique. In conventional soil washing, organic pollutants are detached from large soil particles by mechanical energy input which causes increased adsorption of contaminants at the fine-grain fraction (which must then be deposited or burnt). In soil washing with microemulsions, the detached pollutants are solublilized in the oil fraction of the microemulsions as an extractive step in addition to washing.

Microemulsions are also useful in agrochemicals,[6,85,86] food,[87,88] electronic printing and ink-jet,[89-91] biotechnology,[92-94] thin insulators and conductors,[95-98] sensors[99,100] and magnetic media.[101,102]

1.11 SCOPE OF THE PRESENT WORK

1.11.1 ORGANIC REACTIONS IN MICROEMULSION

Organic syntheses are often faced with the problem of reacting water-soluble inorganic reactants with water-insoluble organic reactants. It is current practice in these cases to bring the reactant together and thus cause them to react with aid of polar aprotic solvents, phase transfer catalysts or just by intensive mechanical mixing. Organic reactions in microemulsion media have been widely investigated mainly focussing on the kinetics. Micelles can concentrate the reactants within their small volumes,[103-108] stabilize substrates, products,[109-112] and orient substrates[113-120] so that ionization potentials and oxidation-reduction properties,[121,122] dissociation constants, physical properties and reactivities[123-125] are changed. Thus, they can alter reaction rate, mechanism, and regio- and steriochemistry.[126-128]

A large number of organic reactions with ionic inorganic reactants such as, acids and bases, bromide, chloride etc.[129-133] and Diels-Alder reaction,[134] redox reaction,[135,136] catalytic reactions[137-139] have been studied by different groups. Recently, Kulkarni et al.[140,141] have reported different organic reactions in micellar/microemulsion media.

The concentrations of the counter-ion in the stern layer (local concentration) is much higher than in the polar pseudophase. Due to this local concentration effect, generally rates of the higher order (> 1) reactions are significantly affected (enhanced or decreased). These concepts are illustrated in Chapter 2 by considering synthesis of dihydroxy benzene and octene epoxide.

1.11.2 NANOPARTICLES SYNTHESIS IN MICROEMULSIONS

The synthesis of nano particles in microemulsion systems has recently become an important focus of research. Five aspects are to be taken into consideration for particle synthesis in microemulsions; phase behaviour and solubilization, average concentration of the reacting species in the aqueous domains, intramicellar interactions, water/surfactant ratio and structure and properties of the solubilizing water, and dynamic behaviour of the microemulsion. The dispersed droplets in the microemulsion can be regarded as microreactors and the exchange mechanism involves coalescence and fusion of the droplets upon collisions, which then disintegrate into droplets.[142] The inverse microemulsion technique has been successfully used to synthesise colloidal nano-particles of both polymers and inorganic materials.[143-152] The synthesis of nano particles in W I and W II type microemulsions have not been studied, although these systems are good alternative to two-phase reaction media. These are of interest to overcome incompatibility problems between nonpolar organic compounds and inorganic salts in preparative organic synthesis. Chapter 3 of this thesis explores the use of Winsor type of systems and considers the synthesis of thiol-capped nanoparticles.

1.11.3 MOLECULAR SIEVES SYNTHESIS IN MICELLAR MEDIA

A variety of surfactant-mediated synthesis of inorganic mesoporous materials have been reported.[153-154] Such materials could find applications in catalysis, membranes and separation technology, and molecular engineering. Cationic surfactants act as a template molecule for the synthesis of such materials. At low surfactant concentrations, the templating mechanism

is thought to be a cooperative process involving the interactions of inorganic ions with discrete surfactant aggregates. The synthesis of inorganic microporous materials using different type of surfactants have also been reported.[155-157] There are however, no reports of the synthesis of ferrierite type zeolites in presence of nonionic surfactants. Chapter 4 (part I), reports the synthesis and characterization of ferrierite type zeolits in the presence of nonionic surfactants while part II reports the synthesis of titanium silicalite-1 molecular sieves in the presence of nonionic surfactant.

1.12 THE PRESENT STUDY AND MAIN CONCLUSIONS

The work reported in the present thesis covers various investigations carried out under micellar / microemulsion conditions. More specifically it includes the studies on some industrially important organic reactions, preparation of thiol capped nanoparticles and molecular sieves synthesis. The thesis contains five chapters, each focusing around the study of a particular aspect of micelles / microemulsions.

Chapter 1 gives a brief introduction and background literature on micelles and microemulsions, along with their technological applications to cover chemical reactions, nanoparticles and molecular sieves synthesis in presence of surfactant.

Chapter 2 reports on two industrially important reactions in micellar / microemulsion media:

Part I: Epoxidation of 1-octene in presence of hydrogen peroxide and TS-1 as a catalyst.

Part II: Hydroxylation of phenol to catechol and hydroquinone using anionic and cationic surfactant.

Chapter 3 reports on the synthesis and characterization of different nanoparticles in micellar / microemulsion media. The study includes:

Part I: The synthesis and characterization of thiol-capped CdS nanoparticles in Winsor II microemulsion of diethylether / AOT / water. The dual role of anionic surfactant viz. the formation of microemulsion and facilitating the extraction of oppositely charged ions from aqueous to the organic reverse micellar phase has been successfully used for the synthesis of

dodecanthiol-capped cadmium sulfide (CdS) nanoparticles in a Winsor II type microemulsion. The thiol-capped cadmium sulfide nanoparticles have been characterized by UV-visible, Fourier-transform infrared (FTIR), X-ray photoelectron spectroscopy (XPS), and transmission electron microscopy (TEM).

Part II: The synthesis and characterization of gold nanoparticles stabilized in silicon fluid containing terminal thiol groups in reverse microemulsion diethyl ether/DDAB-DTAB/water. Mixing two reverse microemulsions, one containing gold-dithiol and the other containing sodium borohydride forms gold nanoparticles. The dithiol-passivated gold nanoparticles have been characterized by UV-visible spectroscopy, transmission electron microscopy, fourier-transform infra-red spectroscopy and X-ray photoelectron spectroscopy.

Part III: The synthesis and characterization of dodecanthiol-capped gold nanoparticles in a novel Winsor II type microemulsion of diethyl ether/DDAB / water. Again the dual role of cationic surfactant(s) viz. the formation of microemulsion as well as extraction of oppositely charged tetrachloroaurate ions from aqueous to the organic reverse micellar phase has been profitably used. The formation of the metal nanocomposite is evident from the similarity of the Fourier transform infrared spectrum (FTIR) of the free thiol and the composite. The formation and size of particles have been determined from UV-vis plasmon absorption spectroscopic and transmission electron microscopic (TEM) analysis, respectively. X-ray photoelectron spectroscopy (XPS) investigation confirms the metallic state of gold (Au^0) and the encapsulation by the thiol molecules.

Chapter 4 reports on the synthesis and characterization of molecular sieves in micellar / microemulsion media. The study includes:

Part I: The synthesis of ferrierite type zeolites in the presence of nonionic surfactant containing catalytic amount of template. Pure phase ferrierite (FER) zeolite has been synthesized in presence of small amounts of nonionic surfactants, Tween-20 or Tween-80. The input SiO_2/Al_2O_3 molar ratio has been varied over a range of 25 to 150. The results confirm that small amount of pyrrolidine acts as a template and is necessary. The effects of varying concentration of surfactant on ferrierite crystallization and output SiO_2/Al_2O_3 molar ratio are reported. The results also show that in the absence of pyrrolidine, ZSM-5 co-crystallized with FER whereas in absence of nonionic surfactant the yield and crystallization of FER is very poor. The XRF analysis shows the changes in SiO_2/Al_2O_3 output molar ratio

as the surfactant concentration changes. The XRD data shows that the samples are fully crystalline and pure. The TG/DTA of the sample shows its structural stability. The Scanning Electron Microscopy (SEM) results show changes in particle size with varying concentration of nonionic surfactant. This catalyst is used for the vapor-phase Beckmann rearrangement of cyclohexanone oxime to caprolactam and gas- phase methylation of catechol to *C/O*-alkylated products.

Part II: The synthesis and characterization of titanium silicalite-1 in micellar media containing nonionic surfactant is reported. Titanium silicalite-1 (TS-1) was synthesized in presence of small amount of TPAOH using Tween 20, as nonionic surfactant. The procedure gives highly pure nanometer sized homogeneous crystalline product and higher rate of crystallization. The results are compared with the TS-1 sample prepared without surfactant. Characterization of TS-1 has been carried out by using x-ray diffraction and shows that the samples are fully crystalline, while FTIR spectroscopy shows the presence of characteristic band for TS-1 at 960cm^{-1}, confirming Si-O-Ti linkages present in the product. The UV-visible spectroscopy of the sample prepared without surfactant at low TPAOH concentration shows the presence of extraframework of TiO_2 species. Scanning electron micrograph of the sample shows homogeneous particle size (~ 150nm), while the sample without surfactant shows the presence of particle size ranging between 150-200nm. Catalytic activity of TS-1 sample was also confirmed for octene epoxidation.

Finally chapter 5 provide the summary and conclusions of the present work.

1.13 REFERENCES

1. Hartley, G. S. *Aqueous Solutions of Paraffin Chain Salts,* Hermann et, Ed., Cie, Paris, 1936.
2. Tadros, F. Th. *Surfactants,* Academic Press*,* London,1984.
3. Nagarajan, R. *Adv. Colloid Interface Sci.,* 1986, 26, 205.
4. McBain, M. E. L.; Hutchinson, E. *Solubilization and Related Phenomena*, Academic Press, New York, 1955.
5. Nagarajan, R. and E. Ruckenstein, *Langmuir,* 1991, 7, 2934.
6. Prince, L. M. *Microemulsion Theory and Practice,* Academic Press, New York, 1977.
7. Damodaran, S. *Advance in Food and Nutration Research,* Kinsella. J. E., (Ed.), Academic Press, San Diego, Vol. 34, 1990.
8. Fendler, J. H.; Fendler, E. J., *Catalysis in Micellar and Macromolecular Systems,* Academic Press, New York, 1975.
9. Jungermann, E, *Cationic Surfactant,* Dekker, New York, 1970.
10. Fendler, E. J.; Day, C. L.; Fendler, J. H. *J. Phys. Chem.* 1972, 76, 1460.
11. Schick, M. J. *Nonionoc Surfactant,* Dekker, New York, 1967.
12. Rosen, M. J. *Micelle Formation by Surfactants. In Surfactant and Interfacial Phenomena;* Wiley: New York, 1978; chapter 3, pp 83-121.
13. Lindman B. and Wennerstrom H., Micelles: *Amphiphile Aggregatiion in Aqueous Solution. In Topics in Current Chemistry*; M. J. S. Dewar, H.Hafner, E. Heilbronner, S. Ito, J. M. Lehn, K. Nedenzu, C. W. Rees, K. Schafer and G. Witting, Spring - Verlag; Berlin, **87** (1980) 1.
14. Rathman J.F. Scamehorn F.J. *J. Phys. Chem.* **88** (1984) 5807.
15. Gunnarsson, G.; Jonsson, B.; Wennerstrom H., *J. Phys. Chem.* **83** (1979) 1854.
16. Bravo, C.; Leis, J. R.;.Pena, M.E; J. Phys. Chem. **96**(1992) 1957.
17. Parfitt, G.D., *Principles of Colloidal State*; The RoyalIns. Of Chem.; Adlar and Son: England, 1967; p. 6.
18. Ortega, F., Rodenas, E., *J. Phys. Chem.* **91** (1987) 837.
19. Bunton, C.A.; Carrasco, N.; Huang, S.K.; Paik, C.; Romsted, L.S., J. Am. Chem. Soc. **100** (1978) 5420.
20. Mahieu, N.; Tekely, P.; Canet, D., *J. Phys. Chem.* **97** (1993) 2764.

21. Romsted, L.S., *Micellization Solubilization and Microemulsions*; Mittal, K.L., Ed.; Plenum Press: New York, vol. **2** (1977) 509.
22. Hoar, T. P.; Schulman, J. H. *Nature,* **152** (1943) 102.
23. Schulman, J. H.; Stoeckenius, W.; Prince, L. M. *J. Phys. Chem.* 63 (1959**)** 1677.
24. Sunamoto, J.; Hamada, T. N.; Seto, T. and Yamamoto, S. *Bull.Chem. Soc. Jpn.* **53** (1980) 533.
25. Fendler, J. H. *Membrane Mimietic Chemistry,* John Wiley and Sons, New York, 1984.
26. Myers, D., *Surfaces, Interfaces and Colloids*; VCH Verlagsgesellschaft: Weinheim. 1991; p 333.
27. Winsor, P. A., *Trans. Faraday Soc.* **44** (1948**)** 376.
28. Gan, L. M. and Chew, C. H. *Bull. Singapore Net. Inst. Chem.* 23 (1995**)** 27.
29. Khalweit, M.; Strey, R.; Hasse, D.; Jen, J. and Schomacker, R. *Langmuir,* **5** (1989**)** 305.
30. Charvolin, J.; Levelut, A. M.; Samulski, E. T. *J. Phys. Lett.* **40** (1979**)** L587.
31. Dvolaitzky, M. et al. *J. Chem. Phys.* **69** (1978**)** 3279.
32. Robbins, M. L.; *Micallization, Solubilization and Microemulsions,* Mittal, K. L., Ed., Plenum Press, New York, 1977, Vol. 2.
33. Roux, D.; Coulon, C. and Cates, M. E., *J. Phys. chem.* **96** (1992) 4174.
34. Van Voorst Vader and F. Trans. *Faraday Soc.* **56** (1960) 1067.
35. Kahlweit, M.; Strey, R; Busse, G. *J. Phys. chem.* **94** (1990**)** 3881.
36. Israelachvili, J. *Colloids and Surfaces A: Physicochemical and Eng. Aspects* **91 (**1994**)** 1.
37. Ruasse, M. F.; Blagoeva, I. B.; Krys, S. and Sebastian-Gambaro, M. A. *J. Chem. Soc. Perkin Trans.* **2** (1993**)** 1283.
38. Luise. P.; Giomini, M., Pileni, M. P.; Robinson, B. H. *Biochim. Biophys. Acta.* **947** (1988) 209.
39. Chan, A. F.; Evans, D. F.; Cussler, E. L. *A. I. Chem. E. J.* **22** (1976) 1006.
40. Hartley, G. S. and Graham-Bryce, I.J., *"Physical Principle of Pesticide Behavior",* Academic Press, New York, **947** (1980) 209.
41. Al-Lohedan, H.; Bunton, C. A.; Mhala, M. M., *J. Am. Chem. Soc.* **104** (1982) 6654.
42. Quina, F. H. et al. J. Phys. Chem. **84** (1980) 361.

43. Dennis, K. J., Luong, T., Reshwan, M. L., Minch, M. J., *J. Phys. Chem.* **97** (1993) 8328.
44. Fendler, J. H., Fendler, E. J., Medary, R. T., Woods V. A., *J. Am. Chem. Soc*., **94** (1972) 7288.
45. Konno, K., *Surf. Colloid Sci.* **15** (1993) 125.
46. Mazumdar, S., *J. Phys. Chem.* **94** (1990) 5974.
47. Jonnson, B., *J. Phys. Chem.* **96** (1992) 945.
48. Bacaloglu, R.; Bunton, C. A.; Cerichelli, G.; Ortega, F., *J. Phys. Chem.* **93** (1989) 1490.
49. Rao, U. K. R; Manohar, C.; Valaulikar, B. S.; Iyer, R. M. J., *J. Phys. Chem.* **91** (1987) 3286.
50. Bunton, C. A.; Minch, M. J., *J. Phys. Chem.* **78** (1974) 1490.
51. Fernandez, M. S.; Fromherz, P. *J. Phys. Chem.* **81** (1977) 1755.
52. Mukerjee, P. *J. Pharm. Sci.* **60** (1971) 1528.
53. Harada, S. Okada, H.; Sano, T.; Yamashita, T.; Yano, H. *J. Phys. Chem.* **94** (1990) 7648.
54. Overbeek, J. Th. G. *Faraday Discuss. Chem. Soc.* **65** (1973) 7.
55. Mitchell, D.J.and Ninham, B. W. *J. Chem. Soc., Faraday Trans. 2,***77** (1981), 601.
56. Ruckenstein, E. and Chi, J.C. *J. Chem. Soc., Faraday Trans.2,* **71** (1975**)** 1691.
57. Amrhar, J.; Chevalier, Y.; Gallot, B.; Perchec, P. Le; Auray, X. and Petipas, C., *Langmuir*, **10** (1994) 3435.
58. Chatenay, D. Langevin, D. and Meunier, J. *J. Dispersion Sci. and Technology,* 3 (1982**)** 245.
59. Vrij, A., Nieuwanhuis, E. A., Fijnaut, H. M. and Agterof, W. G. M., *Faraday Disc. Chem. Soc.* **65** (1978**)** 101.
60. Cayias, J. L., Schecter, R.S. and wade, W. H. *"Adsorption at Interfaces." ACS Symposium Serease.* **8** (1975**)** 234.
61. Fletcher, S. et al. *"Microemulsions"* Robb, I. D., Ed., Plenum Press, New York, London. 1977, 221.
62. Lindman, B., Kamenka, N., Brun, B. and Nilsson, P. G., "*Microemulsions"* Robb, I. D.,Ed., Plenum Press, New York, London. 1977, 115.

63. Bansal, V. K. and Shah, D. O. *Microemulsion Thory and Practice,* Academic Press,New York, 1977, 149.
64. Neumann, H. J. *Tensid Taschenbuch,* 2nd ed., Wine, 1981, 433.
65. Gillberg, G. *In Emulsuion and Emulsion Technology* (Ed. Lissant K. J.), Marcel Dekker, New York, 1984, 1.
66. Schwab, A. W.; Fattere, R. S. and Pyrde, E. H., *J. Disper. Sci. Technol.* **3** (1982) 5.
67. Gollan, F.; Clark, L. C. *Physiologist* **9** (1966) 101.
68. Wesseler, E. P.; Iltes, R., Clark, L. C. *J. Flurine Chem,* **9** (1977) 137.
69. Luisi, P. L.; Imer, V. E.; Kackle, H. and Pande A. *Topics in Pharmacutical Science,*
70. Birrenbach, G. and Speiser, P., *J. Pharm. Sci.* **65** (1976) 1763.
71. Breimer, D. D. and Speiser, P. P., (Eds.), Elsevier, New York, 1983, 243.
72. Reiss J-G.; and Le Blanc M. *Pure Appl. Chem.* **54** (1982) 2383.
73. Mathis, G.; Leempoel, P.; Ravey, J. C.; Selve, C.; Delpuech, J. J. *J Am. Chem. Soc*. **106** (1984) 6162.
74. Kumar, P.; Mittal, K. L. (eds), *Handbook of Microemulsion Science and Technology*, Marcel Dekker Inc. New York, 1999, 755-771, 483-497.
75. Attwood D., *In Colloidal Drug Delivary System* (ed. J. Kreuter), Marcel Dekker, New York, 1994, 31.
76. Muller, E. A.; Kovarik, J. M.; Van Bree, J. B.; Grevel, J.; Luecker, P. W. and Kutz K., *Pharm. Res.*, **11** (1994) 151.
77. Jain, T. K., Roy, I.; De, T. K.; Maitra, A. N. *J. Am. Chem. Soc.* **120** (1998) 11092.
78. Briscoe, B. J.; Evans, C. B. and Tabor, D. *J. Colliod and Interface Sci.* **61** (1977) 9.
79. Sillion, B. *"Pertoleum Refining Crude Oil Petrolium Products Process Flowsheet",* Wauquire, J. P.(Ed.), Editions Teachnip, Paris, pp 345, 1994.
80. Prince, L. M. *"Microemulsion Theory and Practice",* Academic Press, New York, 1977, 21.
81. Leung, P. S. in *Ultrafiltration Membranes and Applications,* Ed. Cooper, A. R., Plenum Press, New York, 1979, p 415.
82. Bhat S. N., Smith, G. A., Tucker, E. E., Christian, S. D.; Scamehorn, J. F. in *Ind. Eng. Chem. Res.* **26** (1987) 1217.

83. Scamehorn, J. F.; Christian, S. D.; Ellingtion, R. T. in *Surfactant-based Separation Process,* Eds. Scamehorn, J. F. and Harwell, J.H., Marcel Dekker, New York & Basal, 1963.

84. Christian, S. D.; Bhat, S. N.; Tucker, E. E.; Scamehorn, J. F. and E1-Sayed, D. A. *AIChE J.,* **34** (1988) 189.

85. Solans, C. and Kuniedan, H. (eds), *Industrial Applications of Microemulsions*, Marcel Dekker Inc., New York, 1997.

86. Moilliet, J. L., Collie, B. and Black, W., *Surface Activity,* Spon, London, 2nd Edn., 1961.

87. El-Nokaly, M.; Hiler, G. and McGrady, J. *In Microemulsions and Emulsions in Foods*.(eds. M. El-Nokaly and D. Cornell) Am. Chem.Soc. Washington DC, 1991, pp 26-43.

88. Larsson, K.; Osborne, D. W.; Pesheck, C. V. and Chipman, R. J., *In Microemulsions and Emulsions in Foods*.(eds. M. El-Nokaly and D. Cornell) Am. Chem.Soc. Washington DC, 1991, pp 44-50 and pp 62-79.

89. Novotry, V. in *Colloids and Structures in Reprographic Technology,* Ed. Hair. M. L. and Croucher, M. D. ACS Symposium Series **200** (1982) 281.

90. Dalquist. J. A. and Brodie, I. *J. Appl. Phys.* **40** (1960) 3020.

91. Ashley. C. T., Edds. K. E. and Elbert, D. L. *IBNJ. Res, Develop.* 21 (1977) 69.

92. Gupte, A.; Nagarajan, R. and Kilara, A., *In Food Flavors: Generation, Analysis and Process Influence* (ed. G. Charalambous) Elsevier, London, 1995, p 1.

93. Levashov, A. V.; Khmelnitsky, Y. L.; Klyachko, N. L.; Chernyak, V. Y.; Martinek, K., *J. Colloid Interface Sci.*, **88** (1992) 444.

94. Larsson, K., *Lipids: Molecular Organisation*, *Physical Functions, and Technical Applications,* Oily Press, Dundee, Scotland, 1994, ch. 9.

95. Nakamura, T.; Matsumoto, M.; Takei, F. Tanaka, M. Skiguchi, T.; Manda, E. and Kawabata, Y. *Chem. Lett.(Jap),* **5** (1986), 709.

96. Mann, B. et al. *J. App. Phys.* **42** (1971) 4398.

97. Winter, C. S. and Tredgold, R. H. *J. Phys. D.* **17** (1984) L123.

98. Barraud, A.; Ruaudel-Tei-nier, A.; Vandevyver, M. and Leiseur, P. *Nouv. J. Chem*. **9** (1985) 365.

99. Blinov. L. M.; Dubinin. N. V.; Mikhenev, L. V. and Yudin, S. G., *Thin Solid Films*, **120** (1984) 161.
100. Smith, G. W.; Daniel, M. F.; Barton, J. W. and Rateliffe, N. *Thin Solid Films,* **1985,**132, 125.
101. Pomeranytz, M. in *Phase Transitions in Surface Films,* Eds. Dash, J. G. and Ruvalds, J. Plenum Press, New York, 1980, p 317.
102. Seto, J.; Nagai, T.; Isimoto, C. and Watanabe, H. *Thun Solid Films,* **134** *(*1985) 101.
103. Duynstee, F. F. J.; Grunwald, E. *J. Am. Chem. Soc.* **81** (1959) 4540.
104. Funasaki, N. *J. Phys. Chem.* **83** (1979) 1998.
105. Quina, F. H.; Chaimovich, H. *J. Phys. Chem.* **83** (1979) 1844.
106. Bunton, C. A.; Romsted, L. S., Thamavit, C., *J. Am. Chem. Soc.* **102** (1980) 3900.
107. Vera, S.; Rodenas, E. *Tetrahedron,* **42** (1986) 143.
108. Bunton, C. A.; Savelli, G. *Adv. Phys. Org. Chem.* **22** (1986) 213.
109. Romsted, L. S.; Cordes, E. H. *J. Am. Chem. Soc.* **90** (1968) 4404.
110. Dunlap, R. B.; Cordes, E. H. *J. Am. Chem. Soc.* **90** (1968) 4395.
111. Gan, L. -H. *J. Chem.* **63** (1985) 598.
112. Bunton, C. A.; Moffatt, J. R.; Rodenas, E. *J. Am. Chem. Soc.* **104** (1982) 2653.
113. Bunton, C. A.; Minch, M. J.; Hidalgo, J.; Sepulveda, L. *J. Am. Chem. Soc.* **95** (1973) 3262.
114. Stilbs, P. *J. Colloid Interface Sci.* **94** (1983) 463.
115. Kallick, D. A. *J. Am. Chem. Soc.* **115** (1993) 9317.
116. Jeager, D. A.; Shinozaki, H.; Goodson, P. A. *J. Org. Chem.***56** (1991) 2482.
117. Broxton, T. J.; Marcou,V. *J. Org. Chem.* **56** (1991) 1041.
118. Ranganathan, D.; Ranganathan, S.; Singh, G. P.; Patel, B. K. *Tetrahedron Lett.* 1993, 34, 525.
119. Kang, Y. S.; Baglioni, P.; McManus, H. J. D.; Kevan L. *J. Phys. Chem.* **95** (1991) 7944.
120. Broxton T. J. *Aust. J. Chem.* **44** (1991) 667.
121. Mandal, A. B.; Nair, B. U. *J. Phys. Chem.* **95** (1991) 9008.
122. Rusling, J. F. *Acc. Chem. Res.* **24** (1991) 75.
123. Grand, D., *J. Phys. Chem.* **94** (1990) 7585.
124. Hu, M.; Kevan, L. *J. Phys. Chem.* **94** (1990) 5348.

125. Scaiano, J. C.; Shi, J. L. *Chem. Phys. Lett.* **173** (1990) 271.
126. Bunton, C. A.; Rubin, R. J. *Tetrahedron Lett.* 1975, 55.
127. Brown, J. M.; Bunton, C. A.; Diaz, S. *J. Chem. Soc. Chem. Comm.* 1974, 971.
128. Weijnen, J. G. J.; Koudijs, A.; Engbersen, J. F. J. *J. Mol. Catal.* **73** (1992) L5.
129. Martin, C. A.; McCrann, P. M.; Angelos, G. H.; Jaeger, D. A. *Tetrahedron Lett.* **23** (1982) 4561.
130. Varughese, P.; Broge, A., *J. Indian Chem. Soc.***68** (1991) 323.
131. McGuiness E. T., Brown, H. D., Chattopadhyay, S. K., Chan F., *Biochem Biophys Acta* **530** (1978) 247.
132. Menger, F. M.; Donohue, J. A.; Williams, R. F., *J. Am. Chem. Soc.* **95** (1973) 286.
133. Schomacker, *R. . J. Chem. Res. (S)* 1991, 92.
134. Gonzalez, A., Holt, S. L., *J. Org. Chem*. **47** (1982) 3186.
135. Briffaud, T., Larpert, C., Patin, H., *J. Chem. Soc. Chem. Commun***.** 1990, 1193.
136. Streitwieser, A. and Reuben, D. M. E. *J. Am. Chem. Soc*. **93** (1971) 1794.
137. Choux, G. and Benoit, R. L., *J. Am. Chem. Soc.* **93** (1969) 6221.
138. Bunton, C. A. and Rubin, R. J., *Tetrahydron Ltters*, **1** (1975) 55.
139. Menger, N. and Elrington, A. R., *J. Am. Chem. Soc*. **113** (1991), 9621.
140. Jha, B. K. and Kulkarni, B. D., *Ind. Eng. Chem. Res.* **1995,** 34, 3826.
141. Chhatre, A. S.; Joshi, R. A. and Kulkarni, B. D., *J. Colloid Interface Sci.* **1993,** 158, 18369.
142. Eric H. F.; Shepherd, J. C. W.; Steinemann, A. *J. Colloid Interface Sci.* 1979, 56, 168.
143. Gan, L. M.; Lee, C. K.; Chew, C. H.; Tok, E. S.; Ng, S. C. *J. Polym. Sci. A:Polym. Chem.* **1995,** 33, 1161.
144. Lumfimpadio,N., Nagy, J. B., Derouane, E. G., *Surfactants in Solution,* Mittal, K. L.and Lindman, B.; Eds., Plenum Press, New York, 1986, Vol. 3, p 483.
145. Chew, C. H., Gan, L. M. and Shah, D. O., *J. Dispersion Sci. Technol.* **1990,** 11, 593.
146. Ayyub, P.; Maitra, A. N.; and Shah, D. O. et al. *Physica C* **1990,** 168, 571.
147. Kortan, A. R.; Hull, R.; Opila, R.L.; Bawendi. M. G.; Steigerwald, M. L.; Carroll,P.J.; Brus, L. E. *J. Am. Chem. Soc.* **1990,** 112, 1327.
148. Joselevich, E., Willner, I., *J. Phys. Chem.* **1994,** 98, 7628.
149. Gan, L. M., Chan, H. S. O., Zhang, L. H., Chew, C. H., Loo, B. H., *Mater. Chem. Phys*. **1994**, 37, 263.

150. Kon-no, K., *Surface and Colloid Science,* Matijevic, E., Ed., Plenum Press, NewYork, 1993, Vol. 15, p 194.
151. Lewis, L. N., *Chem. Rev.* **1993,** 93, 2693
152. Pileni, M. P., *J. Phys. Chem.* **1993,** 97, 6961.
153. Krasge, C. T.; Leonowicz, M. E.; Roth, W. J.; Vartuli, J. C.; Beck, J. S., *Nature* **1992,**359, 710.
154. Enderby, J. C.;Howells, W. S.,;Howe, R. A. *Chem. Phys. Lett.* **1973,** 21, 109.
155. Attard, G. S.; Glyde, J. C.; Goltner, C. G. *Nature* **1995,** 378, 366.
156. Tromp, R. H.; Postorino, P.; Nielson, G.W.; Ricci, M. A.; Soper, A. K. *J. Chem. Phys.* **1994,** 101, 6210.
157. Myatt, G. J.; Budd, P. M.; Price, C.; Hollway, F.; Carr, S. W. *Zeolite* **1994,** 14, 90.

CHAPTER 2

ORGANIC REACTIONS IN MICELLES AND MICROEMULSIONS

PART I

EPOXIDATION OF 1-OCTENE IN REVERSE MICROEMULSION

In this part we report the epoxidation of octene with hydrogen peroxide in reverse (w/o) micremulsion containing bis (2-ethylhexyl) sulfosuccinate (AOT). This is a co-solvent free method where an anionic surfactant (AOT) overcomes the limitation of homogenization. The catalyst used was a titanium molecular sieve, TS-1 with a Ti to Si molar ratio of 30. The influence of reaction time, temperature, surfactant concentration and octene to hydrogen peroxide molar ratio on the conversion and selectivity has been studied. Improved yield and total selectivity to epoxide are obtained.

2.1 INTRODUCTION

Alkene epoxidation is a very useful reaction in industrial organic synthesis. Epoxides are key raw materials for a wide variety of products[1,2] and much efforts are devoted to the development of new active and selective epoxidation catalysts for processes that avoid the formation of large amounts of by-products. In organic synthesis one often encounters the problem of bringing about the reaction of water-soluble inorganic reactants with water-insoluble organic reactants. Micelles and microemulsions are pseudo-homogeneous mixtures of aqueous and organic phases which show remarkable stability in the presence of large amount of additives like inorganic salts, organic substrates, and complexes.[3] More significantly, the solubilization of non-polar organic molecules and inorganic salts in such a phase brings about variation in rates that can be attributed to hydrophobic, electrostatic, electrophilic and/or nucleophilic interactions resulting in changing the free energy of activation of the process.[4-7]

It is well recognized that microenvironment can enhance the reaction by concentrating reagents in the stern layer.[8,9] Micelles and microemulsions are low viscous, transparent but compartmentalized, and thermodynamically stable dispersions in the presence of surface active agent. The dynamic nature of the micelles/microemulsions facilitates the exchange of various reactants solubilized in microdroplets. Owing to the excellent solubilization, particular orientation and local concentration gradient effects at the interfaces, micelles and microemulsions serve as batter media for several organic reactions. The counter environments (hydrophobicity and hydrophilicity) of a microdroplet leads to organized assembly as well as specific orientation of substrate molecules. This, in turn, helps the product selectivity for a specific reaction.[10] In addition to the above mentioned properties, this technique allows the reaction to be conducted under conditions of low viscosity and interfacial tension, higher stability of surfactant molecules and reduced toxicity. These attributes have proven to be especially useful in various biocatalytic synthesis of a range of important pharmaceuticals,[11-16] synthesis of nanoparticles for ceramic and electronic processing and as a solvent for the selective recovery of proteins. It is also known to be a better media for conducting numerous organic and inorganic reactions such as acid, base, cyanide, bromide, hypochlorite, permanganate, cyclization, molecular rearrangement and decarbamoylation reaction.[17-23]

Recently, epoxidation of 1-octene over titanium molecular sieves TS-1 by aqueous hydrogen peroxide has acquired considerable interest. The reaction is customarily a liquid-solid heterogeneous catalytic system, where a co-solvent like acetone, methanol or acetonitrile acts as a homogenizer of aqueous and organic phases. The use of large quantities of organic solvents is not only detrimental to environment but also economically unfavorable. Further, the separation of solvent after reaction is cumbersome, expensive and energy intensive.

Thus we report in this part a new eco-friendly and efficient synthetic method for octene epoxide in microemulsion medium over TS-1. A detailed study of influence of various reaction parameters such as 1-octene/H_2O_2 molar ratio, reaction temperature, and AOT concentration on the conversion of 1-octene is carried out systematically.

2.2 EXPERIMENTAL SECTION

2.2.1 REAGENTS

1-octene (Aldrich, 98%), AOT (SIGMA, 99%), hydrogen peroxide (Loba Chemie, 50 wt.% aqueous solution). Titanium silicalite-1 was used as a catalyst and prepared using a reported procedure.

2.2.2 CATALYST PREPARATION

TS-1 of Ti/Si molar ratio 30, was synthesized according to modified literature procedure.[24,25] In brief, in a teflon beaker 31.5 g of TEOS was added dropwise to 76.2 g TPAOH under vigorous stirring for 2 h. The reaction mixture was stirred by a magnetic stirrer at around 600 RPM all the time. A solution of 1.69g TNBT in 8.55 g dry IPA was added slowly to the above solution under vigorous stirring and stirring was continued for another 30 min. Then 1.18 g H_3PO_4 in 3.3 g water was added slowly under vigorous stirring which was continued for another 1 h. The final molar composition of the reaction mixture was:

30 TEOS : 15 TPAOH : TNBT : 28.5 IPA : 2 H_3PO_4 : 750 H_2O

The whole reaction mixture was packed in a Teflon jacketed stainless steel autoclave and immediately put into the preheated oven. After being heated at 433 K for 10 h the autoclave was quenched under cold tap water. The precipitate was filtered, washed with deionized water and dried at 393K for 12h. The calcination was carried out in a furnace at

828 K for 15 h with an initial rate of temperature increment of 2°/min. The catalyst prepared was characterized by XRD, FT-IR, SEM, and UV-visible spectroscopy.

2.2.3 CHARACTERIZATION OF CATALYST

The XRD pattern of TS-1 sample shows the characteristic of MFI topology. The scanning electron micrograph shows that the crystallites have the particle size in between 100-200nm. UV-visible spectrum of TS-1 shows a sharp absorption peak at ca. 214nm. The absence of any peak in the range 250- 355nm clearely indicates the absence of extraframework TiO_2 species. FT-IR spectrum of the TS-1 shows a sharp band at 962 cm^{-1} which is a characteristic of TS-1 (believed to be due to stretching vibrations of SiO_4 tetrahedron bound to Ti atoms as Si-O-Ti linkages).

2.2.4 REACTION PROCEDURE

The microemulsions of different compositions were prepared according to the titration method. To a fixed amount of 1-octene, a pre-calculated amount of AOT has been dissolved to form a micellar solution. Required quantity of H_2O_2 (50 wt. % aqueous solution) was then added to this solution while stirring. The transparent mixture thus prepared is water in oil type microemulsion. Pre-determined amount of this microemulsion along with the required amount of catalyst were charged into a RB (50 ml) and stirring was continued till the end of the reaction. The reaction mixtures were analyzed by a capillary GC using a FID. The exact percentage of H_2O_2 was determined by titration with standard potassium permanganate solution. The temperature was controlled using oil bath.

2.3 RESULT AND DISCUSSIONS

2.3.1 EFFECT OF H_2O_2 MOLAR RATIO

Table 2.1 depicts the effect of octene: H_2O_2 molar ratio. It can be seen from the table that increase in the octene: H_2O_2 ratio (from 1 to 10) increases the octene conversion and H_2O_2 effeciency. The maximum H_2O_2 efficincy is observed at molar ration 10, while minimum H_2O_2 efficiency is observed at molar ratio 1. This may be due to the self-decomposition of H_2O_2 which is minimum at higher ratios. The selectivity

towards octene epoxide was always 100%. Generally size and number of microemulsion droplets increases with increase in molecular ratio of H_2O_2 to AOT, which results in increase in interfacial area. These droplets perform Brownian motion and the collisions between the surface of TS-1 and the droplets result in the formation of reactive transition state which translates into product. The conversion of octene is directly proportional to the number of collisions and reactive interfacial area. However, after attaining the limiting value of H_2O_2 to octene molar ratio, the system undergoes structural changes leading to decrease in number of collisions and hence, rate of the reaction.

Table 2.1: Effect of Octene to H_2O_2 molar ratio on H_2O_2 efficiency and Octene epoxide selectivity.

Octene : H_2O_2	1	2	4	5	10
H_2O_2 efficiency (mole %)	12	40	65	90	91
Epoxide selectivity (mole %)	98	100	100	100	100

Reaction conditions: Catalyst TS-1 = 10 wt. % with respect to substrate; Temperature 333 K; Reaction time = 3h.

Table 2.2: Effect of reaction temperature on H_2O_2 efficiency and Octene epoxide selectivity.

Reaction Temp. (^oC)	30	40	50	60
H_2O_2 efficiency (mole %)	24	40	67	85
Epoxide selectivity (mole %)	100	100	100	100

Reaction conditions: Catalyst TS-1 = 10 wt. % with respect to substrate; octene to H_2O_2 = 10 (mole); Reaction time = 3h.

2.3.2 EFFECT OF REACTION TEMPERATURE

Table 2.2 shows the effect of temperature on the H_2O_2 efficiency and epoxide selectivity at a fixed octene : H_2O_2 (10:1) molar ratio. The H_2O_2 efficiency is low at 30^oC and maximum at 60^oC. This may be attributed to the fact that total number of reactant molecules in the vicinity of stern layer (reactive interface) decreases with temperature. In addition, the thermal motion produces a disrupting effect on the packing of surfactant molecules at high temperature. This disrupting effect cause an increase in molecular distance between the surfactant molecules at the interface, which in turn influence the viscosity, surface tension and stability of micelles.

2.3.3 EFFECT OF THE AOT CONCENTRATION

It can be seen from table 2.3 that as the concentration of AOT increases the H_2O_2 efficiency goes through a maximum and then decreases at high concentration (0.25M) of AOT. Low efficiency of H_2O_2 utilization and selectivity towards epoxide are observed at low concentration of AOT (0.01M). This may be due to the absence of the proper microenvironment of the medium in the system. At 0.12M concentration of AOT the H_2O_2 efficiency was maximum and selectivity towards epoxide was 100%. Above this concentration of AOT the H_2O_2 efficiency goes on decreasing. This may be due to an increase in concentration of Na^+ ions, accumulated near the interface. These unreacted Na^+ ions may decrease the reactivity of the catalyst by decreasing the acidity. In addition, adsorption of the AOT molecules at higher concentration on the reactive sites of the catalyst may also be considerable.

Table 2.3: Effect of AOT concentration on H_2O_2 efficiency and octene epoxide selectivity.

AOT concentration (M)*	0.01	0.05	0.12	0.18	0.25
H_2O_2 efficiency (mole %)	42	55	90	88	85
Epoxide selectivity (mole %)	95.3	98.8	100	100	100

Reaction conditions: Catalyst TS-1 = 10 wt. % with respect to substrate; Temperature 333 K; Reaction time = 3h; Octene to H_2O_2 = 10

*= AOT concentration with respect to total volume of the reaction mixture.

PART II

HYDROXYLATION OF PHENOL IN MICELLAR MEDIA

Hydroxylation of phenol to hydroquinone and catechol has been successfully carried out in micellar media over titanium silicalite-1 in the presence of anionic surfactant. Hydrogen peroxide was used as an oxidant. The influence of reaction time, temperature, surfactant concentration and phenol to hydrogen peroxide molar ratio on the conversion and selectivity is studied.

2.4 INTRODUCTION

The use of TS-1 in the oxidation of phenols to diphenols is described by Taramasso et al [26-28] The first commercial process utilizing titanium silicalite (TS-1) as a catalyst was the hydroxylation of phenol to hydroquinone and catechol introduced by Enichem, Italy.[29,30] Several reports have since appeared on the influence of various parameters, such as the titanium content, phenol to H_2O_2 mole ratio, the solvent used, etc., on the conversion of phenol and various products of hydroxylation.[31-33] TS-1 was the most effective material in the utilization of H_2O_2 in forming oxidized phenols but it gives hydroquinone and tars in addition to dihydroxy compounds. The hydroquinone (p-isomer) was the major product. So increasing the selectivity towards dihydroxy benzenes and control of regioselectivity of isomers is very important from the industrial point of view. This can be achieved in presence of micelles and led us to carry out hydroxylation of phenol over titanium silicalite-1 in the presence of anionic surfactant.

Micelles not only catalyze chemical reactions but can also increase the selectivity as well as yield. Use of a micelle based systems to control the selectivity of an organic reactions is therefore. It is significant that in some reactions of phenol and its ethers, selectivity changes in substitution have been caused by surfactant. Chlorination of phenol is promoted at the ortho position by SDS micelles[34] and conversely para chlorination can be obtained for n-pentyl phenyl ether.[35]

In this part we report the hydroxylation of phenol over titanium silicalite-1 in micellar media containing anionic surfactant. The phenol hydroxylation scheme is given as below:

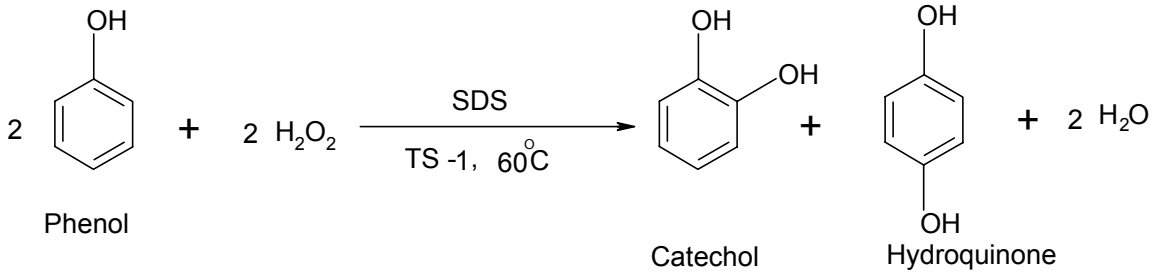

2.5 EXPERIMENTAL SECTION

2.5.1 REAGENTS

Phenol (Aldrich, 99%), SDS (s.d. FINE CHEM. 99%), hydrogen peroxide (Loba Chemie, 50 wt.% aqueous solution). Titanium silicalite-1 was used as a catalyst and prepared using a reported procedure.

2.5.2 CATALYST PREPARATION

The detailed procedure for the synthesis of catalyst is reported in the part I. (section 2.2.2).

2.5.3 REACTION PROCEDURE

The micellar solution of different compositions were prepared by the following method. Sodium dodecyl sulfate was dissolved in appropriate quantity of distilled water. To this clear surfactant solution required quantity of phenol was added to form a micellar solution. Required quantity of H_2O_2 (50 wt. % aqueous solution) was then added to this solution while stirring. The micellar solution along with the calculated amount of catalyst has charged into a RB (50 ml) and stirring was continued till the end of the reaction. The reaction mixtures were analyzed by a capillary GC using a FID. The exact percentage of H_2O_2 was determined by titration with standard potassium permanganate solution. The temperature was controlled using oil bath.

2.6 RESULT AND DISCUSSION

2.6.1 EFFECT OF PHENOL TO H_2O_2 MOLAR RATIO

Table 2.4 shows the effect of phenol : H_2O_2 molar ratio on phenol conversion. With increase in the phenol : H_2O_2 ratio (from 1 to 5) the H_2O_2 efficiency also increases. It is observed that the H_2O_2 efficiency is higher at ratio 5. The self decomposition of H_2O_2 is minimum at higher phenol: H_2O_2 ratio. It can also be seen from the table that selectivity to the o-isomer is always higher as compared to the p-isomer. This may be due to orientation effects of the micellar media.

Table 2.4: Effect of H_2O_2 concentration on phenol conversion and selectivity towards o- and p- hydroxy phenols.

Phenol:H_2O_2 (mole)	Phenol conv.[a] (mole%)	H_2O_2 efficiency [b](mole%)	Product (%)	
			catechol	hydroquinone
1	8	40	78	22
2	10	50	71	29
3	13	65	64	36
5	18	90	60	40

Reaction conditions: catalyst 15 wt. % with respect to substrate, reaction temperature = 60^oC; Time = 3h

[a]= conversion is based on the number of moles of H_2O_2 taken with respect to phenol.

[b] = H_2O_2 efficiency is defined as the number of moles of H_2O_2 utilized for the formation of hydroxylated phenol products.

2.6.2 EFFECT OF THE SURFACTANT CONCENTRATION

It can be seen from table 2.5 that with an increase in concentration of SDS the H_2O_2 efficiency increases. At 0.1M concentration of SDS the H_2O_2 efficiency of 90 % reached. Further increase in concentration of SDS however decreases the H_2O_2 efficiency. This may be attributed to the fact that addition of large amount of SDS brings about an increase in concentration of Na^+ ions which accumulate in the stern layer (the reactive interface). These unreacted Na^+ ions may decrease the reactivity of the catalyst by decreasing the acidity. Also at higher concentration, the SDS molecules may get adsorbed to the reactive sites. Low H_2O_2 efficiency at low concentration of SDS may be due to absence of proper microenviornment. It can also seen from table that by varying the surfactant concentration selectivity towards the o- and p- isomer also changes.

2.6.3 EFFECT OF REACTION TIME

Table 2.6 shows the effect of reaction time on phenol conversion. When the progress of the reaction was followed with time during the hydroxylation of phenol in

micellar media, it was observed that the reaction is very fast at the beginning and gives high selectivity towards the o-isomer. Further with the progress in time the selectivity for the p-isomer increases with corresponding decrease in the selectivity for the o- isomer.

Table 2.5: Effect of SDS concentration on phenol conversion and selectivity towards o- and p- hydroxy phenols.

SDS conc.	Phenol conv.[a] (mole%)	H_2O_2 efficiency [b](mole%)	Product (%)	
			catechol	Hydroquinone
0.01	7	35	75	25
0.04	11	55	66	34
0.1	18	90	60	40
0.15	17	85	45	55

Reaction conditions: catalyst 15 wt. % with respect to substrate; phenol: H_2O_2 = 5 (maximum theoretical phenol conversion = 20 mole).

[a, b] defined in Table 2.4.

Table 2.6: Effect of reaction time on phenol conversion and selectivity towards o- and p-hydroxy phenols.

Rection time (h)	Phenol conv.[a] (mole%)	H_2O_2 efficiency [b](mole%)	Product (%)	
			catechol	hydroquinone
1	12	60	85	15
2	15	75	70	30
3	18	90	60	40
4	17.5	87.5	65	35

Reaction conditions: catalyst 15 wt. % with respect to substrate; phenol: H_2O_2 = 5 (maximum theoretical phenol conversion = 20 mole).

[a, b] defined in Table 2.4.

2.6.5 EFFECT OF REACTION TEMPERATURE

Table 2.7 shows the effect of temperature on the hydroxylation of phenol. At 30°C both the H_2O_2 efficiency and p-isomer selectivity were low. At 60°C maximum H_2O_2 efficiency is observed.

Table 2.7: Effect of reaction temperature on phenol conversion and selectivity towards o- and p- hydroxy phenols.

Reaction temp. (^oC)	Phenol conv.[a] (mole%)	H_2O_2 efficiency [b](mole%)	Product (%)	
			catechol	hydroquinone
30	5	25	70	30
40	9	45	68	32
50	12	60	62	28
60	18	90	60	40

Reaction conditions: catalyst 15 wt. % with respect to substrate; phenol: H_2O_2 = 5 (maximum theoretical phenol conversion = 20 mole).

[a, b] defined in Table 2.4.

2.7 CONCLUSION

In conclusion, use of co-solvent for epoxidation of 1-octene can be successfully avoided by carrying it out in reverse microemulsion containing AOT. Presence of anionic surfactant, AOT helps to i) avoid the limitation of homogenization, ii) increase the rate of reaction and iii) gives 100% epoxide selectivity with better conversion.

The hydroxylation of phenol was also successfully carried out in micellar media. It is also possible that by varying the surfactant concentration one can control the regioselectivity of the products.

2.8 REFERENCES

1. Franz, G; Sheldon, R.A. in: Elvers, B.; Hawkins, S.; Shulz, G. (Eds.), *Ullmann's Encyclopedia of Industrial Chemistry,* Vol. A (18), 5th Edition, VCH, Weinheim, 1991, pp. 261–311.
2. Lutz, J.T.; in: Kirk-Othmer, Grayson, M.; Eckroth, D.; Bushey, G.J.; Eastman, C.I.; Klingsberg, A.; Spiro, L. (Eds.), *Encyclopedia of Chemical Technology,* Vol. 9, 3rd Edition, Wiley, New York, 1980, p. 251.
3. Fendler J. H. and Fendler E. J., *Catalysis in Micellar and Macromolecular Systems*, Academic Press, New York, 1975.
4. Cordes, E. H. and Dunlop, R. B. Accts. Chem. Res., **2** (1982) 329.
5. Gunnarsson, G., Johnsson, B and Wennerstrom, H., *J. Phys. Chem.* **84** (1980**)** 3114.
6. Bunton C. A.; Nome, F.; Quina, F. H. and Romsted, L. S. *Accts. Chem. Res.,* **24** (1991) 375.
7. Garcia-Rio, L.; Iglesias, E. and Pena, M. E., *Langmuir*, **9** (1993) 1263.
8. Stigter. D. *J. Phys. Chem*. **68** (1964) 3567.
9. Gruen, D. W. R. *Prog. Colloid Polym. Sci.,* **70** (1985) 6.
10. Adachi, M.; Harada, M.; Shioi,A. and Sato, Y. *J.Phys. Chem.* **95** (1991) 95, 7925.
11. Birrenbach, G. and Speiser, P., *J. Pharm. Sci.* **65** (1976) 1763.
12. Gollan, F. and Clark, L. C. *Physiologist* **9** (1966) 101.
13. Wesseler, E. P.; Iltes, R. and Clark, L. C. *J. Flurine Chem,* **9** (1977) 137.
14. Luisi, P. L.; Imer, V. E.; Kackle, H. and Pande A. *Topics in Pharmacutical Science,* Breimer, D. D. and Speiser, P. P., Eds., Elsevier, New York, 1983, 243.
15. Reiss J-G. and Le Blanc, M. *Pure Appl. Chem.* **54** (1982) 2383.
16. Mathis, G.; Leempoel, P.; Ravey, J. C.; Selve, C.; Delpuech, J. J. *J Am. Chem. Soc*. **106** (1984) 6162.
17. Menger, F. M.; Donohue, J. A.; Williams, R. F. *J. Am. Chem. Soc.* **95** (1973) 286.
18. Hamilton, J. F. and Baetzold, R. C. *Science* **205** (1979) 1213.
19. Boutonnet, M. and Kizling, J. Stenius, P., Maire, G. *Colloids Surf.* **5** (1982) 209.
20. Kurihara, K.; Kizling, J.; Stenius, P.; Fendler, J. H. *J. Am. Chem. Soc.* **105** (1983) 2574.
21. Colvin, V. L.; Schlamp, M. C. and Alivisatos, A. P., *Nature* **370** (1994) 354.

22. Martin, C. A.; McCrann, P. M.; Angelos, G. H.; Jaeger, D. A. *Tetrahedron Lett.* **23** (1982) 4561.
23. Lumfimpadio,N.; Nagy, J. B.; Derouane, E. G. *Surfactants in Solution,* Mittal, K. L. and Lindman, B., Eds., Plenum Press, New York, **3** (1986) 483.
24. Gao, H.; Lu, G.; Suo, J. and Li, S. *Applied Catal. A: General,* **138** (1996) 27.
25. Kumar, S. B.; Mirajkar, S. P.; Pais, G. C. G., Kumar, P. and Kumar, R. *J. Catal.* **156** (1995) 163.
26. Esposito, M. Taramasso, C. Neri and F. Buonomo, U.K. patent 2 116 974 (1983).
27. Esposito, M. Taramasso, C. Neri and F. Buonomo, US patent 4 396 783 (1983).
28. M. Taramasso, G. Perego and B. Notari, US patent 4 410 50 (1983) assigned to SNAM Progetti Italy.
29. U. Romano, A. Esposito, F. Maspero, C. Neri and M.G. Clerici, Chem. Ind., (Milan) **72** (1990) 610.
30. Notari, *Stud. Surf. Sci. Catal*., **60** (1991) 343.
31. Kraushar-Czarnetzki and J.H.C. Van Hoof, *Catal. Lett*., **2** (1989) 43.
32. Thangaraj, R. Kumar and P. Ratnasamy, *J. Catal*., **131** (1991) 294.
33. D.R.C. Huybrechts, P.L. Buskens and P.A. Jacobs, *J. Mol. Catal*., **71** (1992) 129.
34. S. O. Onyriukas, C. J. Suckling, *J. Chem. Soc.: Chem. Commun.* (1982) 833.
35. D. A. Jaeger, R. E. Robertson., *J. Org. Chem*. **42** (1977) 3298.

CHAPTER 3

SYNTHESIS AND CHARACTERIZATION OF NANOPARTICLES IN MICROEMULSIONS

PART I

SYNTHESIS AND CHARACTERIZATION OF DODECANTHIOL-CAPPED CADMIUM SULFIDE NANOPARTICLES IN A WINSOR II MICROEMULSION

Synthesis and characterization of dodecanthiol-capped cadmium sulfide (CdS) nanoparticles in a Winsor II type of microemulsions of diethyl ether / AOT / water are described. The dual role of anionic surfactant viz. the formation of microemulsion and facilitating the extraction of oppositely charged ions from aqueous to the organic reverse micellar phase has been successfully used for the synthesis of dodecanthiol-capped cadmium sulfide (CdS) nanoparticles in a Winsor II type microemulsion. The thiol-capped cadmium sulfide nanoparticles have been characterized by UV-visible, Fourier-transform infrared (FTIR), X-ray photoelectron spectroscopy (XPS), and Transmission electron microscopy (TEM).

3.1 INTRODUCTION

Synthesis of nanometer size particles of metals and semiconductors have gained considerable interest due to their novel size-dependent physicochemical and optoelectronic properties. The quantum properties of the semiconductor particles have potential uses in information-processing devices and, in recognition of this, they are often called "Q particles". These novel properties arise due to the large number of surface atoms (high surface-to-volume ratio) and/or the three-dimensional (3D) confinement of electrons**.** When the electrons and holes are confined within the three dimensional potential well, the continuum of the states in the conduction and valance bands is broken down into descrete states with an energy spacing, relative to band edge, which is approximately inversely proportional to the square of the particle size[1]. Altering the size of the particle changes the degree of confinement of the electrons and tunes the electronic structure of the solid (particularly 'band edges'). These nanomaterials have found promising applications in various fields such as in microelectronic systems[2-3] (light-emitting diodes and photovoltaic cells), photocatalysis,[4-5] electroluminescence,[6] reprography,[7] etc.

"Water-in-oil" (w / o) microemulsions consist of nanometer size water droplets dispersed in a continuous oil phase and stabilized by surfactant molecules localised at water/oil interface.[8] The reverse micellar systems are heterogeneous on a molecular scale and are thermodynamically stable and transparent. They provide a suitable reaction media for the synthesis of nanoparticles, since water droplets represent nanoreactors where the formation of small crystallites with a narrow size distribution will be favoured.[9-12] In addition to single-phase reverse microemulsions, multiphase microemulsion- containing systems such as Winsor I (W I), Winsor II (W II), Winsor III (W III), Winsor IV (W IV) systems are known.[13] A Winsor I (W I) system consists of an o/w microemulsion which is in equilibrium with an excess oil phase, while a Winsor II (W II) system is a w/o microemulsion which is in equilibrium with an excess aqueous phase. The Winsor III (W III) system is a bicontinuous microemulsion while a macroscopically single-phase microemulsion is denoted as a Winsor IV (W IV) system.11 All of these systems maintain a certain microenvironment; the applications of W I and W II type systems in

the synthesis of "quantum dot" particles is expected to avoid the limitations that may arise due to solubility constraints as mentioned earlier. Recently, Manna et al. have synthesized dodecanethiol-capped silver and gold nanoparticles in Winsor II microemulsion.[14]

Brust et al.[15] first reported the use of a two phase method wherein the metal ions were transferred to the organic layer using a phase transfer reagent and thereafter reduced in the organic medium in the presence of suitable capping agents. This method is, however, not applicable to other common water-soluble salts of the metals (e.g. salts of silver, copper, cadmium etc.) as the transferable metal ions are not present in the form of anionic complexes. Sarathy et al.[16] have demonstrated that colloidal gold, platinum, and silver particles synthesized in aqueous media may be transferred into a hydrocarbon environment such as toluene by acid-facilitated coordination of the particles with alkanethiols present in toluene. The serious drawback of this method is the requirement of relatively large quantity of concentrated HCl. Very recently Kumar et al.[17] have synthesized octadecanethiol-capped CdS nanoparticles in a biphasic liquid-liquid system in the presence of excess (> 20 times) octadecanethiol. The system may be suitable for very low salt (10^{-4} M) concentration.

In this part I of this chapter, we demonstrate a new method for the synthesis of dodecanthiol capped-cadmium sulfide nanoparticles in Winsor II microemulsion of AOT / diethyl ether / H_2O. Sodium bis (2-ethylhexyl) sulfosuccinate, $CH_3(CH_2)_3CH(C_2H_5)CH_2O_2CCH_2CH(SO_3Na)CO_2CH_2CH(C_2H_5)(CH_2)_3CH_3$, commercially known as AOT, is a double tailed anionic surfactant. The CMC value of AOT is 0.0025M. It is known to form spherical, nanometer sized, molecular aggregates in a variety of non-polar organic solvents. The solubility and micelles forming ability of AOT are well established. We prefer AOT as an anionic surfactant due to its higher solubility in organic phase (diethyl ether). Further the anionic polar head groups help to extract metal cations from the aqueous to reverse micellar phase. The metal ions concentrated in the reverse microdroplets can be capped by dodecanthiol present in the system. The nanoparticles so prepared have been characterized by FT-IR, TEM, XPS, and UV-visible to reveal the nature of thiol-capped cadmium sulfide.

3.2 EXPERIMENTAL SECTION

3.2.1 CHEMICALS

Cadmium nitrate (Sarabhai M. Chem. Ltd., 99%), diethyl ether (Merck, 98%), sodium sulfide nonahydrate (Loba Chemie, 99%), dodecanthiol (Aldrich, 98 %), sodium bis-(2-ethylhexyl) sulfosuccinate, AOT (Sigma, 99%).

3.2.2 PARTICLE SYNTHESIS

Nanoscale dodecanthiol-capped cadmium sulfide particles were prepared using Winsor II microemulsion system. Twenty cubic centimeter of aqueous salt solution [[Cd $(NO_3)_2$] 0.04 mol dm^{-3}] and 80 mL of 0.05 mol dm^{-3} AOT solution in diethyl ether were mixed together and stirred vigorously for 30 min. Next, 90 milligrams of dodecanthiol (4.45 x 10^{-4} mol) was then added to the rapidly stirring microemulsion for 10 min and allowed to stand. Next, 20 mL of 0.04-mol dm^{-3} aqueous sodium sulfide (Na_2S. $9H_2O$) solution was slowly added to the mixture with vigorous stirring for 1 h to complete the reaction. The yellow reverse micellar phase containing the precipitate was in equilibrium with a clear aqueous phase and this aqueous phase was separated. The solvent was removed under reduced pressure with a rotary evaporator, and the resulting sample was thoroughly rinsed with ethanol to remove adsorbed AOT, excess thiols, and other reaction by-products. The particles so obtained were soluble in solvents like n-hexane, n-heptane, toluene, tetrahydrofuran, etc.

3.2.3 CHARACTERIZATION

The FT-IR spectra were recorded on a Perkin-Elmer 16PC FT-IR instrument, using KBr pellet. The sample for the transmission electron microscope (TEM unit Philips EM 301) was prepared by evaporating a drop of dilute n-hexane solution of the particles onto an amorphous carbon-coated copper TEM grid. A Perkin Elmer Lambda 3B double beam UV-vis absorption spectra of dodecanthiol-capped CdS nanoparticles dispersed in different non-polar solvents was also recorded. UV-visible spectroscopy is particularly effective in characterizing semiconductor-type nanoparticles or metal particles whose plasmon resonance lies in the visible range. UV-Vis has also been used to determine both particle size and the degree of cluster aggregation in the sample.

The X-ray photospectroscopy signals were recorded on a V. G. Scientific ESCA - 3000 spectrometer fitted with separate sample preparation chamber. All the spectra were recorded using Mg Kα radiation (1253.6 eV). The spectrometer was calibrated by determining the binding energies (BE) of Au $4f_{7/2}$ (84.0 eV), Ag $3d_{5/2}$ (368.3 eV) and Cu $2p_{3/2}$ (932.4 eV) levels using spectroscopically pure metals (M/s Johnson and Matthey). All the spectra were recorded with a pass energy of 50eV and 4mm slit. Under this condition, the line width (FWHM) for Au $f_{7/2}$ level was 1.6 eV. The vacuum in the analyzer chamber was better than 10^{-9} Torr. Elemental analysis was conducted with a C, H, N, S, O elemental analyzer (Carlo Erba Instrument, Modekl EA 1108).

3.3 RESULTS AND DISCUSSION

3.3.1 FT-IR ANALYSIS

Figure 3.1 shows a comparison of the FT-IR spectra (4000-400 cm^{-1}) for (a) the free thiol and (b) the composite nanoparticles. The band positions and their assignments are listed in Table 3.1. The figure clearly shows that all the important bands of the pure dodecanthiol (Figure 3.1a) are also seen in the composite nanoparticles (Figure 3.1b). The commonality of the features confirm the presence of thiol as an essential component of the nanoparticles. The figures also show that the band assigned to C-C twisting, wagging, and rocking vibrations in the broad region of 1200-800 cm^{-1} are much stronger in figure 1b due to an encapsulation effect. The increase in intensities of the symmetric bending vibration ($\delta_s CH_3$) at around 1379 cm^{-1} and asymmetric bending vibration ($\delta_{sa} CH_3$) at around 1462 cm^{-1} of methyl group is due to capping. The methylene asymmetric and symmetric vibrational modes occurred at 2923 and 2852 cm^{-1}, respectively and shows a slight increase in intensity that may be assigned to the capping effect.

Table 3.1: FT-IR bands for free thiol and nanoparticles.

assignment	Band position in cm^{-1}	
	Free thiol[a]	CdS nanoparticles
CH_2 anitsymmetric stretching	2925 (s)	2923 (s)
CH_2 symmetric stretching	2855 (s)	2852 (s)
CH_2 scissoring	1465 (m)	1462 (m)
CH_3 bending (U tupe)	1375 (w)	1379 (w)
CH_2 twisting, wagging, and rocking	1187 (w)	1185 (sh)
”	-	1222 (m)
”	1044 (m)	1043 (m)
”	725 (w)	723 (w)
”	620 (w)	620 (w)

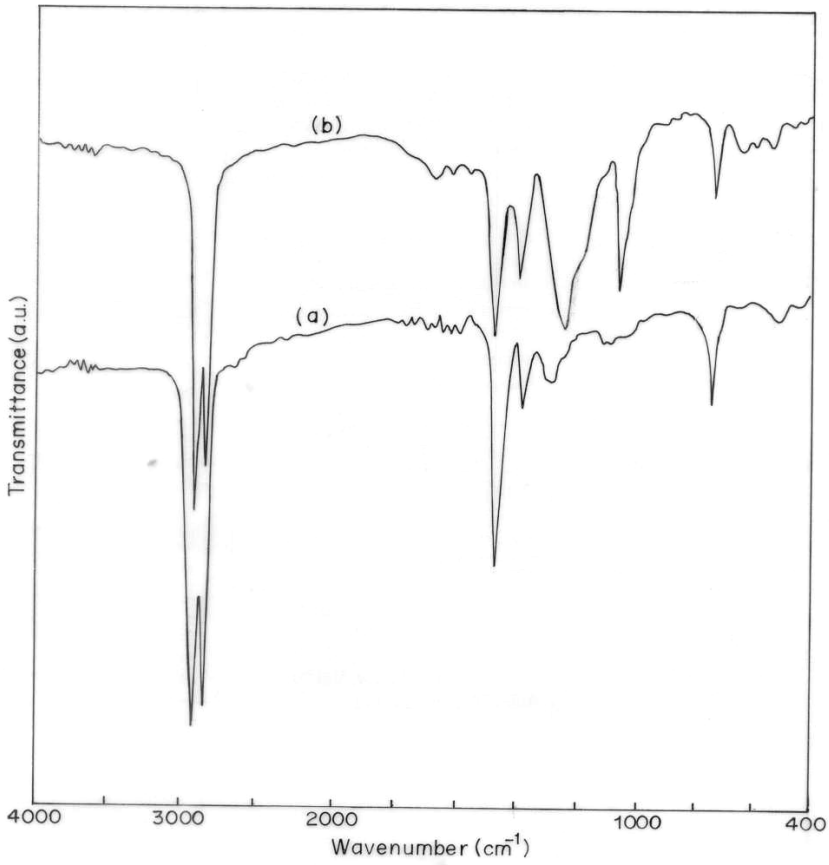

Figure 3.1: FT-IR spectra of (a) free dodecanthiol and (b) nanoparticles. KBr technique is used for recording of these spectra.

3.3.2 X-RAY PHOTOELECTRON SPECTROSCOPY

Figure 3.2 gives the survey scan of the thiol-capped CdS nanoparticles prepared in Winsor II microemulsion. C, Cd, S and O were the elements which could be detected. It can be seen from Figure 3.2 that there are no impurities present except for a small amount of oxygen. The XPS signals (Figure 3.3a and b) show the presence of principle S *2p,* and Cd *3d* core levels in the composite particles synthesized in Winsor II

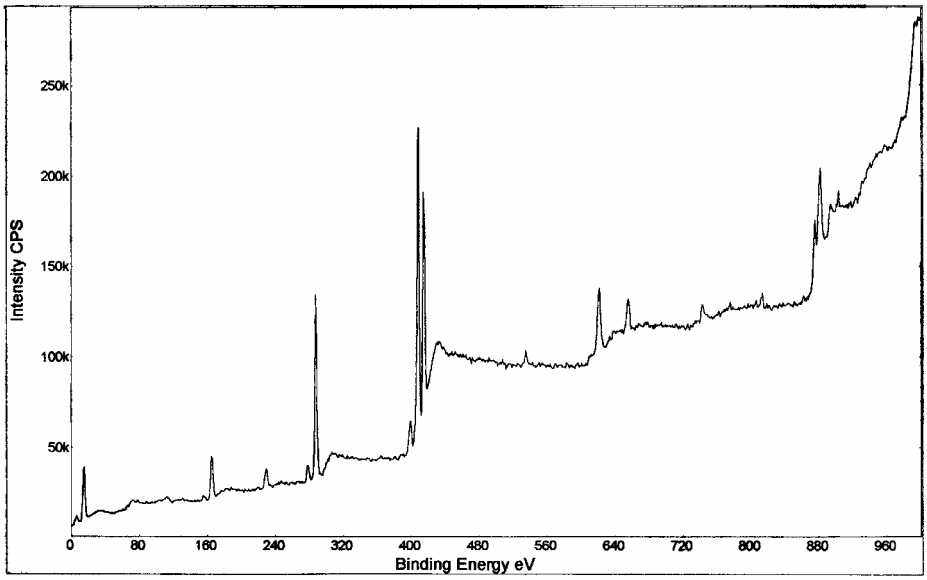

Figure 3.2: XPS survay scan of the dodecanthiol-capped CdS nanoparticles prepared in Winsor II microemulsion.

microemulsion system. The absence of XPS signal between 166 – 169 kV BE region provides evidence to the absence of the impurities (surfactant). It is clear from the high resolution spectrum of the Cd *3d* core level (Figure 3.2a) that there are two chemically distinct species in the spectrum and they have been individually fit to the *3d* spin-orbit components as shown in the figure. The Cd $3d_{5/2}$ peak at 406.1 eV and Cd $3d_{3/2}$ peak at 412.86 eV is in good agreement with the published results[19]. Figure 3.2b, over the range 158-166 eV reveals two peaks in the S *2p* core level spectrum of nanoparticle with the peak of the S $2p_{3/2}$ BEs at 162.06 and $2p_{5/2}$ at 163.67 eV. These BE values are in excellent agreement with published values for the S *2p* signal from self-assembled monolayers of alkanethiols on CdS nanoparticles[18,19]. Thus, the XPS analysis of the material is consistent with DDT-stabilized CdS nanoparticles.

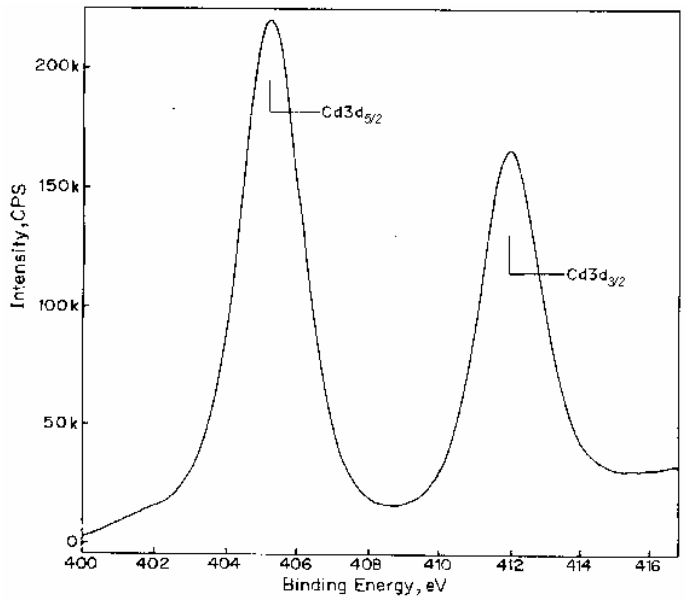

Figure 3.3 a: XPS spectra of the nanoparticles (a) showing the Cd $3d_{5/2}$ and Cd $3d_{3/2}$ doublet with binding energies of 405.1 and 412.2 eV respectively.

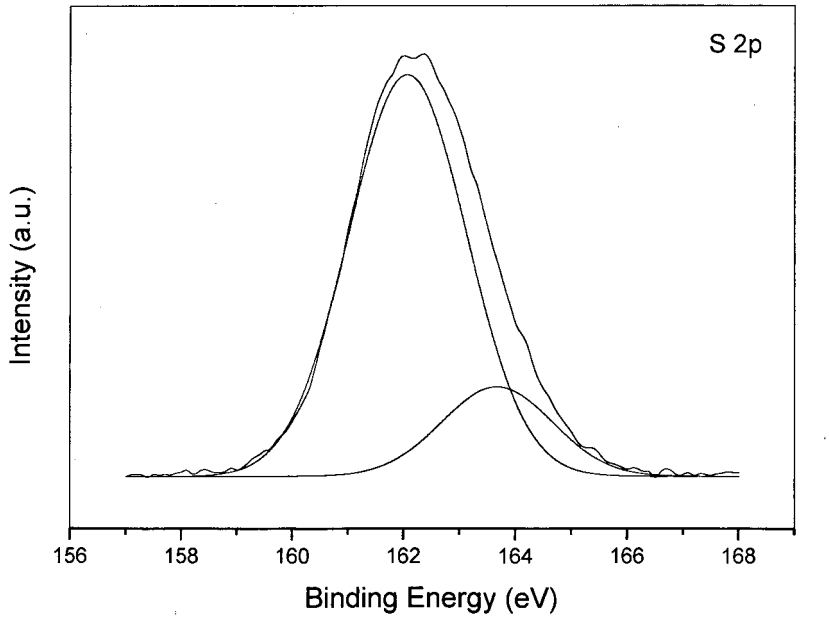

Figure 3.3b: S 2p core level spectrum recorded from the dodecanthiol-capped CdS nanoparticles prepared in Winsor II microemulsion.

3.3.3 TEM ANALYSIS

The Figure 3.4 shows the transmission electron micrograph of thiol-capped CdS particles prepared in Winsor II type microemulsion of diethyl ether / AOT/ water. It can be seen from the figure that the particles are monodispersed, almost spherical and are within 1-7 nm size range. The TEM micrograph also shows that the particles taking part in the formation of nanostructure maintain their distinct character and do not agglomerate into large clusters. Figure 3.5 shows the particle size distribution histogram for the corresponding TEM micrograph given in Figure 3.5. Histogram shows that more than 55% of particles possess a diameter of 4 nm.

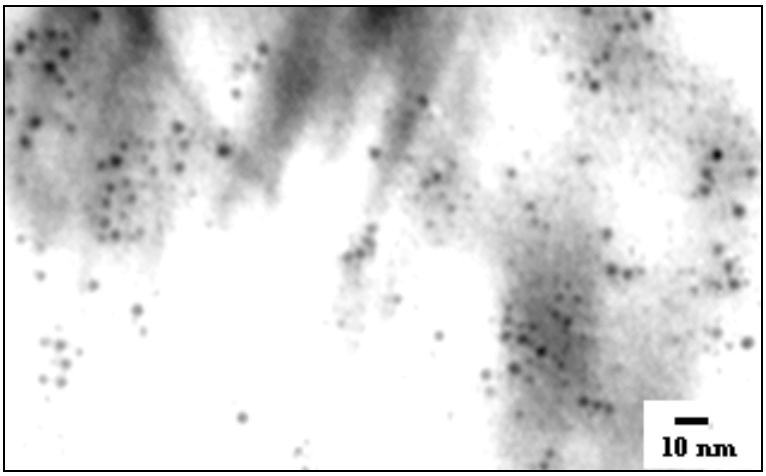

Figure 3.4: Transmission Electron Micrograph (TEM) of thiol-capped CdS nanoparticles.

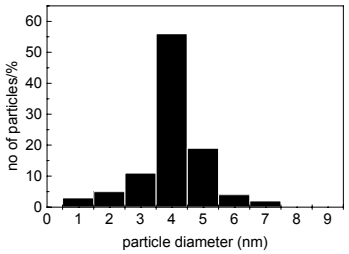

Figure 3.5: Histogram of particle size distribution corresponding to the TEM given in Figure 3.4

3.3.4 UV-VISIBLE SPECTRAL ANALYSIS

Colloidal dispersions of metals display absorption in the UV-vis region, these are caused by the excitation of plasmon resonance or interband transition and thus are characteristic properties of metals. The UV-visible spectrum of the dodecanthiol-capped CdS nanoparticles is presented in Figure 3.6. The nanoparticles are redispersed in n-hexane solvent for the measurement of optical absorption. The absorption occurs at ca. 425nm. This peak is due to the surface plasmon absorption of the CdS nanoparticles.

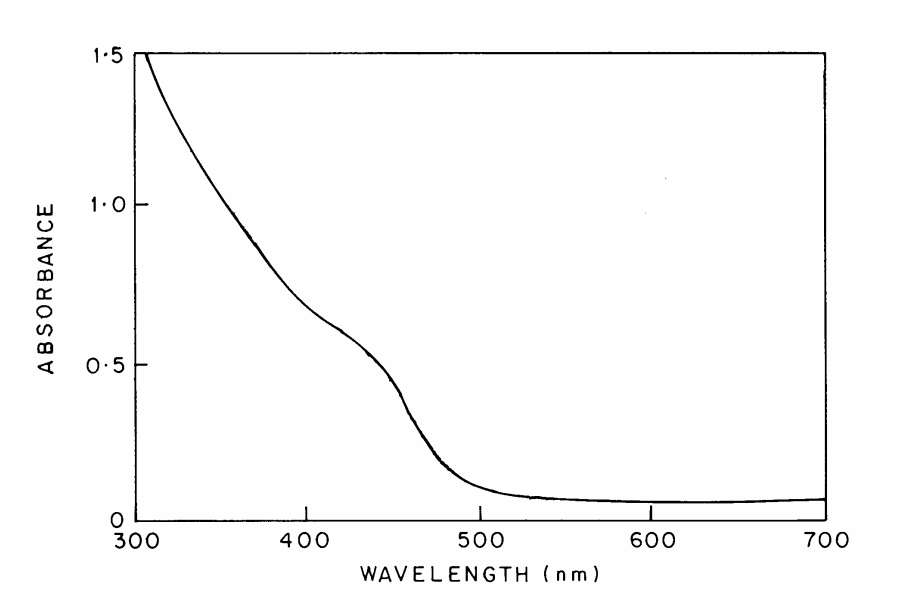

Figure 3.6: UV-vis spectrum of the thiol-capped CdS nanoparticles redispersed in the n-hexane solvent.

3.3.5 ELEMENTAL ANALYSIS

Elemental analysis of the thiol-capped cluster compound for C, H and S gave the values of 24.25, 4.44 and 16.43, respectively. The atomic percentage of C, H, S work out to be 63,44, 9.87 and 36.44. The percentages of C & H, gave the values of (considering the total atomic weight percent of carbon and hydrogen equal to 100 %) C = 84. 61 % and H = 15.38 %, that are consistent with the literature reports. Thus, atomic weight percentages of C and H found in the elemental analysis are in close agreement with the composition of dodecane chain of a thiol molecule, which supports the encapsulation. The excess atomic percentage of S present (based the theoretical value of the same in dodecanethiol) in the composite material was also calculated. We found that ~ 20.6 wt % of S is present in excess. The contribution of this excess S is from the CdS particles.

PART II

SYNTHESIS AND CHARACTERIZATION OF GOLD NANOPARTICLES IN REVERSE MICROEMULSION STABILIZED BY MERCAPTO FUNCTIONAL SILICONE FLUID

Synthesis and characterization of gold nanoparticles in a reverse microemulsion of diethyl ether / DDAB / water are described. The gold nanoparticles are stabilized with 3-mercaptopropyldimethoxysilyl end-blocked dimethyl silicone fluid (GP-506). The formation of the metal nanocomposite is evident from the similarity of the Fourier transform infrared spectrum (FTIR) of the free thiol and the composite. The UV-visible spectroscopy shows the characteristic surface plasmon absorption peak at 520 nm for Au nanoparticles. The sizes of particles have been determined from transmission electron microscopic (TEM) analysis. The evidence from X-ray photoelectron spectroscopy (XPS) investigation confirms presence of mercapto functional silicone molecules. It is observed from the experimental data that the average particle size changes as a function of the DTAB concentration.

3.4 INTRODUCTION

Recently there has been an extensive interest in the development of new methods for the synthesis of nanoparticles because of size dependant properties of particles. For example, as gas-evaporation,[20] sputtering,[21] coprecipitation,[22] sol-gel method,[23] hydrothermal,[24] microemulsion,[25-28] and so on. These nanometer-sized particles have found many applications in microelectronic devices,[29,30] photocatalysis,[31,32] electroluminance and electrocatalysis,[33] reprography,[34] sensors and molecular electronics. The morphology of the gold nanoparticles is controlled by various properties of the capping ligands.

One of the most widely studied nanoparticles, gold nanoparticles have attracted great attention due to their potential applications in biological markers,[35] DNA sensors,[36] molecular recognition system,[37] and nanoscale electronics.[38] For the preparation of gold nanoparticles with small sizes, narrow size distributions, and long-term stability, various stabilizers such as low molecular weight (MW) surfactants and various polymers have been used.[39-47] These materials are essentially classified as "nanoreactors", which allows for control of several parameters for nanoparticle synthesis.

Many synthesis routes have been developed for the preparation of thiol derivatized gold/ nanoparticles. Brust et al.[15] have developed thiol-derivatized gold nanoparticles in biphasic medium. Duff et al.[48] have synthesized new hydrosols of gold clusters. Badia et al.[49] have studied the properties of the gold nanoparticles which are prepared in the presence of thiols. Recently, Green et al.[50] have synthesized organically capped gold nanoparticles.

The synthesis of nanoparticles using microemulsions may be classified into two types. The first is a single microemulsion type in which nanoparticles are produced in a microemulsion by adding a reducing or precipitating agent, in the form of gas or liquid, to a microemulsion containing the primary reactant dissolved in its aqueous droplets. The particles produced by this type of process could be much bigger than the original droplet size. The second is the double or multiple microemulsion type, in which two or more water-in-oil microemulsions each containing respective reactants are mixed together. The droplets of the mixed microemulsion go through numerous collisions and thereby the reactants are mixed and react to form solid particles as a product of the chemical reaction.

Experimental data indicate that the particles formed by this type are generally smaller than the original droplets.

When two microemulsions each containing respective reactants are mixed, the contents of the aqueous droplets are mixed and redistributed very rapidly because of the collisions that involve temporary merging of the droplets into a larger droplet (fusion) and subsequent breakup of this larger droplet (fission). It was found that the mass exchange between the droplets can be extremely fast and consequently, the mass exchange is limited by the collision of the droplets. For a first approximation, we may assume that once two droplets are merged through a collision, the contents of the two droplets are mixed rapidly and thoroughly before breakup into two droplets of identical size.

Although synthesis of nanodimensional colloids in biphasic system was known earlier, the problems such as their stability and precise control of reactivity have been tackled only recently using different methodologies. Size control is often sought either through the appropriate protecting agents, such as gelatinus albumins, other peptides and macromolecules, such as polyethylene imine or polyvinylimidazole, on the surface of the cluster or to one another without leading to coalescence which results into the loss of their size-induced electronic properties.

We now report here the use of two reverse microemulsions of diethyl ether / DDAB / water one containing salt of gold and poly (siloxane) containing terminal thiol groups (GP-506, Figure) and another containing sodium borohydride. GP-506 is a 3-mercaptopropyldimethoxysilyl end-blocked dimethyl silicone fluid (Figure 3.7). The molecular weight of the silicone fluid is 3700 (calculated). It is soluble in aliphatic solvents. Thiol content is 1.75% by weight thiol (SH) (calculated).

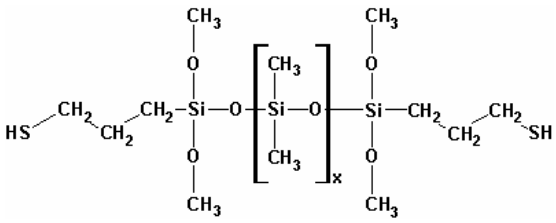

Figure 3.7: 3-mercaptopropyldimethoxysilyl end-blocked dimethyl silicone fluid (GP-506). Where x = 46.

The metal ions concentrated in the dynamic reverse micellar phase were reduced with sodium borohydride and consequently stabilised by mercapto functional silicone fluid. It is observed from experimental results that by changing the DDAB: DTAB molar ratio in the reverse microemulsions, it is possible to change the nanoparticle size distribution.

3.5 EXPERIMENTAL SECTION

3.5.1 CHEMICALS

Potassium tetrachloroaurate (III) ($KAuCl_4$, 99.999%, Aldrich), Didodecyldimethylammonium bromide (DDAB, 98%, Aldrich), 3-mercaptopropyldimethoxysilyl end-blocked dimethyl silicone fluid (Genesee Polymers Corporation), sodium borohydride (99%, Aldrich), diethyl ether (Loba Chemie) and ethanol (BDH, 99.7-100%).

3.5.2 PARTICLE SYNTHESIS

The preparation of gold nanoparticles was achieved by mixing equal volumes of two w/o microemulsion solutions one containing an aqueous solution of the metal salts (M I) and the other containing an aqueous solution of sodium borohydride (M II).

Microemulsion I (M I): Thirty milliliter 0.01 M solution of DDAB in diethyl ether is prepared. To this solution 0.1M 60mg aqueous solution of gold is added. This forms a clear reverse microemulsion. Then 60mg mercapto functional silicone fluid olegomer is added.

Microemulsion II (M II): Thirty milliliter 0.01 M solution of DDAB in diethyl ether is prepared. To this solution 100mg of 0.2M aqueous solution of sodium borohydride is added. Finally, M II reverse microemulsions is added to the above M I microemulsion slowly under stirring and stirring was continued for 2 h. The mixture turned dark red-brown immediately. All the gold nanoparticles were prepared using the same procedure except by varying the DDAB concentration.

3.5.3 CHARACTERIZATION

The FT-IR spectra were recorded on a Perkin-Elmer 16PC FT-IR instrument, using KBr pellet. The sample for the transmission electron microscope (TEM unit Philips EM 301) was prepared by evaporating a drop of dilute n-hexane solution of the particles onto an amorphous carbon-coated copper TEM grid. A Perkin Elmer Lambda 3B double beam

UV-vis absorption spectra of gold nanoparticles dispersed in n-hexane solvent was also recorded. UV-visible spectroscopy is particularly effective in characterizing semiconductor-type nanoparticles or metal particles whose plasmon resonance lies in the visible range. UV-Vis has also been used to determine both particle size and the degree of cluster aggregation in the sample. The X-ray photospectroscopy signals were recorded on a V. G. Scientific ESCA - 3000 spectrometer fitted with separate sample preparation chamber. All the spectra were recorded using Mg Kα radiation (1253.6 eV). The spectrometer was calibrated by determining the binding energies (BE) of Au $4f_{7/2}$ (84.0 eV), Ag $3d_{5/2}$ (368.3 eV) and Cu $2p_{3/2}$ (932.4 eV) levels using spectroscopically pure metals (M/s Johnson and Matthey). All the spectra were recorded with a pass energy of 50eV and 4mm slit. Under this condition, the line width (FWHM) for Au $f_{7/2}$ level was 1.6 eV. The vacuum in the analyzer chamber was better than 10^{-9} Torr. Elemental analysis was conducted with a C, H, N, S, O elemental analyzer (Carlo Erba Instrument, Modekl EA 1108).

3.6 RESULTS AND DISCUSSIONS

3.6.1 FT-IR ANALYSIS

Figure 3.8 shows a comparison of the IR spectra (4000-400 cm -1) for (a) the free mercapto functional silicon fluid, and (b) the composite nanoparticles. Both IR spectra are similar, which confirms that mercapto functional silicone fluid is an essential component of composite nanoparticles.

3.6.2 UV-VISIBLE SPECTROSCOPY ANALYSIS

It is known that optically, both intensity and energy of the surface plasmon (SP) resonance bands of nanoparticles are strongly dependent on size. We have carried out the UV-visible measurement of nanoparticles synthesized at different concentration of surfactant. Figure 3.9 shows UV-visible spectra of the gold nanoparticles stabilized by mercapto functional silicone fluid. The well-defined surface-plasmon band is observed at 520 nm. This absorption is characteristic for gold nanocrystals in a size regime below 10 nm and are due to a localized surface plasmon oscillation.[33] It can be seen from figure 3.9

that there is no shift in energy but there is difference in intensity of the surface-plasmon bands, which indicate that the difference in core size of nanoparticles.

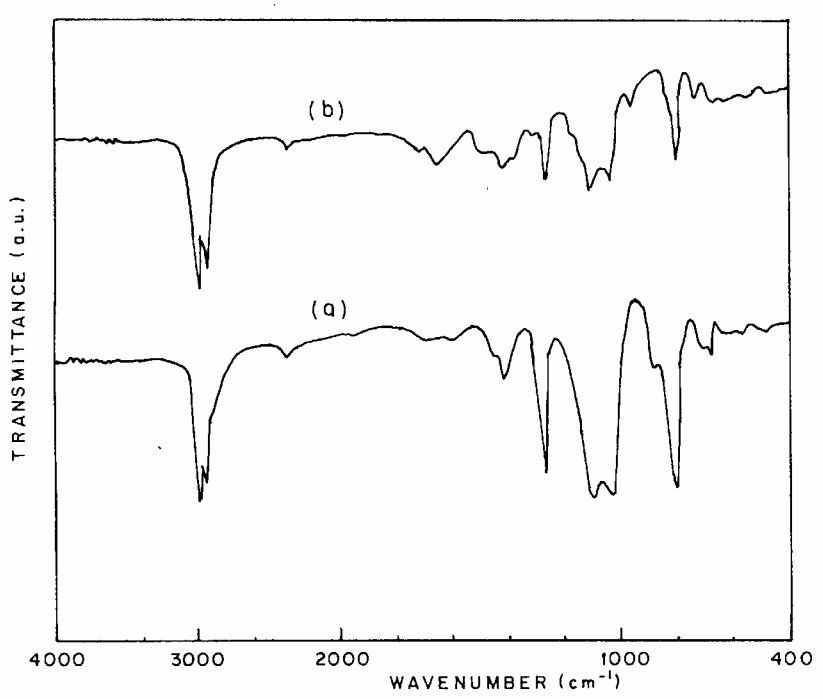

Figure 3.8: Comparison of IR spectra of (a) pure mercapto functional silicone fluid and (b) gold composite particles.

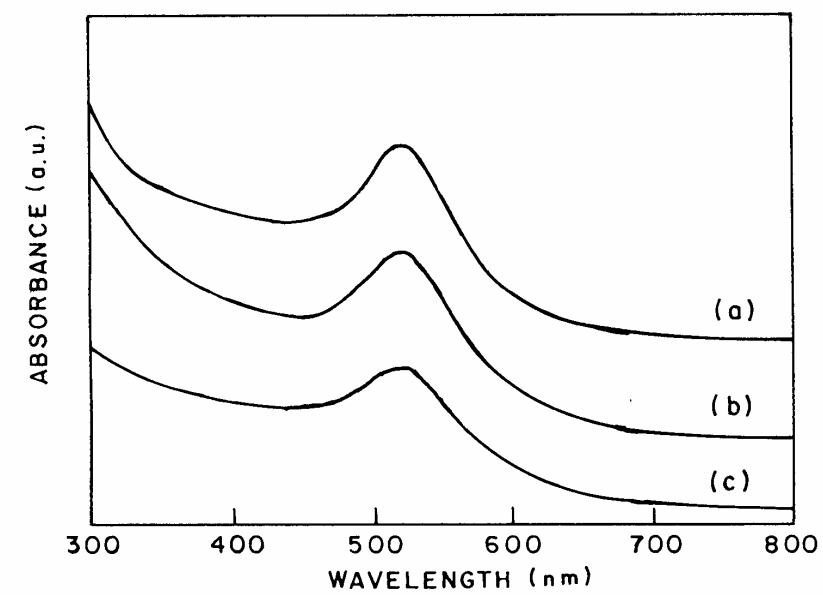

Figure 3.9: UV-visible spectra of the gold nanoparticles prepared in reverse microemulsion and stabilized by GP-506. The ratio of DDAB : DTAB are (a) 1:0; (b) 1:1; and (c) 2:1.

3.6.3 X-Ray Photoelectron Spectroscopy

X-ray photoelectron spectroscopic studies of the Au nanoparticles stabilized by mercapto functional silicone fluid prepared in reverse microemulsion confirms the presence of C, Au, S, Si and O in the composite particles.

3.6.4 TEM ANALYSIS

The size of nanoparticles prepared using reverse microemulsion in presence of mercapto functional silicone fluid at different concentrations was examined by TEM. Figure 3.10 shows the typical bright field photographs. The photographs shows that all of the particles are almost spherical. The photographs also shows that the mercapto functional stabilized particles taking part in the formation of nanoscale structure maintain less aggregation of metal cores into flocs. It can be seen from these micrographs that the particles synthesized at different concentrations of DDAB show the different sizes and morphologies.

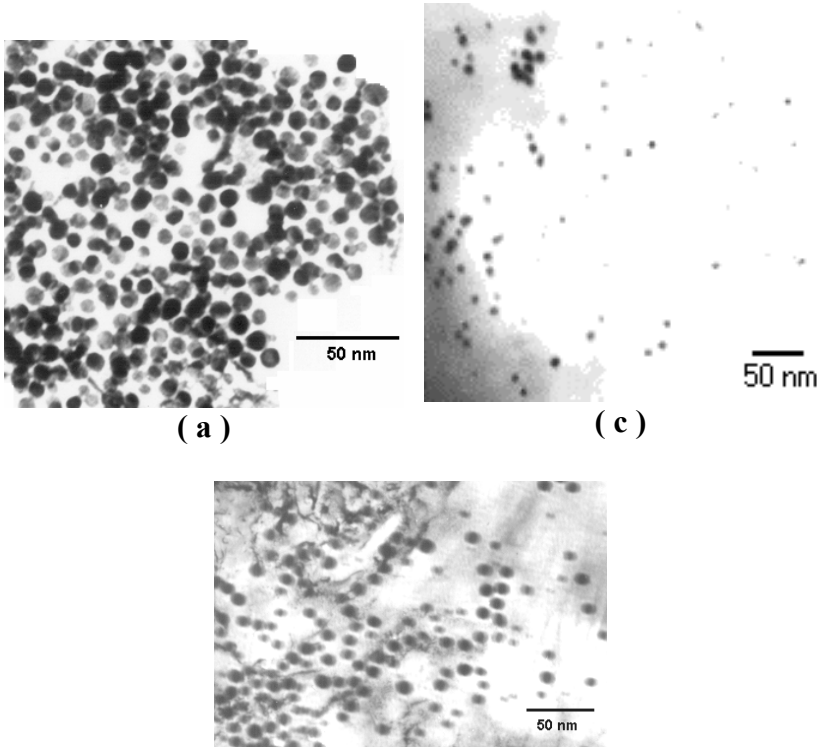

(a) **(c)**

(b)

Figure 3.10: Transmission electron micrographs of gold nanoparticles stabilized by mercapto functional silicone fluid by varying the surfactant mole ratio of DDAB : DTAB, (a) 1:0 (b) 2:1and (c) 1:2. The average particle sizes for a, b, and c are 8, 10 and 6nm receptively.

PART III

SYNTHESIS OF THIOL-CAPPED GOLD NANOPARTICLES IN MICROEMULSIONS

Synthesis and characterization of thiol-capped gold nanoparticles in a novel Winsor II type microemulsion of diethyl ether / DDAB / water are described. The dual role of cationic surfactant(s) has been found for the formation of microemulsion as well as extraction of oppositely charged tetrachloroaurate ions from aqueous to the organic reverse micellar phase. The formation of the metal nanocomposite is evident from the similarity of the Fourier transform infrared spectrum (FTIR) of the free thiol and the composite. The formation and size of particles have been determined from UV-visible plasmon absorption spectroscopic and transmission electron microscopic (TEM) analysis, respectively. The evidence from X-ray photoelectron spectroscopy (XPS) investigation confirms the metallic state of gold (Au^0) and the encapsulation by the thiol molecules. It is observed from the experimental data that the average particle size changes (4 nm to 9 nm) by varying the DDAB: DTAB molar ratio (1:0 to 1:2).

3.7 INTRODUCTION

The reverse microemulsions have been quite successfully used for producing colloidal nanoparticles of both polymers and inorganic materials. In the part II we have successfully reported the reverse microemulsion technique for the preparation of gold nanoparticles stabilized by mercapto functional silicone fluid. Reverse microemulsion, however have the probleam of limited solubilization of metal salt and reducing agent. These limitations can be overcome by applying the Winsor II type of microemulsions for the preparation of nanoparticles as it can solubilize more amount of metal salt and hence can use it for large-scale synthesis of metal, metal oxide and semiconductor nanoparticles. Also these systems can be regarded as an alternative to two-phase reaction media. In this part we demonstrate the successful application of the Winsor II microemulsion for the synthesis of gold nanoparticles.

Winsor II type microemulsion of diethyl ether / DDAB-DTAB / water was for the synthesis. We prefer DDAB and DTAB as surfactants because they form stable W II microemulsion with gold salts. Also their cationic head groups which help to form complex with metal anion present in aqueous phase and extract it to reverse micellar organic phase. The metal ions concentrated in the dynamic reverse micellar phase were reduced with sodium borohydride and consequently capped by dodecanthiol, which is already present in the organic reverse micellar phase. It is observed from experimental results that by changing the DDAB: DTAB molar ratio in the W II microemulsion, it is possible to modify the nanoparticle size distribution.

3.8 EXPERIMENTAL SECTION

3.8.1 MATERIALS

Potassium tetrachloroaurate (III) ($KAuCl_4$, 99.999%, Aldrich), Didodecyldimethylammonium bromide (DDAB, 98%, Aldrich), 1-dodecanthiol (DDT, 98%, Aldrich), sodium borohydride (99%, Aldrich), diethyl ether (Loba Chemie) and ethanol (BDH, 99.7-100%).

3.8.2 PREPARATION OF AU NANOPARTICLES

Twenty cubic centimeter of aqueous salt solution of potassium tetrachloro aurate (KAuCl4) 0.02 mol dm^{-3}] and 80 mL of 0.02 mol dm^{-3} DDAB solution along with 0.00, 0.002, 0.006 mol dm^{-3} DTAB in diethyl ether were mixed together and stirred vigorously for twenty minutes. It was allowed to separate into two distinct phases for 5-10 min, resulting in a quantitative transfer bright red colored [Au $(Cl_4)]^-$ ions from aqueous to reverse microemulsion phase. 110 mg of dodecanthiol was then added to the rapidly stirring microemulsion for 5 min. Next, 0.2 mol dm^{-3} of 20 mL of freshly prepared $NaBH_4$ aqueous solution was slowly added to the reaction mixture with vigorous stirring; stirring was continued for 2h to complete the reaction, and two phase separation was observed to follow. The dark brown / black reverse micellar phase containing a large quantity of precipitate was in equilibrium with a clear aqueous phase and this aqueous phase is separated. The solvent was then removed under reduced pressure with a rotary evaporator, and the resulting sample were thoroughly rinsed with ethanol and acetone to remove DDAB and DTAB adsorbed on the surface of the particles and also excessive thiols and other reaction byproducts. The particle appeared to be stable and very soluble in non-polar solvents (e.g. n-hexane, n-heptane, toluene, chloroform, benzene etc.) but seems to be insoluble in polar solvents (e.g. alcohols and acetone).

3.8.3 CHARACTERIZATION TECHNIQUES

FT-IR spectra were recorded on a Perkin-Elmer 16PC FT-IR instrument, using KBr pellet. The TEM analysis was performed with a transmission electron microscope (TEM unit Philips EM 301) for which the sample was prepared by evaporating a drop of dilute n-hexane solution of the particles onto an amorphous carbon coated copper TEM grid. The normal incidence selected area electron diffraction pattern was obtained using the Philips EM 301 transmission electron microscope.

A Perkin Elmer Lambda 3B double beam UV-vis absorption of dodecanthiol-capped Au nanoparticles dispersed in different non-polar solvents. The X-ray photospectroscopy signals were recorded on a VG scientific ESCA-3 - MK - II spectrometer fitted with separate sample preparation chamber. All the spectra were recorded using Mg K_α radiation (1253.6 eV). The spectrometer was calibrated by

determining the binding energies (BE) of Au 4f 7/2 (84.0 eV), Ag 3d5/2 (368.3 eV) and Cu 2p3/2 (932.4 eV) levels using spectrscopically pure metals (M/s Johnson and Matthey). The thermal stability of the nanoparticles were investigated by thermogravimetric (TG) and differential thermal analysis (DTA) (Sieco SH, SSC5100, instrument) at a heating rate of 10^{o}C min under nitrogen atmosphere. The sample used for the analysis of FT-IR, XPS, and elemental analysis was prepared with 0.02 molar salt concentration.

3.9 RESULTS AND DISCUSSION

3.9.1 FT-IR SPECTROSCOPY

FT-IR spectra of the free thiol and nanoparticles were shown in Figure 3.11 a and b respectively. A comparison of both spectra shows that all the characteristic bands of pure thiol are present in the gold particles. The similarity of the spectra shows that the thiol is indeed part of the composite. A band assigned by C-C stretching vibrations in the broad region of 1200-800 cm^{-1} is stronger compared to free thiol, this indicates the formation of Au-S bond (encapsulation effect). The asymmetric (γ_{as} CH_2) and symmetric (γ_s CH_2) stretching of the methylene groups observed at 2924 and 2853 cm^{-1}, respectively. The intensities of the symmetric (δ_s CH_3) and asymmetric (δ_{as} CH_3) bending vibrations of the methyl group occur at 1377 and 1466 cm^{-1}, respectively and are found to increase due to capping effect. The C-S stretching vibration occurs in the region 700- 600 cm^{-1} in both the spectra.

3.9.2 UV-VISIBLE SPECTROSCOPY

It is known that optically, both intensity and energy of the surface plasmon (SP) resonance bands of nanoparticles are strongly dependent on size[51]. We have carried out the UV-visible measurement of nanoparticles synthesized at different concentration of surfactant. Figure 3.12 shows UV-visible spectra of the dodecanthiol-capped gold nanoparticles. The well-defined surface-plasmon band is observed at 520 nm, which is in well agreement with the data published for gold nanoparticles in the literature. It can be seen from figure 3.12 that there is no shift in energy but there is difference in intensity of the surface-plasmon bands, which indicate that the difference in core size of nanoparticles.

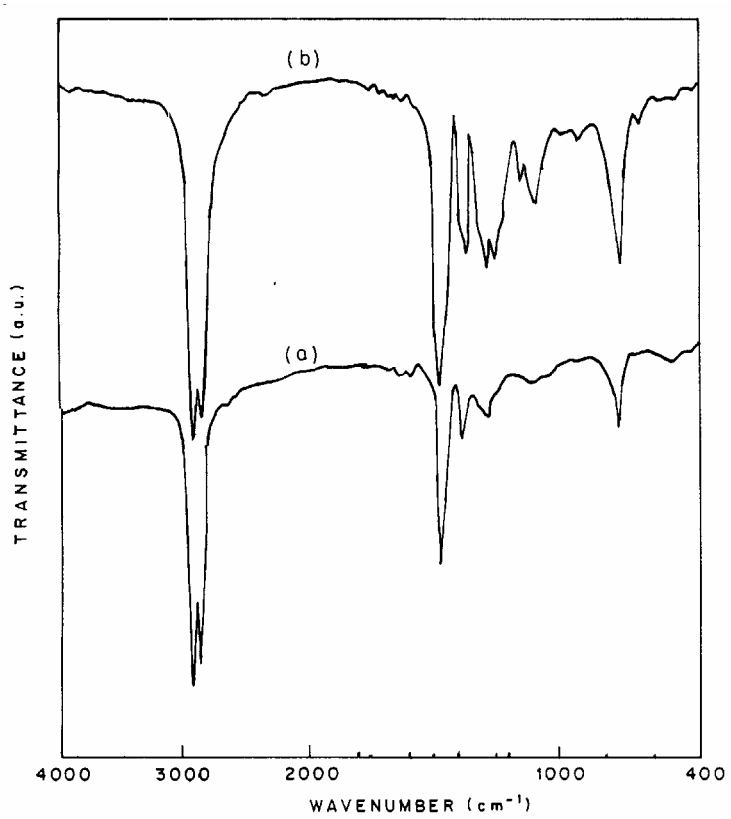

Figure 3.11: Comparison of the IR spectra of the (a) free thiol and (b) composite nanoparticles.

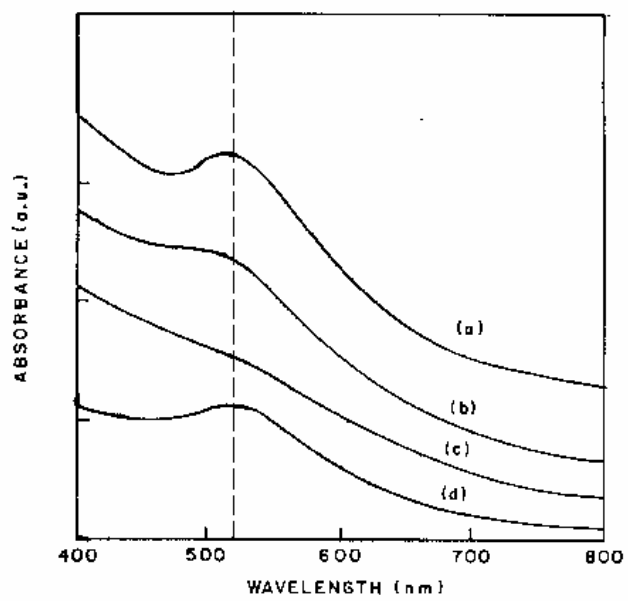

Figure 3.12 : UV-visible spectrum of the thiol-capped gold nanoparticles synthesized in Winsor II microemulsion of diethyl ether / DDAB / water. The ratio of DDAB : DTAB are (a) no DTAB; (b) 1:1; (c) 2:1; and (d) 1:2.

3.9.3 X-RAY PHOTOELECTRON SPECTROSCOPY

Figure 3.13a gives the survey scan of the thiol-capped gold nanoparticles prepared in Winsor II microemulsion of diethyl ether / DDAB / water. C, Au, S and O were the elements which could be detected. It can be seen from XPS results that the resolution

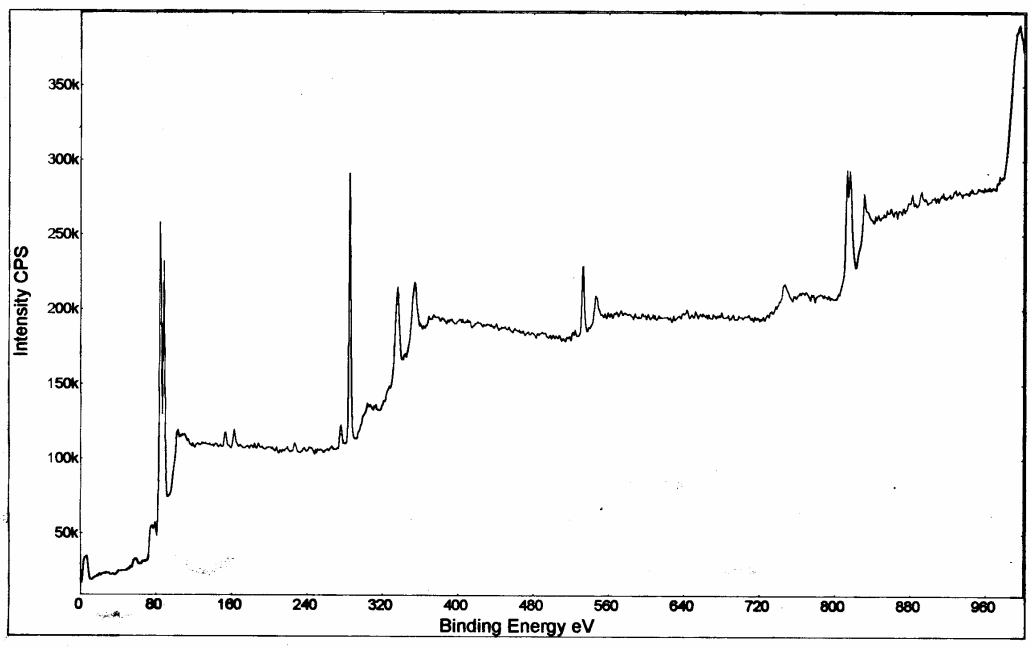

Figure 3.13a: XPS survay scan of the dodecanthiol-capped gold nanoparticles prepared in reverse microemulsion.

scan over the range 80- 94 eV (Figure 3.13b) reveals a doublet of the Au $4f_{7/2}$ peak at 83.9 eV and the Au $4f_{5/2}$ peak at 87.6eV corresponding a peak separation of 3.7 eV which is a characteristic of the Au^0. A peak at 163.1eV (Figure 3.13c) due to S (2p) showing that the thiol molecules were chemisorbed on the surface of the gold particles. The absence of a peak at 84.9 eV which is due to Au^I indicate that the gold atoms in the clusters must be present largely as Au^0.

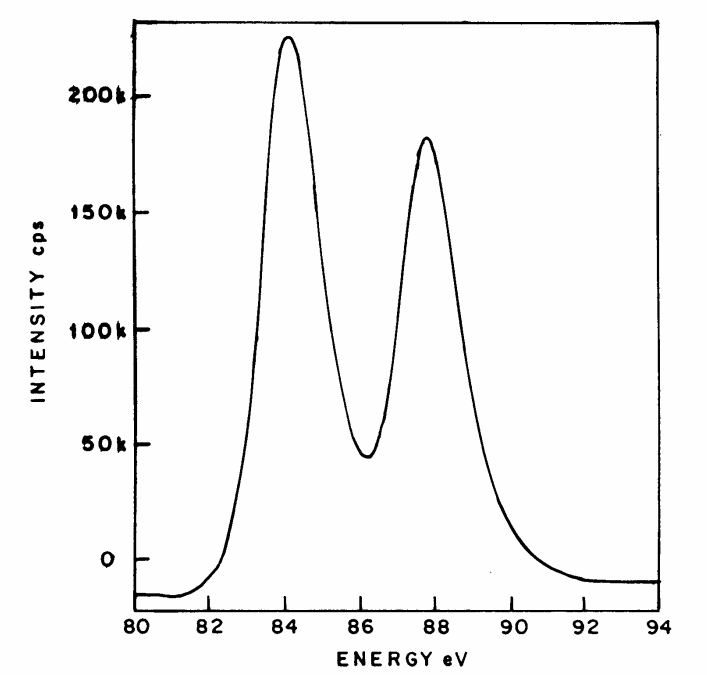

Figure 3.13b: XPS spectrum of the nanoparticles showing the Au $4f_{7/2}$ and $4F_{5/2}$ doublet with binding energies of 83.9 and 87.6eV respectively. These are typical values for Au^0.

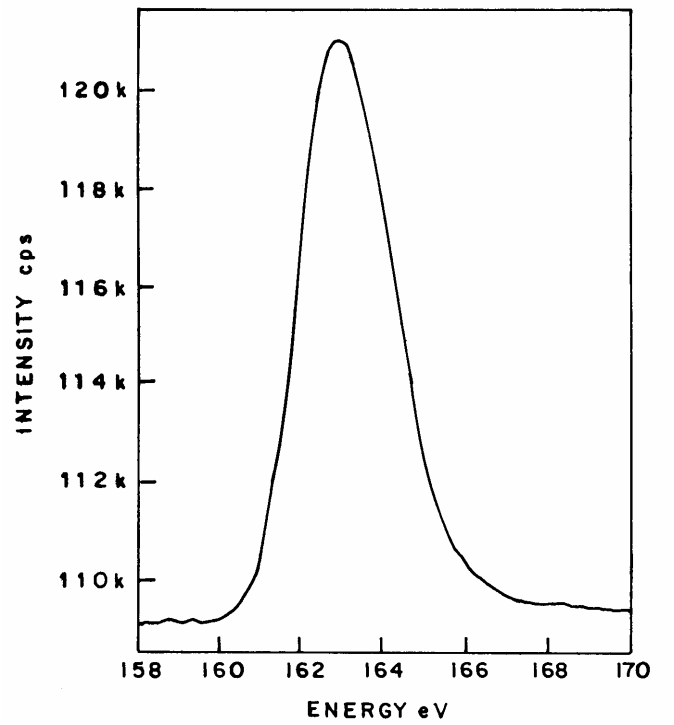

Figure 3.13c: S 2p core level spectrum recorded from the dodecanthiol-capped gold nanoparticles prepared in Winsor II microemulsion.

The size of the gold nanoparticles prepared in Winsor II microemulsion were examined by the transmission electron micrographs (TEM). The TEM photographs are shown in Figure 3.14. The particles are quite small and in the size range of 1-10 nm. The average particle size (~4 to 8 nm) changes by varying the molar ratio of DDAB and DTAB surfactants.

The high resolution TEM Figure 3.14 (a) inset shows the crystalline nature of the gold cores by the appearance of lattice fringes.

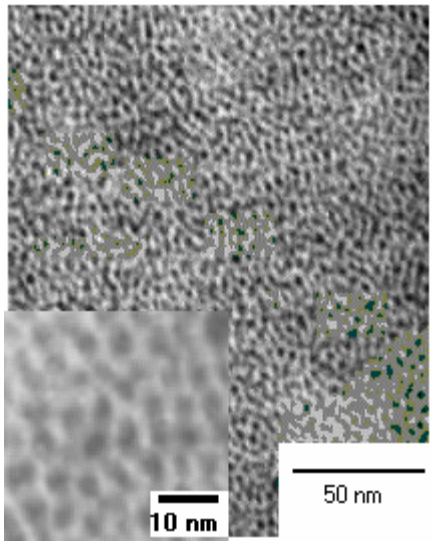

(a)

(b)

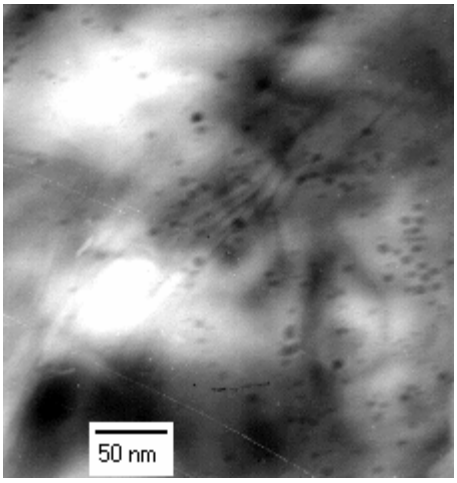

(c)

Figure 3.14: Transmission electron micrographs of thiol-capped nanoparticles prepared in Winsor II microemulsions by varying molar ratio of DDAB: DTAB (a) 1:0 (b) 2:1 and (c) 1:2. Average partcle sizes for a, b and c are 4, 8 and 6 respectively.

3.10 CONCLUSION

In conclusion, the synthesis of stable dodecanthiol-capped cadmium sulfide nanoparticles of an average particle size of ~4 nm, using Winsor II microemulsion have been carried out successfully. The dual role of anionic surfactant viz. the formation of microemulsion and facilitating the extraction of oppositely charged ions from aqueous to the organic reverse micellar phase has been successfully used for the synthesis of dodecanthiol-capped Cadmium Sulfide (CdS) nanoparticles in a Winsor II type microemulsion. UV-vis spectroscopy shows the surface-plasmon band at ca. 425 nm. FT-IR and XPS results confirm that the yellow powder product is the dodecanthiol-capped cadmium sulfide cluster.

Reverse microemulsions have been successfully used for the synthesis of gold nanoparticles stabilized by mercapto functional silicone fluid (GP-506). In this method it is observed that by adjusting the molar ratio of surfactants one can control the growth of nanoparticles. We have also successfully synthesized stable dodecanthiol-capped nanoparticles of an average particle size 4 nm, using Winsor II type microemulsion, and demonstrate the dual role of the cationic surfactants in the formation of microemulsion and extraction of oppositely charged metal ions from aqueous to organic phase. By varying the concentration of DTAB surfactant in the mixed micelles one can control the particle size of the gold nanoparticles. UV-vis spectroscopy shows the well-defined surface-plasmon band at 520 nm. FT-IR and XPS results confirms that the dark brown / black powder product is the dodecanthiol-capped metallic gold clusters. TEM shows the monodisperse particles having the average diameters varying from 4 nm to 8nm by changing the molar composition of two surfactants.

3.11 REFERENCES

1. Schmid, G. *Chem. Rev*. **92** (1992) 1709.
2. Colvin, V. L.; Schlamp, M. C.; Alivisatos, A. P. *Nature*, **370** (1994) 354.
3. Shim, M. and Guyot-Sionnest, P. *Nature*, 407 (2000) 981.
4. Beydoun, D.; Amal, R.; Low, G.; McEvoy S. *J. Nanopart. Res.* **1** (1999**)**, 439.
5. Thurston, T.R. and Wilcoxin, J. P. *J Phys Chem B* **103** (1999) 11.
6. Mattoussi, H.; Radzilowski, L.H.; Dabbousi, B.O.; Thomas, E.L.; Bawendi, M.G. and Rubner, M.F. *J. Appl. Phys.* **83** (1998) 7965.
7. Hamilton, J. F.; Baetzold, R. C. *Science* **205** (1979) 1213.
8. Ko-no, K., , In: Esumi, K., Veno, M. (Eds.). Structure-Performance Relationship in Surfactant, S. S. Series, 70. 1997, Marcel Dekker, New York.
9. Pileni, M.P. *Langmuir*, **13** (1997) 3266.
10. Sato, H., Hirai, T., Komasawa, I., *Ind. Eng. Chem. Res*. **34** (1995) 2493.
11. Petit, C., Jain, T.K., Billoudet, F., Pileni, M.P.,*Langmuir*, **10** (1994) 4446.
12. Tanori, J., Duxin, N., Petit, C., Veillet, P., Pileni, M.P., *Colloid. Polym. Sci.* **273** (1995) 886.
13. Lattes, A.; Rico, I.; de Savignac, A.; Samii, A. *Tetrahedron*, **43** (1987) 1725.
14. Manna, A.; Kulkarni, B. D.; Bandyopadhyay, K. and Vijayamohanan, K. *Chem. Mater.* **9** (1997) 3032.
15. (a) Brust, M.; Walker, M.; Bethell, D.; Schiffrin, D. J.; Whyman, R. J. *J. Chem. Soc., Chem. Comm*. 1994, 801. (b) Brust M.; Bethell, D.; Schiffrin, D. J.; Kiely, C. J. *Adv. Mater*. **7** (1995) 795.
16. Sarathy, K. V.; Thomas, P. J.; Kulkarni, G. U.; Rao, C.N.R. *Journal of Physical Chemistry B,* **103** (1999) 3399.
17. Kumar, A.; Mandale, A. B. and Sastry, M. *Langmuir* **16** (2000) 9299.
18. Terrill, R. H.; et al. *J. Am. Chem. Soc.* **117** (1995) 12537.
19. Kundu, A.; Khosravi, A. A.; Kulkarni, S. K. and Singh, P. *J. Mater. Sci.* **32** (1997) 245.
20. (a) Siegel, R. W. *J. Mater. Res.* **3** (1998) 1367. (b) Uyeda, R. *J.Cryst. Growth* **24** (1974) 69.
21. Fayet, P.; Woste, L. *Z. Phys. D* **3** (1986) 177.

22. Tang, Z. X.; Sorensen, C. M.; Klabunde, K. J.; Hadjipanayis, G. C. *J. Colloid Interface Sci.* **146** *(*1991) 38.
23. Fegley, B., Jr.; White, P.; Bowen, H. K. *Am. Ceram. Soc. Bull.* **64** (1985) 1115.
24. Komarneni, S.; Roy, R.; Breval, E.; Ollinen, M.; Suwa, Y. *Adv. Ceram. Mater.* **1** (1986) 87.
25. Osseo-Asare, K.; Arriagada, F. J. *Ceram. Trans.* **12** (1990) 3.
26. Pileni, M. P. *J. Phys. Chem.* **97** (1993) 6961.
27. (a) Fendler, J. H. *Chem. Rev.* **87** (1987) 877. (b) Henglein, A. *Chem. Rev.* **89** (1989) 1861.
28. Pillai, V.; Kumar, P.; Hou, M. J.; Ayyub, P.; Shah, D. O. *Adv.Colloid Interface Sci.* **55** *(*1995) 241.
29. Colvin, V. L.; Schlamp, M. C.; Alivisatos, A. P. *Nature*, **370** (1994) 354.
30. Shim, M. and Guyot-Sionnest, P. *Nature*, **407** (2000) 981.
31. Beydoun, D.; Amal, R.; Low, G.; McEvoy S. *J. Nanopart. Res.* **1** (1999) 439.
32. Thurston, T.R. and Wilcoxin, J. P. *J Phys Chem B* **103** (1999) 11.
33. Mattoussi, H.; Radzilowski, L.H.; Dabbousi, B.O.; Thomas, E.L.; Bawendi, M.G. and Rubner, M.F. *J. Appl. Phys.* **83** (1998) 7965.
34. Hamilton, J. F.; Baetzold, R. C. *Science* **205** (1979) 1213.
35. Slot, J. W.; Geuze, H. J.; Cell. Biol. **90** (1981) 533.
36. Elghanian, R; Storhoff, J. J.; Mucic, R. C.; Letsinger, R. L.; Mirkin, C. A. Science **277** (1997) 1078.
37. Liu, J.; Xu, R.; Kaifer, A. E. Langmuir **14** (1998) 7337.
38. Sato, T.; Ahmed, H.; Brown, D.; Johnson, B. F. G. J. Appl. Phys. **82** (1997) 696.
39. *Nanoparticles and Nanostructured Films*; Fendler, J. H., Ed.; Wiley-VCH: Weinheim, 1998.
40. Leff, D. V.; Brandt, L.; Heath, J. R. *Langmuir* **12** (1996) 4723.
41. Weisbecker, C. S.; Merritt, M. V.; Whitesides, G. M. *Langmuir* **12** (1996) 3763.
42. Mayer, A. B. R.; Mark, J. E. *J. Macromol. Sci., Pure Appl. Chem.* **A34** (1997) 2151.
43. Garcia, M. E.; Baker, L. A.; Crooks, R. M. *Anal. Chem*. **71** (1999) 256.
44. Esumi, K.; Suzuki, A.; Yamahira, A.; Torigoe, K. *Langmuir* **16** (2000) 2604.

45. Mo¨ssmer, S.; Spatz, J. S.; Mo¨ller, M.; Aberle, T.; Schmidt, J.; Burchard, W. *Macromolecules* **33** *(*2000) 4791.
46. Spatz, J. P.; Mo¨ssmer, S.; Hartmann, C.; Mo¨ller, M. *Langmuir* **16** (2000) 407.
47. Tuzar, Z.; Kratochvil, P. *Surface and Colloid Science*; Plenum Press: New York, 1993; Volume 15. (b) *Colloid-Polymer Interactions*; Farinato, R. S., Dubin, P. L., Eds.; Wiley & Sons: New York, 1999.
48. Duff, D. G. Baiker A. and Edwards, P. P. *J. Chem. Soc., Chem. Comm.* 1993, 96-98.
49. Badia, A. Cuccia, L. Demers, L. Morin, F. Lennox, R. B. *J. Am. Chem. Soc.* **119** (1997) 2682.
50. Green, M, O'Brien, P. *J. Chem. Soc., Chem. Comm.* (2000) 183.
51. Templeton, A. C.; Wuelfing, M. P.; Murray, R. W. *Acc. Chem. Re*s. **33** (2000) 27.

CHAPTER 4

MOLECULAR SIEVES SYNTHESIS IN MICELLAR MEDIA

PART I

SYNTHESIS AND CHARACTERIZATION OF FERRIERITE TYPE ZEOLITE IN MICELLAR MEDIA AND ITS CATALYTIC APPLICATIONS

Part I of the chapter reports on the synthesis of pure phase ferrierite (FER) zeolite in presence of small amounts of nonionic surfactants, Tween-20 or Tween-80. The input SiO_2/Al_2O_3 molar ratio has been varied over a range of 25 to 150. The results confirm that small amount of pyrrolidine acts as a template and is necessary. The effects of varying concentration of surfactant on ferrierite crystallization and output SiO_2/Al_2O_3 molar ratio are reported. The results also show that in the absence of pyrrolidine, ZSM-5 co-crystallized with FER whereas in absence of nonionic surfactant the yield and crystallization of FER is very poor. The XRF analysis shows the changes in SiO_2/Al_2O_3 output molar ratio as the surfactant concentration changes. The XRD data shows that the samples are fully crystalline and pure. The TG/DTA of the sample shows its structural stability. The Scanning Electron Microscopy (SEM) results show changes in particle size with varying concentration of nonionic surfactant. The catalyst synthesized used for vapor-phase Beckmann rearrangement of cyclohexanone oxime to caprolactam and catechol methylation to *O/C*-alkylated products.

4.1 INTRODUCTION

Zeolites belong to a family of microporous metal oxides commonly referred to as '**molecular sieves**' due to their ability to differentiate between molecules based on their shapes and sizes. They are water containing crystalline aluminosilicates of natural or synthetic origin with highly ordered structures[1-6]. These crystalline materials are characterized by well defined pore systems composed of channels or cage-like structures. Zeolites are attractive materials as catalyst supports because of their high surface area and stability as well as the shape selectivity that arises from their uniform pore dimensions. These materials have found widespread application as adsorbents, ion exchange materials, detergent builders and catalysts, especially in petroleum refining, petrochemicals, and as Fluidized Cracking Catalysts.[6] Their microporosity also provides the means for physically trapping of guest molecules as opposed to external surface attachment. The interior of the pore system, with its atomic-scale dimensions, is the catalytically active surface of the zeolites. The inner pore structure depends on the composition, the zeolite type, and the cations. Thus, zeolites are represented by the general formula:

$$\mathbf{Mx/n\ ^{n+}[(AlO_2^-)x\ (SiO_2)y].\ zH_2O}$$

Where 'n' is the valency of the charge compensating cation M; x assumes values between 0 and 0.5. M represents the exchangeable cation (eg. Alkali or alkaline earth metals or an organic cation). According to the Lowenstein rule,[7] the ratio x/y is smaller than or equal to 1. The Si/Al molar ratio corresponds to the acid sites in the zeolites. **z** represents the number of water molecules, which can be reversibly adsorbed or desorbed in the pores.
The characteristic features of zeolites, which make them effective catalysts, are: i) High surface area and adsorption properties, ii) active acid sites; to use as solid acid, iii) shape selectivity (due to uniform pores and channels), iv) easy regeneration, v) high thermal stability and vi) eco friendly.

4.1.1 NOMENCLATURE

The Structure **C**ommission of **I**nternational **Z**eolite **A**ssociation and IUPAC has assigned structural codes to synthetic and natural zeolites.[8,9] The codes for zeolite identification have generally been derived from the names of the type of species, and do

not include numbers and characters other than Roman letters. Structure type codes are independent of chemical composition, distribution of various possible T atom, (e.g. Si^{4+}, Al^{3+}, P^{5+}, Ti^{4+}, etc.), cell dimension or crystal symmetry.

4.1.2 CLASSIFICATION

Zeolites have been classified in accordance with the chemical composition,[10] effective pore diameter,[11,12] morphology[13] and crystal structure.[14] Zeolites have been also classified structurally on the basis of differences in the secondary building units.[15-17] Flanigen[10] has classified zeolites according to their chemical composition as shown below and some of their salient features are described.

Table 4.1: Classification of zeolites on the basis of chemical composition.

Low silica zeolites	Si/Al = 1- 1.5	A, X, sodalite, etc.
Intermediate silica zeolites	Si/Al = 2.0 - 5.0	Erionite, mordenite, X,Y,L, Ω, etc.
High silica zeolites	Si/Al = 5 – 500	MFI, FER, BEA, etc.
Pure silica zeolites	Si/Al = ∝	Si-MFI (silicalite-1), Si-MEL (silicalite -2Si-MTW, Si-ZSM-48, Si-FER, etc.

The thermal stability increases from low silica zeolites to high silica zeolites. The high silica zeolites are hydrophobic in nature while low silica zeolites are more hydrophilic. The acidity tends to increase in strength with increase in Si/Al ratio. The cation concentration and ion exchange capacity (which is directly proportional to the aluminum content) decreases with the increase in Si/Al ratio. Low silica zeolites are formed predominantly with 4-, 6- and 8- rings of tetrahedra while in case of intermediate silica zeolites there is an onset of 5- rings and in case of high silica zeolite 5-ring tetrahedra predominate in the structure.

Zeolites are also classified according to their effective pore diameter, which is dependent on the number of tetrahedra present in the ring aperture, which circumscribes the pore.[18,12]

4.1.3 FERRIERITE (FER)

Ferrierite (FER) is a natural zeolite mineral, which occurs near Kamloops Lakes, British Columbia. Staples[19] in 1955 reported the unit cell composition as:

$$(Na,K)_4\ Mg_2\ (Si_{30}Al_6)O_{72}\ (OH)_2.\ 18H_2O$$

Vaughan[20] and Kerr[21] solved its crystal structure. Breck[22] classified ferrierite zeolite along with mordenite, dachiardite, epistilbite and bikatite.

Ferrierite (FER) is a medium pore type zeolite,[23-27] containing chains of five membered rings, which are linked to give [5^4] polyhedral unit from which the three-dimensional framework can be built. FER contains two dimensional network of 10-MR pore (4.3 x 5.5 A^o) and 8-MR (3.4 x 5.5 A^o) intersecting channels. FER is used as a catalyst for skeletal isomerization of n-butene to iso-butene,[28-30] which in turn is used to produce methyl tertiary butyl ether (MTBE). Cobalt exchanged ferrierite is reported to be active for selective reduction of NO_x.[31] Additionally isomerization of m-xylene to p-xylene on ferrierites[32,33] and alkylation of toluene with methanol over H- on rare earth zeolite have also been found to be active catalysts in comparison to the conventional Friedel-Crafts catalyst because of their high acidity, easy separation from the product, regenerability, absence of corrosive substances and lack of environmental hazards.[34-36]

In 1964, Barrer and Marshall[23] first synthesized the ferrierite under hydrothermal conditions using strontium as an inorganic cation. The process, however, required high synthesis temperature (613K) and longer crystallization period (10 days). Since then, many workers have reported on the synthesis of ferrierite,[37-39] but most of these studies again require high temperature and obtain ferrierite with low Si/Al ratios. Kibby et al.[39] have reported synthesis of ferrierite using tetramethylammonium hydroxide as a template. Since then a number of N- containing molecules and also oxygenated hydrocarbons have been used in FER synthesis. Kim et al.[40] have succeeded in synthesizing FER in absence of inorganic cations using pyrrolidine, 1,4-diaminobutane and ethylene diamine as a structure directing agents. Plank et al.[41] have reported synthesis of ferrierite using hexamethylenediamine as an organic template. Borade and Clarified [42] have reported synthesis of ferrierite in presence of trimethylcetylammonium hydroxide as a template. Ferrierite have synthesized in presence of sodium bis- (2-ethyl hexyl)

sulfosuccinate (AOT),[43] but it requires longer crystallization period (80hr). Recently Guo et al.[44] have synthesized ferrierite with tetrahydrofuran as the template.

In this chapter we report for the first time the synthesis of ferrierite in presence of small amount of nonionic surfactants (Tween-20 and Tween-80), which are the ethoxylated derivatives of the fatty esters of sorbitan. Compared with other surfactants (anionic, cationic), polyethylene oxide (PEO) molecules are relatively inexpensive, non-toxic, and biodegradable. In presence of these nonionic surfactants comparable yields of highly crystalline ferrierite was obtained.

4.2 EXPERIMENTAL SECTION

4.2.1 REACTANT

The following chemicals were used: sodium silicate (28.2% SiO_2, 8.4% Na_2O (Aldrich), aluminum sulfate hexadecaanhydrate (Loba Chemie), pyrrolidine (99% SRL), sulfuric acid (98% BDH), Polyoxyethylene sorbitan monooleate (Tween-20) and Polyoxyethylene sorbitan monostearate (Tween-80) (s.d.FINE CHEM. Ltd.). Demineralized water was used throughout all the experiments.

4.2.2 METHOD

In a typical synthesis 0.6 g of Tween-80 was dissolved in 3ml pyrrolidine and added to 52.5g of sodium silicate containing 30 ml of distilled water under vigorous stirring. The gel was stirred for one hour. To this solution 2.4 g of aluminum sulfate hexadecaanhydrate in 30 ml water and 1.8gm of sulfuric acid in 10ml water was added in a dropwise fashion resulting in the formation of a thickened gel. Finally, 20 ml of water was added to this thickened gel, stirred for one hour and was transferred to a 300 ml stainless steel autoclave and put into the preheated oven at $160^oC \pm 2\ ^oC$ for 35 hours. The autoclave was quenched in cool tap water and the precipitate was filtered, washed with distilled water and dried at 100^oC. The input gel molar composition was as follows:

20 Na_2O: 9.45 Py: 66 SiO_2: Al_2O_3: 6.3 H_2SO_4: 0.12 Tween-X: 1600 H_20

(Where Py = pyrrolidine and X = 20, 80). The as synthesized sample was then calcined in air at 550^oC at the rate of 2^o/min. for 15 hours. Various samples with input SiO_2/Al_2O_3 molar ratios ranging between 25 to 150 were synthesized using similar procedure.

4.2.3 CHARACTERIZATION

4.2.3.1 X-RAY DIFFRACTION

Among the various spectroscopic techniques employed for structural evaluation of zeolites, x-ray diffraction is one of the most important and useful technique to identify zeolite structure, and determining phase purity, percent crystallinity, unit cell parameters, crystallite size and further in understanding the kinetics of crystallization. As the powder pattern is the finger print of the individual zeolite structure, phase purity and percent crystallinity of the synthesized zeolite can be ascertained by comparing with the standard pattern for the zeolite under investigation. Isomorphous substitution of a hetero atom in zeolitic framework results in changes in the unit cell parameters, unit cell volume. This is one way of confirming isomorphous substitution.

The extent of crystallization and phase purity was evaluated for all the FER samples by recording X-ray diffractograms using Cu Kα radiation, (Philips Analytical, PW1710, λ=1.54056 A^o). The XRD patterns were recorded in the 2θ range 5-50 degrees. The degree of crystallinity of the ferrierite samples was estimated by measuring the peak area of the characteristic diffraction peaks at $2\theta = 8.9^o$ and between 22^o-25.5^o, 100% crystallinity being arbitrarily assigned to the most crystalline material obtained during crystallization kinetics.

4.2.3.2 FRAMEWORK IR SPECTRA

The framework IR vibration spectra (400-1400 cm^{-1}) of FER samples (NUJOL MULL) were recorded using Perkin-Elmer 221 spectrophotometer.

4.2.3.3 NITROGEN ADSORPTION

Nitrogen adsorption measurements were performed to estimate BET surface area and pore diameter (Omnisorb 100CX, Coulter, USA) of ferrierite zeolite at room temperature and relative pressure (P/P_o) range between 0.005-0.05. About 200mg of calcined sample was degassed at 450^{o}C and a pressure better than 10^{-5} Torr before adsorption measurements.

4.2.3.4 THERMOGRAVIMETRY (TG) AND DIFFERENTIAL THERMAL ANALYSIS (DTA)

Generally zeolites are thermally stable, but heating at elevated temperatures may lead to structure breakdown and therefore decrease in crystallinity. Thermo analytical data obtained from TG, DTA and DTG study are useful in evaluating the thermal properties of zeolites. The shape and splitting of the endotherms (low temperature) helps to identify the location of water molecules and also helps in studying kinetics of dehydration of water molecules. Zeolites are known to possess high thermal stability, which increases with increase in silica to alumina ratio. Ferrierite zeolite is found to be stable up to 1273 K.

Thermal analysis was carried out using Differential Scanning Calorimeter, Sicko S II, SSC5100, Japan Instrument. About 3mg sample was placed in a container, which is suspended directly on the balance beam. The heating rate was 10^{o}C/min from room temperature to 1000^{o}C. Nitrogen was used as a carrier gas with flow rate of 100ml/min. The temperature sensing thermocouple is positioned very close to the sample (within 1mm) to indicate accurate temperature. Mass change of sample was plotted as a function of temperature using an internal X-Y recorder. The DTA curve was obtained simultaneously with TGA curve during a sample analysis.

4.2.3.5 X-RAY FLUORESCENCE SPECTROSCOPY

The Chemical composition of fully crystalline Na-FER products was established using wavelength despersive XRF (3070, Rigaku), using lithium tetraborate as a flux.
Infrared spectroscopy can yield information about the structural details of the materials. In addition, it can be used to confirm acidic characteristics and isomorphous substitution as well as aid in relating different zeolite materials by their common structural features. The IR spectrum in the range 200 - 1300 cm^{-1} is used to characterize and to differentiate various zeolite framework structures.

4.2.3.6 SCANNING ELECTRON MICROSCOPY

The morphology and the habit of the crystalline phase of ferrierite product was examined on Model Leica Sterioscan 440, manufactured by M/S Cambridge Leica Ltd.

The micrographs of the samples were recorded by a 35-mm camera attached to the high-resolution recording unit with a 10-KV EHT and a 50-μA beam current.

The crystal morphology of zeolite samples are investigated using Scanning Electron Microscopy (SEM JEOL, JSM-5200). Cathode rays are bombarded on the sample and the scattered Secondary Electrons are used to form image. A thin layer (~ 0.1 mm) of the sample was mounted on a carrier made from alumina and was coated with a film of Gold to prevent surface charging and to protect the zeolite material from thermal damage by the electron beam. The major advantage of the SEM is that bulk samples can be studied by this technique.

4.3 RESULTS AND DISCUSSION

4.3.1 X-RAY DIFFRACTION ANALYSIS

Figure-4.1 (a-d) shows the x-ray diffraction patterns of ferrierite zeolite prepared using different concentration of Tween-80 and figure-4.1e shows the x-ray diffraction

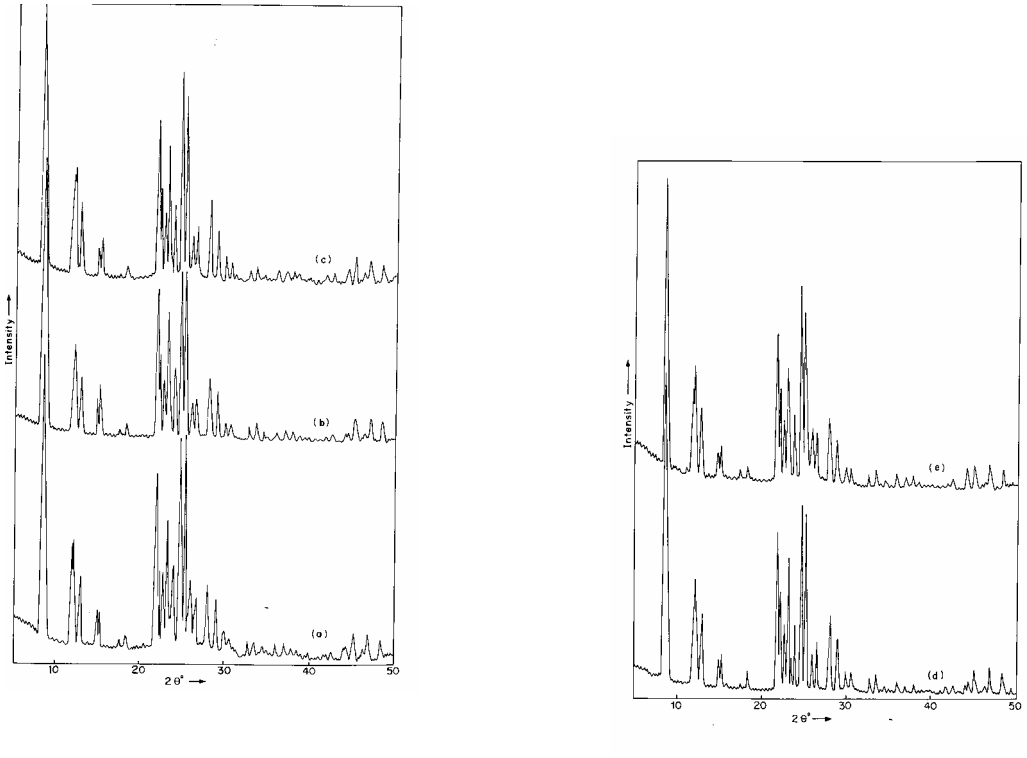

Figure4.1: X-ray diffraction pattern of the ferrierite zeolite with input SiO_2/Al_2O_3 molar ratio 66 synthesized in presence of different concentrations of nonionic surfactant, Tween-80: a) 0.00305 mol/lit., b) 0.0061 mol/lit., c) 0.00916 mol/lit., d) 0.0122 mol/lit. and e) 0.00305 mol/lit. of Tween-20.

patterns of ferrierite zeolite prepared using Tween-20 in presence of catalytic amount of pyrrolidine. The input Si/Al molar ratio for all the samples was 66. The x-ray pattern shows the product to be fully crystalline and pure FER phases, in good agreement with the synthetic FER framework topology.[45,46] The enhancement of the characteristic peak at 8.9^{o} (2θ) on calcination confirms the structural stability of the FER zeolite.

4.3.2 FRAMEWORK IR SPECTRA

The framework IR spectra of the samples synthesized with varying input SiO_2/Al_2O_3 molar ratios of 25, 66 and 150 using Tween-80 surfactant in combination with pyrrolidine are presented in Figure- 4.2a, b and d respectively. Figure-4.2c shows the sample graph for input molar ratio 66 using Tween-20 surfactant. The IR spectra of the samples have been found to be similar to the samples obtained in presence of pyrrolidine alone. The absorption bands around 1080 cm^{-1} and 721 cm^{-1} and 470-430 cm^{-1} can be assigned to the internal vibration of tetrahedral SiO_2 and have been observed in silica or quartz.[47] It can be observed from IR spectra that the strongest band corresponding to asymmetric

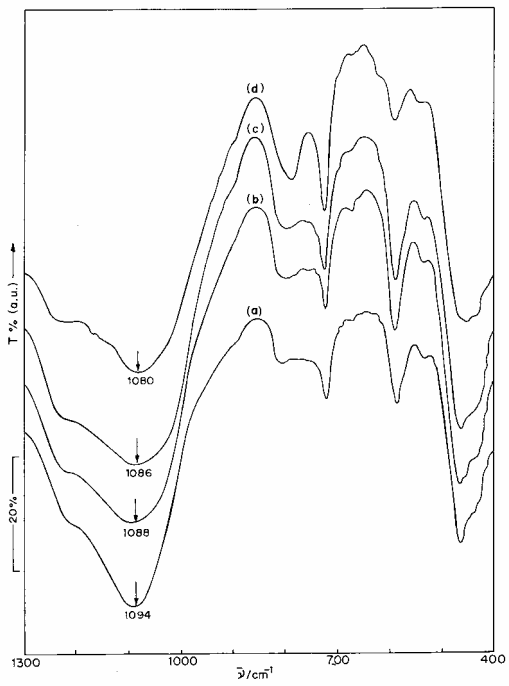

Figure 4.2: Framework IR spectra of the ferrierite sample with different SiO_2/Al_2O_3 input molar ratios synthesized in nonionic surfactant, Tween-80: a) 150 c) 66, d) 25 and b) 66 using Tween-20.

stretching (1220 cm^{-1}) is found to shift to lower frequency for sample with low SiO_2/Al_2O_3 molar ratio (Figure- 4.2). This may be due to the change occurring in the force constant of T— O bond by aluminum insertion.[48]

4.3.3 X-RAY FLUORESCENCE SPECTROSCOPY

The XRF analysis shows that for the same input SiO_2/Al_2O_3 molar ratio, ferrierite zeolite obtained using different concentrations of nonionic surfactant shows different output SiO_2/Al_2O_3 molar ratio (Table-4.2). It can also be observed from XRF data that as the surfactant concentration increases the output SiO_2/Al_2O_3 molar ratio also increases. For the same input SiO_2/Al_2O_3 molar ratio (66), the ferrierite synthesized using different surfactants shows different output SiO_2/Al_2O_3 molar ratio. Thus, sample no.6 synthesized using Tween-20, shows higher output molar ratio as compared to the one synthesized using Tween-80. Ferrierite samples with high output SiO_2/Al_2O_3 molar ratios have been synthesized by this method (Table-4.2, sample no.5 and sample no.8).

Table 4.2 Chemical properties of ferrierite synthesized in different concentration of nonionic surfactants in combination with pyrrolidine.

Sample No.	SiO_2/Al_2O_3 Ratio		SiO_2/Tween-80 (mole/mole)	SiO_2/Pyrrolidine (mole/mole)	Zeolite	% Yield
	Input gel	Product				
1	66	32	No Tween-80	2.1	FER	60
2	66	31.38	551.84	7	FER	62
3	66	28.65	275.92	7	FER	56.6
4	66	29.84	183.95	7	FER	57.3
5	66	38.75	137.95	7	FER	63.3
6	66	ND	183.95	No Pyrrolidine	FER+ZSM-5	ND
7	25	22.07	551.84	7	FER	69
8	150	70.13	551.84	7	FER	53
9	66	35.134	SiO_2/Tween-20 551.84	7	FER	65

4.3.4 BET SURFACE AREA

The BET surface area of the calcined sample synthesized using nonionic surfactant (Tween-80, 0.0061 mol/lit.) is 327 m^2/g which is slightly more than the surface area (~ 300 m^2/g) of the FER sample synthesized by conventional method.[49] It is observed from surface area results (Table-4.3) that using same concentration of different nonionic surfactants gives different surface area.

Ferrierite synthesized using Tween-20 (Table-4.3, sample no.3) shows more surface area as compared to ferrierite synthesized using Tween-80 (Table-4.3, sample no.2) for the same concentration. Surface area goes on increasing as the surfactant concentration increases, reaches a maximum and then decreases. The pore diameter of the FER samples, synthesized using different concentrations of nonionic surfactants however has been found to be nearly same (~0.68nm).

Table 4.3 BET surface area and pore size of ferrierite zeolite synthesized in nonionic surfactants.

Sample No.	Surfactant Concentration	BET Surface Area	Effective Pore Diameter
1	No surfactant	307 m^2/g	0.684nm
2	0.00305 mol/lit.	236 m^2/g	0.680nm
3	0.0061 mol/lit.	327 m^2/g	0.681nm
4	0.00923 mol/lit.	362 m^2/g	0.687nm
5	0.01231mol/lit.	336 m^2/g	0.683nm
6	0.00923 mol/lit.	ND	ND
7	0.00305 mol/lit.	287 m^2/g	0.680nm
8	0.00305 mol/lit.	310 m^2/g	0.688nm
9	0.00305 mol/lit.	280 m^2/g	0.675nm

4.3.5 SCANNING ELECTRON MICROSCOPY (SEM)

The morphologies of the calcined FER samples, having same input SiO_2/Al_2O_3 molar ratio, synthesized at different concentrations of nonionic surfactants are shown in Figure-4.3 (a-h). The SEM photographs shown in figures clearly indicate that the crystal size and morphology of FER is strongly influenced by the presence of small quantities of nonionic

surfactants (Tween-80 or Tween-20) along with pyrrolidine as compared to conventional system,[49] which shows irregular polycrystalline mixture of small and large particles. The figures also indicate the change in particle size with change in surfactant concentration. At low concentration (0.00152 mol/lit. of Tween-80), the particle size is around 3μm (Figure- 4.3a), while at medium concentration (0.0061 mol/lit. of Tween-80), it goes down to 1μm and finally at high concentration (0.0122 mol/lit. of Tween-80) it shows a particle size of 3μm. The sample with high SiO_2/Al_2O_3 molar ratio (150) shows more intricate morphology (Figure-4.3f).

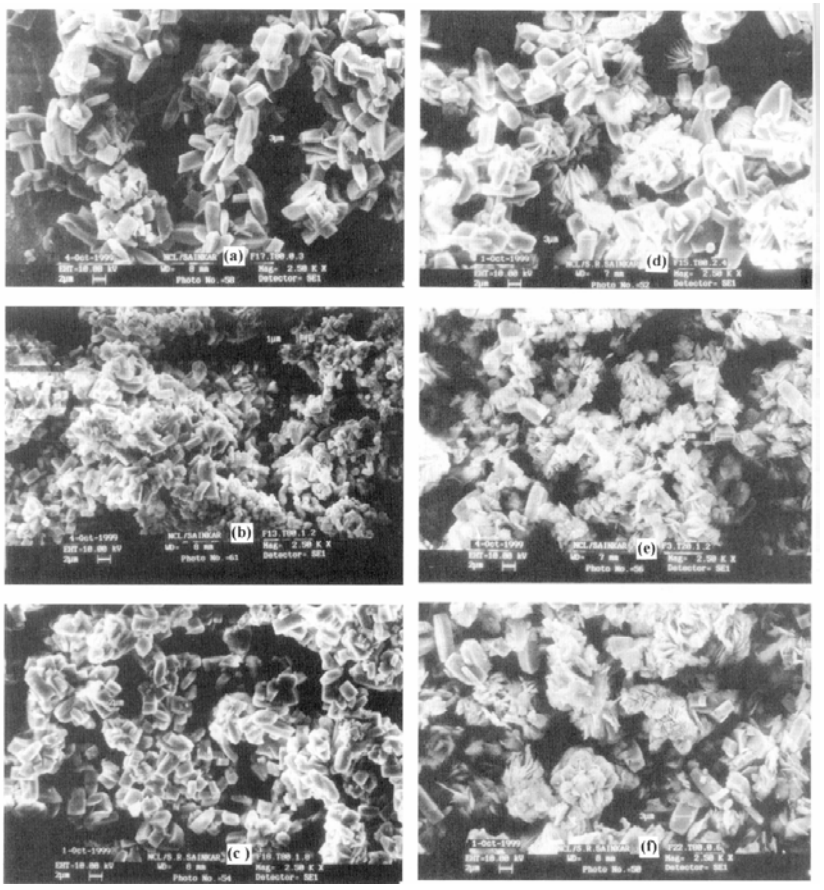

Figure 4.3: Scanning Electron Micrographs of ferrierite crystals obtained in different concentrations of nonionic surfactants, Tween-80: a) 0.00152 mol/lit., b) 0.0061 mol/lit., c) 0.00916 mol/lit., d) 0.0122 mol/lit. and f) 0.00152 mol/lit. and e) 0.0061 mol/lit. of Tween-20.

4.3.6 THERMOGRAVIMETRY (TG) AND DIFFERENTIAL THERMAL ANALYSIS (DTA)

Figure- 4.4, shows the DTA/TGA curve of as-synthesized ferrierite samples having input SiO_2/Al_2O_3 molar ratio 66 using nonionic surfactant (Tween-80), in combination with catalytic amount of pyrrolidine. The TGA curve shows three steps of weight losses between the temperature range of (i) 100-260^oC (weight loss 3.49%), (ii) 260-445^oC (weight loss 3.26%), and (iii) 445-550^oC (weight loss 4.48%). The weight loss in the first case at low temperature is mainly due to dehydration occurring from the FER cavities. The weight loss in second and third steps may be due to the removal of pyrrolidine and surfactant in the FER structure. The DTA curves obtained in air atmosphere for the as synthesized products of varying SiO_2/Al_2O_3 molar ratios reveal significant changes, which are mainly due to oxidative decomposition of the occluded Tween-80 in combination with pyrrolidine. Finally, there are no major changes or transformations observed in the temperature range between 750-1000K which essentially determines the high thermal stability of FER synthesized in presence of surfactant-pyrrolidine system.

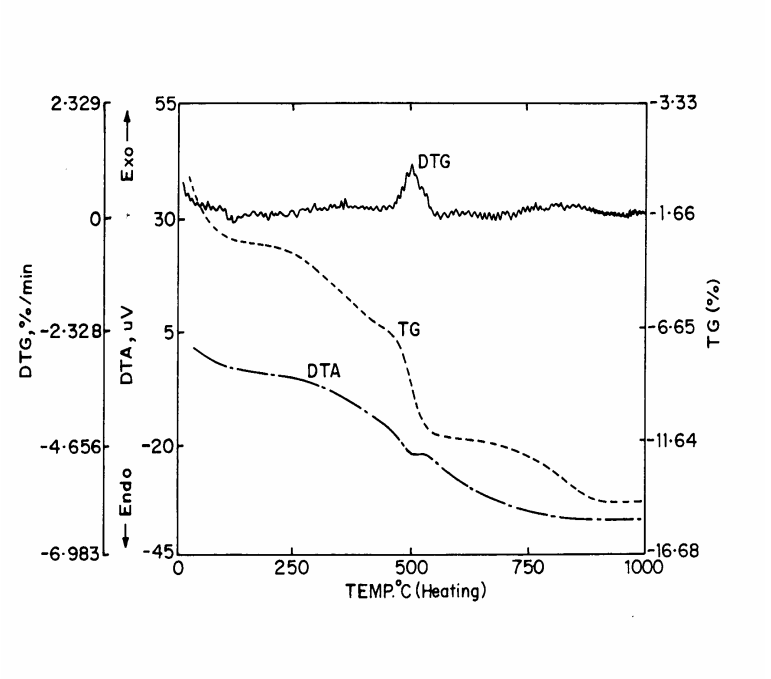

Figure 4.4: TG/DTA curve of as -synthesized ferrierite using Tween 80 in combination with pyrrolidine having input SiO_2/Al_2O_3 molar ratio 66.

Tween surfactants have a short hydrophobic chain with a large hydrophilic head. The head unit consists of three free PEO chains with one PEO chain linking the ring to the hydrophobic tail. When such molecules aggregate into micelles, they have a tendency to orient the free PEO chains as parallel as possible to the alkyl tail, resulting the formation of very short but dense hydrophilic shell around the hydrophobic core. Such type of arrangement helps in increasing the interactions between hydrophilic shell and inorganic species (Si and or Al) and between pyrrolidine and inorganic species which are present very close to hydrophilic shell. The arrangement is also responsible for reducing the quantity of pyrrolidine required as "*space filler*". Recently the role of anionic surfactant, sodium bis (2-ethyl-hexyl) sulfosuccinate (AOT) has been explained on the basis of formation of "*microdroplet*" during ferrierite crystallization.[50]

CATALYSIS

4.4 VAPOR PHASE BECKMANN REARRANGEMENT OF CYCLOHEXANONE OXIME TO CAPROLACTAM

Ferrierite zeolite catalysts prepared using different procedures have been tested for their activity for vapor phase Beckmann rearrangement of cyclohexanone oxime to ∈-caprolactam. We report here the results of a study seeking the influence of temperature, nitrogen feed rate, oxime concentration and solvents on the catalyst performance. At low concentration of oxime (2.5 wt%.), using acetonitrile as solvent the maximum in the conversion of oxime and selectivity to ∈-caprolactam has been obtained. The presence of weak, medium and strong acid sites as indicated by temperature programmed desorption of NH_3 corroborates well with the catalytic activities of various ferrierites shown here. Solvent polarity is found to significantly affect the conversion of cyclohexanone oxime.

4.4.1 EXPERIMENTAL SECTION

4.4.1.1 CATALYST PREPARATION

The vapor phase Beckmann rearrangement of cyclohexanone oxime to ∈-caprolactam was investigated over five different FER zeolite catalysts, Viz., (i) H-FER , (ii) St-H-FER, (iii) Si-H-FER , (iv) H-FER-TT and (v) H-FER-TE. The later two were synthesized in presence of non-ionic surfactants Tween-20 and Tween-80 respectively according to the procedure reported earlier section. In what follows we shall briefly describe the synthesis procedures:

(A) H-FER[49]

52.5 g of sodium silicate (in 25ml of distilled water) was stirred with 10 ml pyrrolidine. To this solution, 2.4 g of aluminum sulphate hexadecahydrate (in 25 ml distilled water) and 1.8 g of sulphuric acid (in 10 ml distilled water) was added. Finally, 30 ml of distilled water was added and the gel (pH 11.5 ± 0.2) was stirred vigorously for

2h and autoclaved in a 300 ml stainless steel Parr autoclave (4842, 300 ml) and heated at 160^{o}C for 60 h. The initial gel composition was:

20 Na_2O : Al_2O_3 : 37 Pyrrolidine : 66.5 SiO_2 : 6.3 H_2SO_4 : 1460 H_2O

The autoclave was quenched, filtered, washed and product was dried at 100^{o}C for 6-8 h. The resulting material was calcined in air at 550^{o}C for 18-20 h. Two more ferrierite samples were prepared using same procedure given above but varying the SiO_2/ Al_2O_3 ratio.

(B) STEAMING OF H-FER

Dealuminated H-FER was prepared by subjecting it to heating in steam at 550°± 10°C for 2-3 h. This steamed sample was then acid treated by making slurry of the powder in 10% oxalic acid solution at 80-90°C for 2 h. The sample was filtered, repeatedly washed with demineralized water, dried and finally calcined in presence of air current at a temperature of 550°C for 6-8 h. The sample so prepared exhibits an excellent hydrothermal stability.

(C) Si-H-FER

The organothermal synthesis of Silicious ferrierite was carried out according to the procedure described by Kuperman *et al.*[51]

4.4.1.2 CHARACTERIZATION

The extent of crystallization and phase purity was evaluated for all the FER samples by recording X-ray diffractograms using Cu Kα radiation, (Philips Analytical, PW1710, λ=1.54056 A^{o}). The XRD patterns were recorded in the 2θ range at 5-50 degrees. The degree of crystallinity of the ferrierite samples was estimated by measuring the peak area of the characteristic diffraction peaks at 2θ = 8.9^{o} and between 22^{o} and 25.5^{o}. The framework IR vibration spectra (400-1400 cm^{-1}) of FER samples were recorded using Perkin-Elmer 221 spectrophotometer. The chemical compositions of ferrierite products were measured using wavelength dispersive XRF (3070, Rigaku). Nitrogen adsorption measurements were performed to estimate BET surface area and pore diameter (Omnisorb 100CX, Coulter, USA) of ferrierite zeolite at room temperature

and relative pressure (P/P_o) range between 0.005 and 0.05. About 200 mg of calcined sample was degassed at a pressure better than 10^{-5} Torr at 450°C before adsorption measurements. The morphology and the habit of the crystalline phase of ferrierite product were examined on Model Leica Sterioscan 440, manufactured by M/s Cambridge Leica Ltd. The micrographs of the samples were recorded by a 35 mm camera attached to the high-resolution recording unit with a 10-KV EHT and a 50-μA beam current.

4.4.1.3 TEMPERATURE-PROGRAMMED DESORPTION OF AMMONIA

The temperature-programmed desorption (TPD) of ammonia was performed in order to determine the distribution of strong acid sites on the catalysts. The analysis was carried out in the Autochem 2910 instrument (Micromeritics, USA). The carrier gas used was He, flowing at a rate of 50 ml/min. The desorption process was monitored by a TCD detector. About 0.4 g of the calcined catalyst was used for each experiment. Prior to the analysis, the catalyst sample was pretreated in situ for 2 h in a He flow (30 ml/min) at 450°C. Adsorption of ammonia was performed by passing a He stream with ammonia vapor over the catalyst for 30 min. The adsorption process was carried out at 80°C. In order to eliminate physically adsorbed ammonia, after the adsorption of ammonia, the sample was flushed with the carrier gas at 105°C for another 1 h. The TPD profile of ammonia was obtained from 50° to 700°C at a heating rate of 10°C/min.

4.4.1.4 REACTOR AND EXPERIMENTAL SETUP

The powdered catalysts are pressed, pelleted, crushed and sieved to obtain 10-20 mesh particles. All the reactions are carried out at atmospheric pressure in a fixed bed down flow reactor. About 3 g of catalyst was placed in a cylindrical glass reactor (1.5 cm i.d; 30 cm length), having thermowell of 4 mm at the centre. The catalyst was packed in-between inert ceramic beeds in such a way that the thermowell top was at the centre of the catalyst bed. Also the portion above the catalyst bed served as preheater. The reactor was placed in a constant temperature zone of an electrically heated furnace. The catalyst was activated at 500° C for 5 h in a flow of dry air. The catalyst was then flushed with dry nitrogen and cooled to the desired temperature. The cyclohexanone oxime was dissolved in acetonitrile (10 wt%) and injected using a high precision feed pump (ISCO, Model

500D,USA) at the required rate. Nitrogen was used as a carrier gas. The reactions were carried out at different temperatures between 300 and 450°C. The liquid products were analyzed by gas chromatography [(HP 6890 series, fitted with HP-1 capillary column and FID as detector, the carrier gas being nitrogen)] and GCMS (QP 2000A, Shimadzu SE-52 column, non-polar silicon fluid).

4.4.2 RESULTS AND DISCUSSION

The XRD data shows that the samples are fully crystalline and pure phase. Framework IR spectra of various FER zeolites showed two bands around 1220 cm^{-1} and 580 cm^{-1}. These two bands can be attributed to the vibrations within the ferrierite framework. Table 4.4 shows the physico-chemical characteristics of the FER samples. Acid strength distribution can be derived from the rate of desorption of corresponding to weak, medium and strong acid sites. For increasing SiO_2/Al_2O_3 ratio (from 34 to 73) the total number of acid sites corresponding to both types, weak as well as strong, decreases as the area under the curve decreases.

Table 4.4 Physico-Chemical properties of ferrierite.

Catalyst	Gel SiO_2 / Al_2O_3 Ratio	Product SiO_2 / Al_2O_3 Ratio *	BET Surface Area (m^2/g)	Average Particle Size (μm)
H-FER	66	34	335.5	**
St- H-FER	-	73	262.5	-
Si-FER	-	-	119.2	-
H-FER-TE	66	29	327	1
H-FER-TT	66	31	225.3	3

* From XRF

** irregular polycrystalline mixture of small and large particles[49]

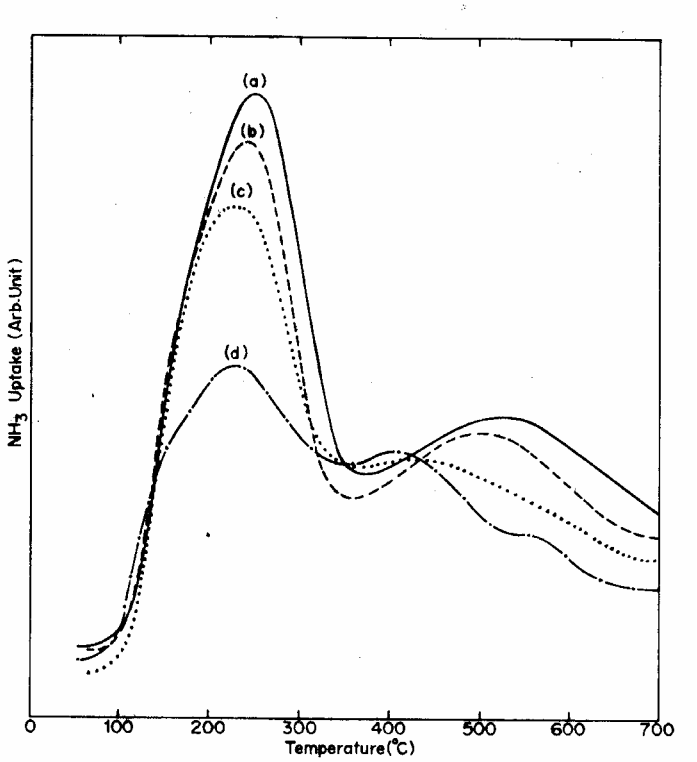

Figure 4.5: NH3-TPD spectra of ferrierite catalysts. (a) H-FER-TE; (b) H-FER-TT; (c) H-FER and (d) St-H-FER.

According to Topse *et al.* [52], the TPD peak around 500°C (550°C in case of FER) is due to Bronsted acid sites. An additional observation is the shift in the TPD peak to the lower temperature as silica to alumina ratio increases. In the case of H-FER-TT (237.7 and 505.8°C) and H-FER-TE (240 and 533°C), in the temperature range studied, the figure shows the presence of only two peaks. It can also seen from the Figure 4.5 that the peaks for Lewis acid sites for H-FER-TE and H-FER-TT have been shifted towards higher temperature and hence these two samples show better performance at 450°C.

The vapor phase Beckmann rearrangement of cyclohexanone oxime mainly yielded ∈-caprolactam and the by-products being cyclohexanone, cyclohexenone, 1-cyanopentane and 1-cyanopentene and polymer of ∈-caprolactam which was shown as in the tables under 'others'.

4.4.2.1 EFFECT OF REACTION TIME

The oxime conversion and selectivity of ε-caprolactam with time is shown in Figure 4.6. The catalyst activity and product selectivity reached an equilibrium level after 3 to 4 h and hence all the experimental data were obtained after the stabilization of the activity.

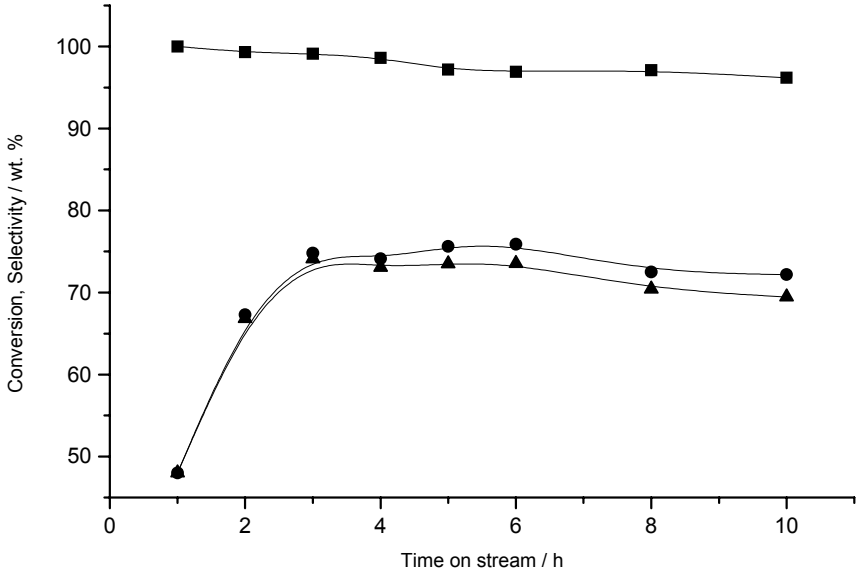

Figure 4.6 Influence of time on the conversion and selectivity for Beckmann rearrangement of cyclohexanone oxime over H-ferrierite (■) conversion, wt. % of oxime; (●) selectivity, wt. % of caprolactam; (▲) yield, wt. % caprolactam.

Reaction conditions: Temp. = 400°C ; Pressure = 1 atm.; WHSV = 1 h^{-1}: Oxime concentration in feed = 10 wt.% in solvent; Nitrogen flow rate = 20 ml min^{-1}; Catalyst wt. = 3 g.

Effects of different parameters on the conversion of oxime and selectvities of different products are discussed below.

4.4.2.2INFLUENCE OF TEMPERATURE

The conversions of cyclohexanone oxime and caprolactam yield at different temperatures over H-FER, H-FER-TE, H-FER-TT, Si-FER and St-H-FER are shown in Table 4.5. It can be seen from Table 4.5 that with increase in temperature from 300 to 450^{o}C, oxime conversion increases and selectivity towards ∈-caprolactam decreases except the sample H-FER-TE. At higher temperature (450^{o}C) the conversion for oxime was 99.9 % while the selectivity towards ∈-caprolactam was 74.2% for the sample H-FER-TE. This low selectivity may be due to decomposition of ∈-caprolactam at high temperature on the catalyst surface. Table 4.5 also shows that H-FER at 350^{o}C gives better performance towards conversion and yield while H-FER-TE and H-FER-TT samples give better performance at 450^{o}C. This is due to the acidic differences as detailed in the TPD studies.

4.4.2.3INFLUENCE OF CATALYST

The results of the catalytic reactions of the cyclohexanone oxime over different ferrierite catalysts at 400^{o}C are presented in Table 4.6. The St.-H-FER catalyst shows good selectivity towards caprolactam. (This is due to the high ratio of SiO_2/Al_2O_3 (73). Increase in SiO_2/Al_2O_3 ratio decreases the total acidity of H-ferrierite zeolites, oxime conversion decreased.) It is known that the catalytic activity for Beckmann rearrangement depends upon the acidity and the nature of hydroxyl group of catalysts. Corma et al.[53] reported that the strong Brönstead acidity of Y zeolite is responsible for the formation of lactam. However, the majority of previous reports have suggested that the very weak [54-56] or medium-strength acidity[57] or almost neutral hydroxyl groups[58] of zeolites are favorable for Beckmann rearrangement reaction, while the strong acid sites accelerate the formation of by-products.[59] This is in good agreement with the results of our study, since St-H-FER is weakly acidic as compared to other samples under study. Si-FER showed poor conversion and yield of ∈-caprolactam towards this reaction and this may be due to large

Table 4.5 Influence of different temperature on the conversion of oxime and selectivity of ∈-caprolactam using ferrierite catalyst.

Catalyst	Temp (°C)	Oxime Conv. (Wt%)	Selectivities (Wt%)[a]				Yield[b]
			A	B	C	D	
H-FER	300	80.6	77	8.2	13.8	0.9	62.06
	350	91.3	78.3	6.8	12.7	2.2	76.96
	400	99.3	74.8	9	13.4	2.8	74.28
	450	99.9	73.5	9.2	14.1	3.2	73.43
H-FER-TE	300	40	74	0	26	0	29.6
	350	91.4	72.9	3.2	23.8	0	66.63
	400	97	71.5	6.2	22.3	0	69.35
	450	99.9	74.2	5.2	18.9	1.7	74.12
H-FER-TT	300	53.6	77.6	0	19.4	3	41.59
	350	82.2	74.3	2.7	18.3	4.6	61.07
	400	89	72	3.1	17.3	7.5	64.08
	450	97.1	70.5	5	19.5	5	68.45
Si-FER	350	43.3	20.7	29.9	38.4	11	8.96
	400	64.2	42.1	19.9	29.5	8.5	27.03
	450	93.1	24	13.7	25.7	36.5	22.34
St-H-FER	300	71.7	79.3	8.1	9.4	3.2	56.85
	350	82.1	79	7.7	8.6	4.6	64.85
	400	84.2	85.3	6.1	6.5	2.1	71.82
	450	95.4	79.9	4.9	6.5	8.6	76.22

[a]Selectivity (wt.%) = (Wt.% of product formed / Wt.% of cyclohexanone oxime formed) x 100

[b]Yield (wt.%) of caprolactam = (Selectivity wt.% x Conversion wt.%) / 100

A= ε-caprolactam; B= Cyclohexanone; C= Cyanopentane + Cyanopentene; D= Others

REACTION CONDITIONS: Pressure = 1 atm.; WHSV = 1 h^{-1}: Oxime concentration in feed = 10 wt.% in acetonitrile; Nitrogen flow rate = 20 ml min^{-1}; Time on stream of the reaction = 3 h; Catalyst wt. = 3 g.

Table 4.6 Conversion of cyclohexanone oxime and selectivity for ∈-caprolactam over various ferrierite type zeolites.

Catalyst	Oxime Conv. (Wt%)	Selectivities (Wt%)[a]				Yield[b]
		A	B	C	D	
Na-FER	92.9	41.2	20.6	20.6	14.7	37.94
Na-H-FER-1 (1.3)[#]	94.4	47.2	19.4	22.2	5.6	44.56
Na-H-FER-2 (1.1)[#]	98.3	65	15.1	16.4	1.9	63.90
H-FER (10)[*]	100	76	5.4	10.9	5.4	76.00
H-FER	99.3	74.8	9	13.4	2.8	74.28
H-FER (25)[*]	98.3	77.5	8.5	9.4	4.6	76.18
St-H-FER	84.2	85.3	6.1	6.5	2.1	71.82
Si-FER	64.2	42.1	19.9	29.5	8.5	27.03
H-FER-TE (12)[*]	100	69.4	10.6	14.5	5.5	69.40
H-FER-TE	97	71.5	6.2	22.3	0	69.35
H-FER-TE (29)[*]	96.1	65.8	6.6	13.2	10.5	63.23
H-FER-TT	89	72	3.1	17.3	7.5	64.08

[*] The value in the parentheses represents the Si/Al ratio by EDX.

[#] The value in the parentheses represents the Na weight percent by EDX.

[a, b] See footnotes in Table 2

A= ε-caprolactam; B= Cyclohexanone; C= Cyanopentane + Cyanopentene; D= Others

REACTION CONDITIONS: Temp. = 400°C; Pressure = 1 atm.; WHSV = 1 h^{-1}: Oxime concentration in feed = 10 wt.% in acetonitrile; Nitrogen flow rate = 20 ml min^{-1}; Time on stream of the reaction = 3 h; Catalyst wt. = 3 g.

zeolite crystals and the reaction on the surface. Also, this is in contrast with other studies,[60] silanol groups (Si-OH) are not active in the case of FER.

The H-FER shows good conversion of cyclohexanone oxime. H-FER-TT shows low conversion of oxime compared to H-FER-TE. This may be due to the difference in particle size and surface area of the catalysts. Also the Si/Al ratio of H-FER and H-FER-TE samples are varied and tested at 400°C for this reaction. As the Si/Al ratio increases, the conversion decreases but there is not much difference in the selectivity towards ε-caprolactum. To know the effect of Na% on activity, Na-FER was exchanged to different levels with NH_4NO_3 and the results are shown in table 3. As the Na % decreases, increase in conversion and selectivity is noticed**.** The following studies were done with H-FER as catalyst.

4.4.2.4 INFLUENCE OF SPACE VELOCITY (WHSV)

The increase in WHSV of the feed on the conversion of oxime and selectivity of the products is shown in Figure 4.7 over H-FER catalyst. It can be seen from Figure 3 that as the WHSV increases there is decrease in oxime conversion and increase in caprolactam selectivity. The formation of cyclohexanone and 5-cyanopentane and 5-cyanopent-1-ene is reduced at higher WHSV because the reactants are in contact for less time and hence secondary product formation is suppressed. The maximum yield of caprolactam is at WHSV = 1.

4.4.2.5INFLUENCE OF SOLVENT

Table 4.7 shows the influences of various solvents for cyclohexanone oxime on the catalytic performance of H-FER. There is not much appreciable change in the conversion but the selectivity of caprolactam was strongly influenced by the type of solvent used. The selectivity increases by increasing the dipole moment of solvent. The selectivity in presence of benzene (0 D) was low (69.4 wt.%), selectivity in presence of ethanol (1.44 D) was 70.7 wt.% while selectivity in presence of acetonitrile (3.92 D) was high (74.8 wt.%). Roseler et al.[61] have reported the deactivation of MFI borosilicate in the Beckmann rearrangement of cyclohexanone oxime using different organic solvents and found that the degree of deactivation depends on the kind of solvent used. Komatsu

et al.[62] have reported that the solvent with medium polarity was preferable for the Beckmann rearrangement on silicalite-1. But for ferrierite it is observed that the solvent with high polarity is preferable for this reaction.

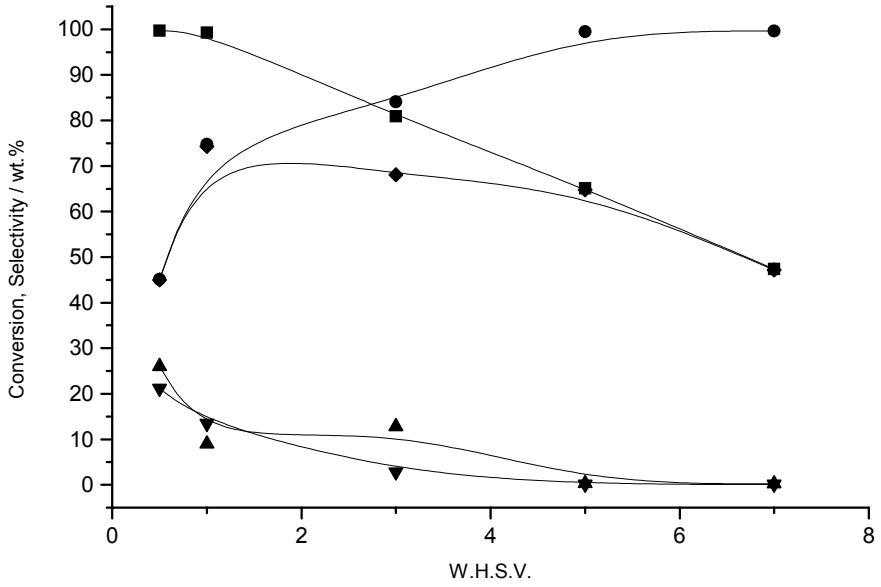

Figure 4.7 Influence of W.H.S.V. data on the conversion and selectivity for Beckmann rearrangement of cyclohexanone oxime over H-ferrierite (■) conversion, wt. % of oxime; (●) selectivity, wt. % of caprolactam; (▲) selectivity, wt. 5 of cyclohexanone; (▼) selectivity, wt.% of 5-cyano-pent-1-ene and (◆) yield, wt.% of caprolactam.

Reaction conditions: Temp. = 400^{o}C ; Pressure = 1 atm.; Oxime concentration in feed = 10 wt.% in solvent; Nitrogen flow rate = 20 ml min^{-1}; Time on stream of the reaction = 3 h; Catalyst wt. = 3 g.

4.4.2.6 INFLUENCE OF CONCENTRATION OF CYCLOHEXANONE OXIME

It can be seen from table 4.8 that the dilution of the cyclohexanone oxime in acetonitrile improves the conversion and the selectivity of caprolactam. At low oxime concentration (2.5 wt.%) the yield of caprolactam was high. At high oxime concentration (20 wt.%) in acetonitrile the formation of by-products cyclohexanone, cyanopentane and cyanopentene were high. Also with higher concentration of oxime deactivation of the catalyst is rather faster.

Table 4.7 Influence of various solvents for cyclohexanone oxime on the catalytic performance of H-FER

Solvent	Oxime Conv. (Wt%)	Selectivities (Wt%)[a]				Yield[b]
		A	B	C	D	
EtOH	99.5	70.7	7.8	20.3	1.2	70.35
Acetonitrile	99.3	74.8	9	13.4	2.8	74.28
Benzene	95.7	69.4	9.5	12.2	8.9	66.41

[a, b] See footnotes in Table 2
A= ε-caprolactam; B= cyclohexanone; C= Cyanopentane + Cyanopentene; D= Others
REACTION CONDITIONS: Temp. = 400^{o}C ; Pressure = 1 atm.; WHSV = 1 h^{-1}: Oxime concentration in feed = 10 wt.% in solvent; Nitrogen flow rate = 20 ml min^{-1}; Time on stream of the reaction = 3 h; Catalyst wt. = 3 g.

4.4.2.7 INFLUENCE OF N_2 FEED

Table 4.9 shows the influence of nitrogen flow on the conversion of oxime and selectivity of ∈-caprolactam. Increase in flow rate of N_2, reduces the residence time of reactants over the catalyst leading to increase in selectivity and decrease in conversion of oxime. The yield of ∈-caprolactam is maximum when the carrier gas flow rate was 20 ml/min. At higher nitrogen flow rate the selectivity of cyclohexanone is seen to increase.

Table 4.8 Influence of oxime concentration on oxime conversion and caprolactam selectivity using H-FER as a catalyst.

Oxime Concentration (Wt%)	Oxime Conv. (Wt%)	Selectivities (Wt.%)[a]				Yield[b]
		A	B	C	D	
2.5	99.8	95.5	3.2	0.9	0.4	95.31
5	99.6	87.7	6.7	4.4	1.2	87.35
10	99.3	74.8	9	13.4	2.8	74.28
20	90.1	49	20.3	18.1	12.6	44.15

[a, b] See footnotes in Table 2

A= ε-caprolactam; B= cyclohexanone; C= Cyanopentane + Cyanopentene; D= Others

REACTION CONDITIONS: Temp. = 400°C ; Pressure = 1 atm.; WHSV = 1 h^{-1};Solvent = acetonitrile; Nitrogen flow rate = 20 ml min^{-1}; Time on stream of the reaction = 3 h; Catalyst wt. = 3 g.

Table 4.9 Influence of nitrogen feed on the oxime conversion and caprolactam selectivity using H-FER as a catalyst.

N_2 Feed	Oxime Conv. (Wt%)	Selectivities (Wt%)[a]				Yield[b]
		A	B	C	D	
140	94.3	70.4	25.9	1.2	2.5	66.39
90	96.6	70.1	22.4	3.4	4.1	67.72
60	98.6	71.4	17	7.7	3.9	70.40
20	99.3	74.8	9	13.4	2.8	74.28

[a, b] See footnotes in Table 2

A= ε-caprolactam; B= cyclohexanone; C= Cyanopentane + Cyanopentene; D= Others

REACTION CONDITIONS: Temp. = 400°C; Pressure = 1 atm.; WHSV = 1 h^{-1}: Oxime concentration in feed = 10 wt.% in acetonitrile; Time on stream of the reaction = 3 h; Catalyst wt. = 3 g.

4.5 GAS - PHASE METHYLATION OF CATECHOL

Gas-phase alkylation of catechol with methanol as an alkylating agent has been carried out over H-FER and modified H-FER zeolites in the temperature range 275-425°C. Guaiacol was obtained as the major product at lower temperature and 4-methylcatechol at elevated temperatures, along with small amounts of veratrole and other *C*-alkylated and polyalkylated catechols. Effects of other reaction parameters like reaction temperature, reaction time, WHSV and molar ratio of the reactants have been studied. Low WHSV and higher methanol concentration in the feed leads to more of *C*-alkylated products with a corresponding decrease in total *O*-selectivity.

4.5.1 REACTOR AND EXPERIMENTAL SETUP

The catechol methylation reaction was carried out using a tubular down-flow glass reactor heated in an electrical furnace. 3g of catalyst (10-20mesh size) was taken in the reactor and was sandwiched between porcelain beads. The catalyst was activated in a flow of dry air at 500C for 5h prior to each run. The catalyst was then cooled to reaction temperature in a flow of nitrogen. Catechol-methanol mixture of 1:3 was fed from the top of the reactor using ISCON syringe pump (Model 500D, USA) The products were collected at the bottom by circulating cold water. The liquid products were analyzed by gas chromatorgraphy using HP-1 capillary column and identified by GC-MS (Shimadzu, QP2000). The major methylation products of catechol, as identified from GC-MS are Guaiacol, Veratrole, 4-methylcatechol (4MC) and 3-methylcatechol (3MC) along with other higher alkylated catechols.

4.5.2 RESULTS AND DISCUSSION

The XRD data shows that the samples are fully crystalline and pure phase. Framework IR spectra of various FER zeolites showed two bands around 1220 cm^{-1} and 580 cm^{-1}. These two bands can be attributed to the vibrations within the ferrierite framework. Table 4.4 shows the physico-chemical characteristics of the FER samples.

4.5.2.1 THE EFFECT OF THE DIFFERENT FER CATALYSTS ON THE PRODUCT DISTRIBUTION.

Table 4.10 demonstrates the relationship between the catalytic activity and Na ion-exchange level in catechol methylation. Catechol conversion increases with decrease in Na content in H-FER zeolite. Na-FER showed lesser conversion; however it is highly selective to the formation of *O*-methylated products (96.5%) with guaiacol to veratrole ratio of 2:1. Also an increase in the Si/Al ratio leads to the decrease in conversion of catechol and polymethylated products. The product distribution however remains almost same with marginally high selectivity for *O*-methylated products as compared to H-FER.

It can be seen from Figure 4.5 that acidity of the FER catalysts increases as follows; H-FER < H-FER-TT<H-FER-TE which is also reflected in the conversion of catechol and other product selectivitites. TE gives slightely higher C-alkylated products compared to other two catalysts.

4.5.2.2 THE EFFECT OF THE REACTION TEMPERATURE ON THE PRODUCT DISTRIBUTION.

The effect of reaction temperature on catechol conversion and product selectivity for methylation of catechol with methanol as methylating agent was investigated in the temperature range 275-425°C over three different H-FER zeolite catalysts. It can be seen from Table 4.11a-c, that maximum conversion of catechol was obtained at 400°C after which it decreases. This may be due to the decomposition of methanol at this temperature. At lower temperatures, these catalyst are more selecitive to O-methylated products guaiacol and veratrole. Among the *C*-alkylated product, 4MPC was obtained as major product at all temperatures, whereas, the 3-MPC, which is considerably low at lower temperatures increases substaitnially at higher temperatures. The conversion of catechol increases from 30% to 70% at temperatures 275°C to 400°C respectively over these catalysts. The catalytic activity decreases in the following order according to conversion of catechol H-FER-TE > H-FER-TT > H-FER. A total O-selecitivity of 82% were obtained over H-FER at 275°C.

4.5.2.3 THE EFFECT OF CONTACT TIME (W/F) ON THE PRODUCT DISTRIBUTION.

Figure 4.8 shows the effect of the space velocity on the catalytic properties of H-FER zeolite for the methylation of catechol at 350°C. When the WHSV decreased from 4 to 0.5h^{-1}, the conversion of catechol increased from 24.5 to 63.7% and the selectivity to *C*-methylated product increases. It is also seen from the figure that the selectivity to guaiacol decreases with increase in contact time.

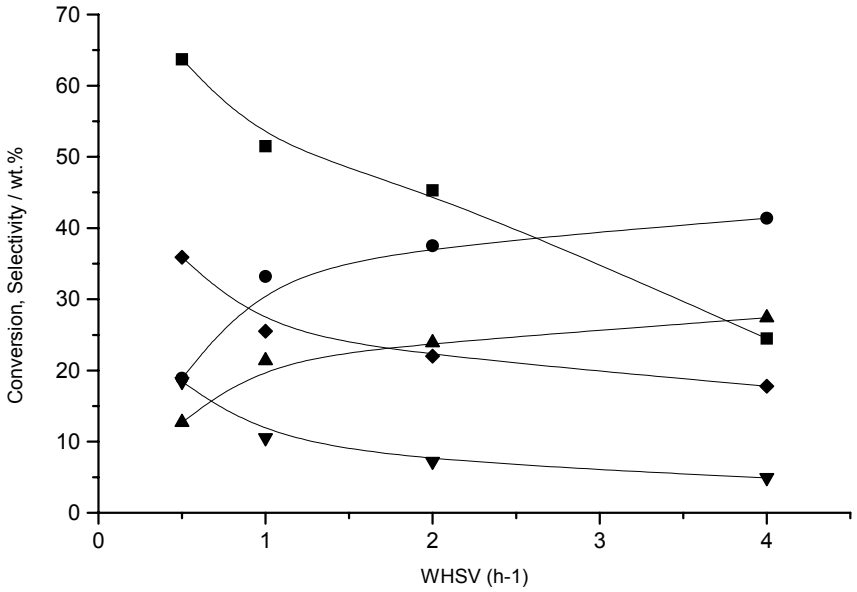

Figure 4.8 Influence of W.H.S.V. data on the conversion and selectivity for catechol methylation over H-ferrierite (■) conversion, wt. % of catechol; (●) selectivity, wt. % of guaicol; (▲) selectivity, wt. veratrole; (▼) selectivity, 3-MPC and (◆) selectivity, wt. % of 4-MPC.

REACTION CONDITIONS: Temp. = 350°C ; Pressure = 1 atm.; Catalyst wt. = 3 g.

4.5.2.4 THE EFFECT OF METHANOL/CATECHOL RATIO ON THE PRODUCT DISTRIBUTION

Catechol conversion and product selectivities as a function of methanol/catechol molar ratio at temperature 350°C, WHSV=0.5h^{-1} are depicted in Figure 4.9. Catechol conversion increased linearly with the methanol concentration in the feed. At a higher methanol/catechol molar ratio, the conversion and polyalkylated product increases with a decrease in *O*-alkylation selectivity. A maximum conversion of catechol 93.5% was obtained at a methanol/catechol molar ratio of 5 with a relatively higher selectivity for *C*-alkylated products. For the reactant molar ratio of 2, the conversion is less (37%), but selectivity to guaiacol increases to 43.2%. A still lower molar ratio was not possible as we faced problem with the solubility of catechol and feeding of the reactants.

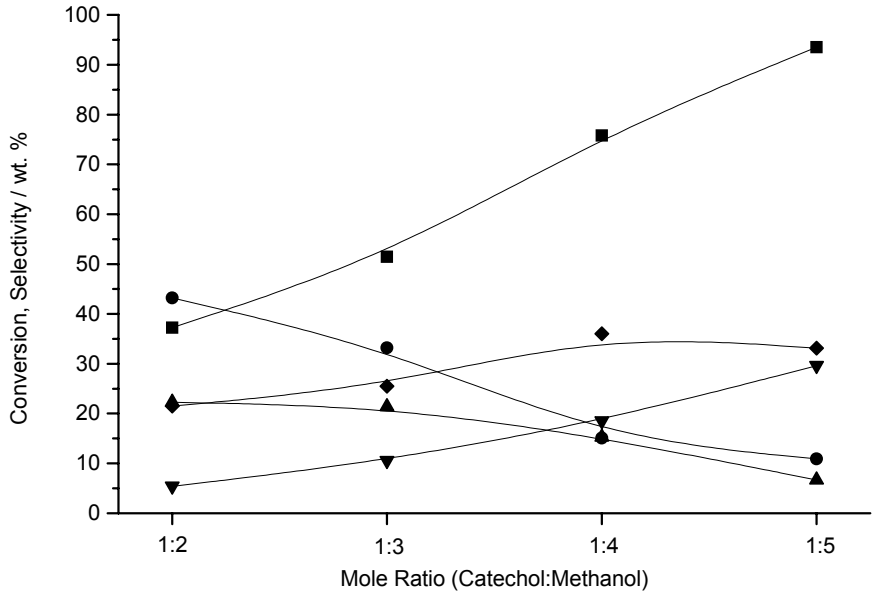

Figure 4.9 Influence of mole ratio of catechol to methanol on the conversion and selectivity for catechol methylation over H-ferrierite (■) conversion, wt. % of catechol; (●) selectivity, wt. % of guaicol; (▲) selectivity, wt. veratrole; (▼) selectivity, 3-MPC and (◆) selectivity, wt. % of 4-MPC.

REACTION CONDITIONS: Temp. = 350^{o}C ; Pressure = 1 atm.; Catalyst wt. = 3 g.

PART II

SYNTHESIS, CHARACTERIZATION AND CATALYTIC PERFORMANCE OF TS-1 PREPARED IN MICELLAR MEDIA

Titanium silicalite-1 (TS-1) was synthesized in presence of small amount of TPAOH using Tween 20, as nonionic surfactant. The procedure gives highly pure nanometer sized homogeneous crystalline product and higher rate of crystallization. The results are compared with the TS-1 sample prepared without surfactant. Characterization of TS-1 has been carried out by using x-ray diffraction and shows that the samples are fully crystalline, while FTIR spectroscopy shows the presence of characteristic band for TS-1 at 960cm^{-1}, confirming Si-O-Ti linkages present in the product. The UV-VISIBLE spectroscopy of the sample prepared without surfactant at low TPAOH concentration shows the presence of extraframework of TiO_2 species. Scanning electron micrograph of the sample shows homogeneous particle size (~ 150nm), while the sample without surfactant shows the presence of particle size ranging between 150-200nm. Catalytic activity of TS-1 sample was also confirmed for octene epoxidation.

4.6 INTRODUCTION

Titanium silicalite-1 has attracted much attention during the last decade because of its interesting catalytic properties in selective oxidation reactions such as aromatic hydroxylation,[63,64] epoxidation of alkenes,[65-67] ammoximation of cyclohexanone[68] and oxidation of alkanes[69,70] and alcoholes[71-73] using hydrogen peroxide as the oxidant. The substitution of Si4+ by Ti4+ in the silicalite-1 was first claimed by Taramasso et al.[63], who synthesized TS-1 by using two different hydrothermal methods. Since then many researchers have prepared TS-1 by using different methods. Kraushaar et al.[74] have shown that the incorporation of Ti^{IV} in the crystal lattice of silicalite occurs when $TiCl_4$ is reacted with dealuminated ZSM-5; Carati et al.[75] have carried out the reaction of $TiCl_4$ with deborated borosilicalite. Though these materials exhibit some catalytic properties, they are not as good as TS-1 in catalytic performance as most of the Ti incorporation occurs at the external lattice. Popa et al.[76] have described the synthesis of TS-1 in the presence of fluoride ions. Lopez et al.[77] have shown that extraframework Ti^{IV} is formed when fluorides are used. Recently Sabde et al.[78] have prepared TS-1 using ethyl silicate-40. Their method however requires more template to hydrolyze the silica precursor. The various methods as described above require the use of a relatively large amount of expensive template (TPAOH), which makes TS-1 costly. It is thus desirable to find an alternative method, which will help to lower the TPAOH concentration and therefore the cost of TS-1. It is known that decreasing the concentration of TPAOH leads to non uniform particles. Also, the particle sizes are larger with lower catalytic performance. It is also very difficult to avoid the precipitation of TiO_2 during the preparation of precursor mixture or during the crystallization of precursor gel leading to presence of extraframework of titanium. However, there is no report on synthesis of TS-1 at low template concentration in micellar media containing nonionic surfactant.

In this part we report for the first time a method for the preparation titanium silicalite-1 using small amount of template in presence of Tween 20. The nonionic surfactant helps to avoid the precipitation of TiO_2 (extra framework of TiO_2). This result is confirmed by UV-VISIBLE spectroscopy. The method also gives highly crystalline uniform particle size that is difficult to obtain by normal method.

4.7 EXPERIMENTAL SECTION

4.7.1 MATERIALS

The following chemicals were used: Tetraethyl ortho silicate (TEOS, Aldrich), tetra n-butyl titanate (TNBT, Aldrich), polyoxyethylene sorbitan monolaurate (Tween 20, s.d. FINE-CHEM, Ltd.), isopropyl alcohol (IPA, s.d. FINE-CHEM, Ltd.), tetrapropyl ammonium hydroxide (TPAOH, Aldrich). Demineralised water was used throughout all the experiments.

4.7.2 SYNTHESIS

2 g of Tween 20 was dissolved in 32 g of distilled water. This surfactant solution was added to 19.2 g of TPAOH (32 % aq. solution) under mild stirring, resulting in the formation of a clear transparent solution. To the above micellar solution 36 g of tetraethyl orthosilicate (TEOS) was added in a dropwise fashion under vigorous stirring. The stirring was continued for another one hour. To this clear solution 1.808 g of tetra n-butyl titanate (TNBT) in 9.12 g of isopropyl alcohol (IPA) was added dropwise under vigorous stirring. Stirring was continued for another one hour. The resulting mixture still remained clear. The mixture was then crystallized at 433K for 18h under autogeneous pressure. The product was recovered by centrifugation, washed with distilled water, dried (383K, 12h). The starting mixture has a molar composition as follows:

0.03TiO_2: SiO_2: 0.12 TPAOH: 0.009 Tween 20: 0.88 IPA: 14.45 H_2O

For normal synthesis the procedure was same as explained above except that only the nonionic surfactant (tween 20) was not used.

The calcination was carried out for both samples in a furnace in a flow of air at 550^{O}C for 15 h with an initial rate of temperature increment of 2^{o}/min.

4.7.3 CHARACTERIZATION

The x-ray powder diffraction (XRD) of calcined TS-1 samples was obtained using a Philips analytical PW1710, X-ray diffractometer using CuK_α radiation (λ = 1.54056 Å). The IR spectra of the calcined samples in the framework region (400-1400cm^{-1}) were recorded using a Perkin-Elmer 221 Spectrometer. Diffuse reflectance UV Visible spectra of calcined TS-1 samples were obtained in a Shimadzu UV-240 spectrometer. The

morphology and the habit of the crystalline phase of TS-1 products was examined on model Leica Sterioscan 440, manufactured by M/s Leica Cambridge Ltd. UK. An Energy Dispersive X-ray Spectrometer EDX (KEVEX) was used to carry out elemental analysis of calcined TS-1. The surface area was determined by N_2 adsorption (surface area analyzer, Quantachrome, Syosset, NY) at 573K. To test the activity of the sample for catalytic reaction of epoxidation of octene was carried out in a liquid phase in a batch reactor. The products were analyzed by Gas Chromatography.

4.8 RESULTS AND DISCUSSION

4.8.1 EPOXIDATION OF1- OCTENE

The samples prepared with and without surfactant were tested for their catalytic activity for epoxidation of octene using H_2O_2. The reaction was carried out in a two-necked glass flask fitted with a condenser and a rubber septum through which aqueous H_2O_2 could be injected through syringe. The temperature of the reaction vessel was maintained using oil bath. In a standard run the reactor content viz. octene (0.5 g), methanol (10 g) and catalyst (0.05 g) were heated it at 333K and an aqueous solution of H_2O_2 (25 wt%) was injected dropwise by syringe. The reaction was continued for 6 h and the reaction mixture was analyzed by gas chromatograph.

Under identical conditions of operation in a batch reactor conversion of H_2O_2, the selectivity of octene epoxide and the utilization of H_2O_2 were monitored. The sample prepared using surfactant shows superior performance viz. 69.5 wt.% (63.7 wt.%) H_2O_2 conversion, 77.7 wt.% (60.2 wt.%) selectivity of octene epoxide and 63.9 wt.% (57.9 wt.%) utilization of H_2O_2. Corresponding figures for sample without surfactant are included in brackets.

4.8.2 X-RAY DIFFRACTION ANALYSIS

Figure 4.10 (a and b) shows the XRD pattern of calcined TS-1 samples synthesized in presence and in absence of nonionic surfactant respectively. The XRD pattern is characteristic of the MFI structure with orthorhombic symmetry. The retention of orthorhombic symmetry on calcination (as opposed to monoclinic symmetry for

calcined ZSM-5) is one of the characteristic features of TS-1 and is believed to arise from the presence of Ti in the framework. XRD patterns of both samples are fully crystalline.

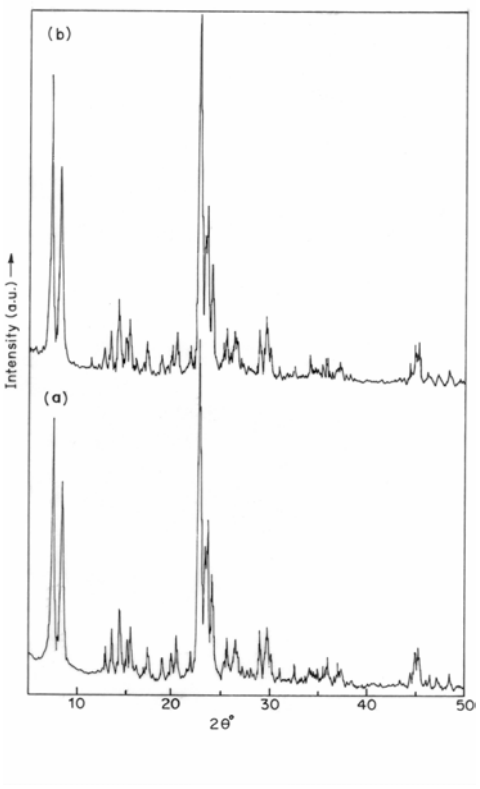

Figure 4.10: XRD patterns of crystalline TS-1 samples (Si/Ti = 33) prepared in presence of tween 20 and in absence of tween 20 (a and b, respectively).

4.8.3 FT-IR ANALYSIS

Figure 4.11 (a and b) shows IR spectra of TS-1 samples prepared in presence and absence of nonionic surfactant respectively. A sharp band present in each spectrum at 962 cm^{-1} is characteristic of TS-1 (believed to be due to stretching vibrations of SiO_4 tetrahedron bound to Ti atoms as Si-O-Ti linkages). FTIR spectra of the two samples are almost identical with each other.

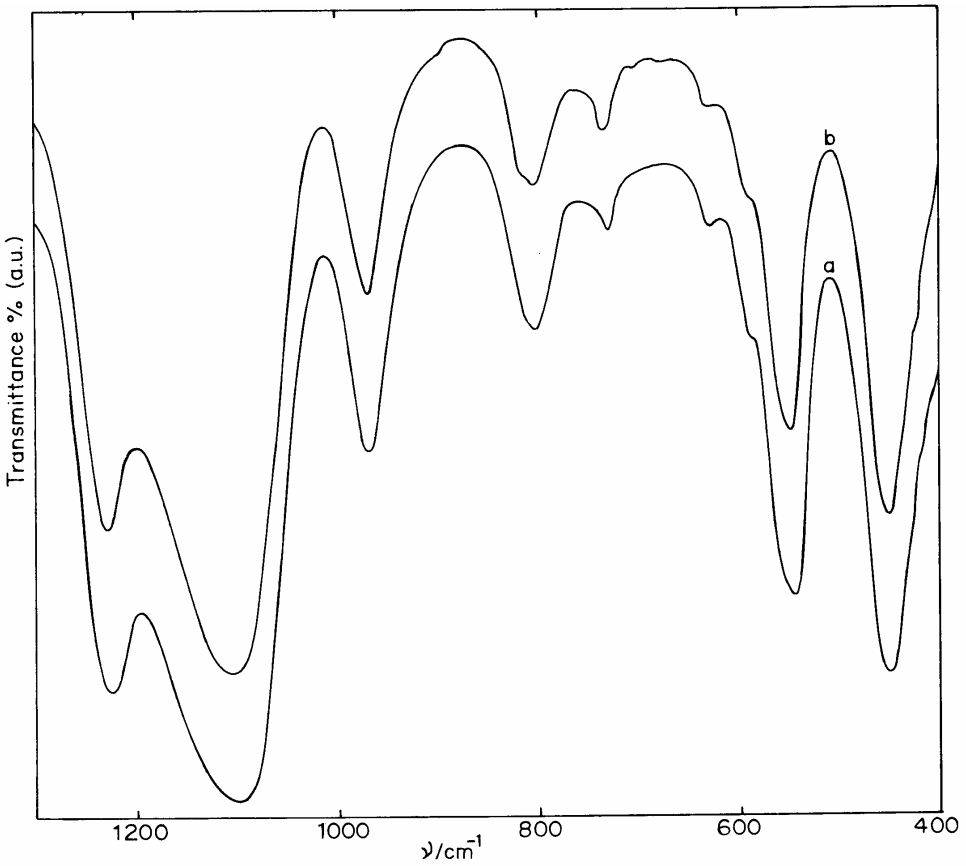

Figure 4.11: FTIR spectra of TS-1 samples: (a) in presence of tween 20 and (b) in absence of tween 20.

4.8.4 UV-VISIBLE SPECTRAL ANALYSIS

UV-VISIBLE spectroscopy is widely used to confirm whether the Ti present in the product is in the tetrahedral position or in the form of extraframework TiO_2. Figure 4.12a shows a charge transfer band at 220nm, which is a characteristic of isolated framework Ti^{4+}. The absence of absorption in the region 280-330nm suggests the absence of extra framework TiO_2. The sample prepared without the use of surfactant on the other hand (see Figure 4.12b) shows band at 330nm, which suggests the presence of extraframework TiO_2.

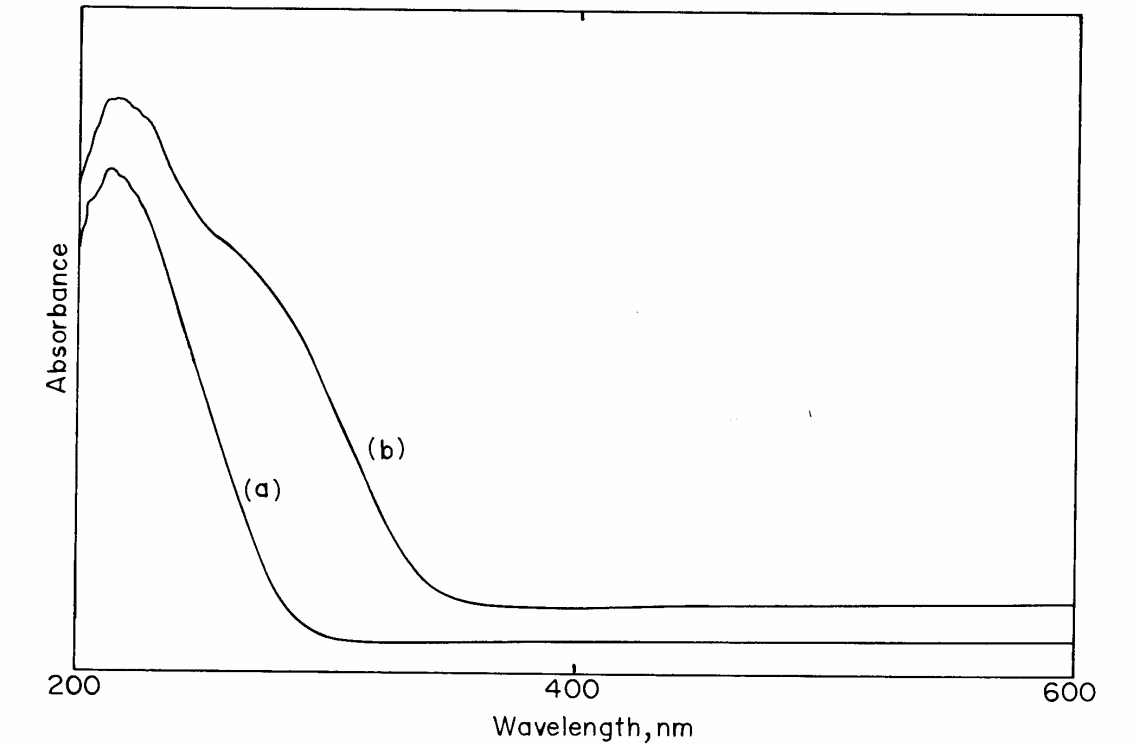

Figure 4.12: UV-VISIBLE diffuse reflectance spectra of TS-1 samples: (a) in presence of tween 20 and (b) in absence of tween 20.

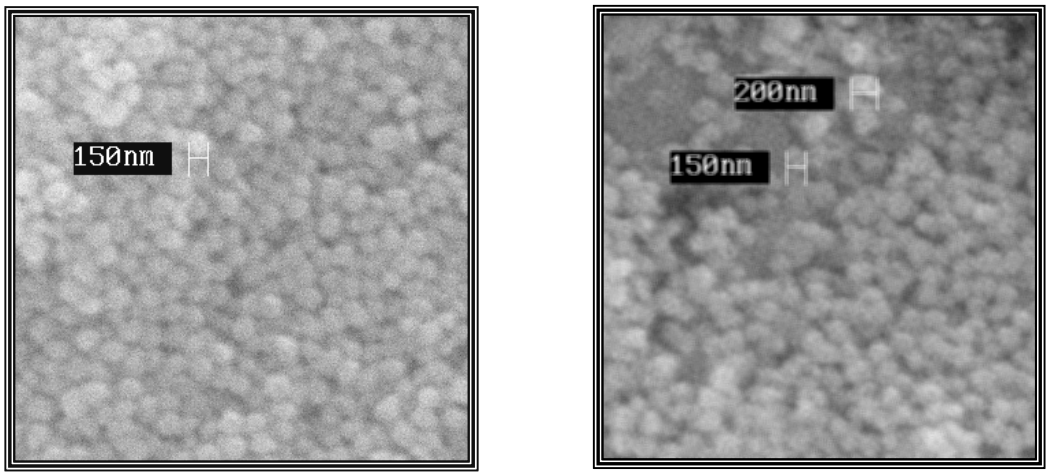

(a) **(b)**

Figure 4.13: SEM photographs of calcined TS-1samples prepared: (a) in presence of tween 20 and (b) in absence of tween 20 (EHT = 20 KV, Mag. = 10 KX).

4.8.5 SCANNING ELECTRON MICROGRAPHS (SEM)

The SEM photographs of TS-1 samples prepared in presence and in absence of surfactant are shown in Figure 4.13a and b respectively. The crystallites in the product obtained in presence of surfactant are smaller and uniform size (150nm) while in absence of surfactant, two types of particles (150-200nm) are seen. The uniform size and small crystals present in figure 4.13a arises due to the cooperative behavior between surfactant and TPAOH at the time of crystallization.

4.8.6 BET SURFACE AREA

The BET surface area of the calcined TS-1 sample (Table 4.12) prepared in presence of surfactant is 425m^2/g, which is more than the sample prepared in absence of surfactant (398m^2/g).

Table 4.12: Physicochemical Properties of Titanium Silicalite-1

Sample	SiO_2/TiO_2		TPAOH/Tween20	S_{BET} (m^2/g)	Particle Size[a]
	Gel	Product	(mol/mol)		(nm)
NTS-1	33	23	No Tween 20	398	150-200
NTS-2	33	27	26.61	425	150

[a] = from SEM.

It is observed that nonionic surfactant (Tween 20) plays an important role during the crystallization of titanium silicalite-1. Tween 20 surfactant has hydrophilic head group containing three PEO chains and one PEO chain linking to short hydrophobic tail. When such molecules aggregate into micelles, the four chains try to orient in a way to remain parallel to hydrophobic tail. Such type of aggregation forms a short but dense hydrophilic shell around the hydrophobic core. The template molecules are located in and around the stern layer. This type of arrangement may increase the interaction between template molecules and silica and or titanium species and induce orientation in template molecules to interact with Si and or Ti species. The cooperative behavior between the surfactant and template molecules thus helps in reducing the concentration of excess

template molecules required as *space filler*. In absence of Tween 20 there is no such environment leading to extraframework of TiO_2 and particle size distribution.

4.9 CONCLUSION

In conclusion, highly crystalline ferrierite zeolite with high output Si/Al molar ratio has been synthesized in presence of nonionic surfactants (Tween-20 or Tween-80) using very small amount of pyrrolidine. The presence of surfactant drastically reduces the requirement of pyrrolidine template although small catalytic amount is still necessary. For the same input SiO_2/Al_2O_3 molar ratio, ferrierite zeolite having different output SiO_2/Al_2O_3 molar ratio can be synthesized by varying concentrations of nonionic surfactant. The micrographs reveal that the morphology and crystal size of ferrierite type zeolite are strongly influenced by the concentration of nonionic surfactant. Also the ferrierite with uniform particle size can be crystallized in good yields and without impurity of any other phase. The surface area data shows that by changing the concentration of nonionic surfactants can control the surface area of ferrierite.

Using appropriate Si/Al ratio or highly dealuminated H-ferrierite and an appropriate diluent can increase catalytic performance of H-ferrierite zeolite catalysts for the vapor phase Beckmann rearrangement of cyclohexanone oxime. The vapor phase methylation of catechol on different ferrierite type zeolites shows that conversion of catechol increases with increase in reaction temperature, catalyst acidity and mole ratio of catechol to methanol.

The use of nonionic surfactant as a additive for the preparation TS-1 offers the following advantages: i) it avoids use of large amount of hazardous template for the preparation of TS-1 and helps to reduce its cost, ii) smaller and uniform size crystallites are formed, iii) it ensures absence of extraframework TiO_2 at low concentration of TPAOH, and iv) gives good catalytic activity as tested for octene epoxidation.

4.10 REFERENCES

1. Barrer, R.M.; *"Hydrothermal Chemistry of Zeolites"* academic press, New York (1982).
2. Barrer, R.M.; *J. Chem. Soc.*(1961) 971.
3. Breck, D.W.; "*Zeolites Molecular Sieves*" Wiley, New York (1974).
4. Liebau, F.; *Zeolites* **3** (1983) 191.
5. Szostak, R.; "*Molecular Sieves: Principles of Synthesis and Identification*" Van Nostrand Reinhold, New York (1989).
6. Rees, L.V.C.; *Nature* **296** (1992) 492.
7. D. W. Breck, " *Zeolite Molecular Sieves*", Wiley, New York, (1974).
8. Barrer, R.M.; *Pure and Appl. Chem.*; **51** (1979) 1091.
9. Meier, W.M. and Olson, D.H.; *Atlas of Zeolite Structure Types*, Butterworths (1987).
10. Flanigen, E.M.; "*In Proceedings of the fifth Interanational Conference of Zeolites"*, (L.V.C Rees Eds.) Naples, Italy, June 2-6, (1980) 760.
11. Barrer, R.M., *"Molecular Sieves"Soc. of chem. Ind.* London (1968) 10.
12. Sand, L.B.; *Econ. Geol.* (1967) 161.
13. Bragg, W.L; *The Atomic Struc. of Miner.* Cornell University Press, Ithaca, New York (1937).
14. Meier, W.M.; "*Molecular Sieves" Soc. of Chem. Ind.* London (1968) 10.
15. Smith, J.V., *Mineral Soc. Amer. Spec.* paper # 1 (1963).
16. Fischer, K.F.; Meier, W.M.; *Fortschi Mineral* **42** (1965) 50.
17. Breck, D.W.; "*Molecular Sieves Zeolites"*, Adv. Chem. Ser., Amer. Chem. Soc., Washington DC, **101** (1971) 1.
18. Meier, W.M. and Olson, D.H. In *Atlas of Zeolite Structure Types,* 2nd edn., Butterworthes, London, 1987.
19. Stapes, L.W.; *Amer. Min.* **40** (1955) 1095.
20. Vaughan, P.A.; *Acta. Cryst*. **21** (1966) 983.
21. Kerr, I.S. *Nature* **210** (1966) 294.
22. Breck, D.W.; *"Molecular Sieve Zeolites"* J. Wiley (1974) 219.
23. Barrer, R.M. and Marshall, D.J., *J. Chem. Soc*. 485 (1964).

24. Barrer, R.M. and Marshall, D.J., *J. Amer. Mineralogist*. 50, 484 (1865).Vaughan, P.A., *Acta Crystall.* **21** (1966) 983.
25. Barrer, R.M. and Lee, J.A., *J. Colloid Interface Sci.* **30** (1969) 111.
26. Meier, W.M. and Olson, D.H., *Atlas of Zeolite Structure Types*, Butterworth, London, 98 (1992).
27. Mooiweer, H.H.; De Jong, K.P.; Kraushaar-Czarnetzki, B.; Stork, W.H.J. and Krutzen, Stud. Surf. Sci. Catal. **84** (1994) 2327.
28. Pellet, R.J., O'Young, C.L., Casey D.G., Ugolini J.R., and Sawicki, R.A., *J. Catal.* **157** (1995) 423.
29. Finelli, Z. R.; Querini, C. A.; Figoli, N. S.; Comelli, R. A.; Appl. Catal. A, **187** (1999) 115.
30. Li, Y. and Armor, J.N., *Appl. Catal*. B, **37** (1993) L1.
31. Sheddon, D., J. Catal. **98** (1986) 1.
32. Rane, S.J.; Satyanarayana, C.V.V. and Chakraborty, D.K., *Appl. Catal*. G, **69** (1991) 177.
33. Lanewala, M.A. and Botlon, A.P., *J. Org. Chem*. **34** (1969) 3107.
34. Bremer, H.; Hoffmann, F.E.; Schoedel, R. and Wendlandt, K.P.; *Chem. Tech*. (Leipzig) **27** (1975) 457.
35. Csicsery, S.M., *J. Org. Chem*., **34** (1969) 3338.
36. Sanderov, E.E.; *Geokimiya*. **9** (1959) 820.
37. Hawkins, D.B.; *Mater. Res. Bull*. **2** (1967) 951.
38. Vaughen, D.E.W. and Edwards, G.C., *US Pat. 3,966,883* (1976) assigned by W.R. Grace.
39. Kibby, C.L., Perotta, A.J., and Massoth, F.E., *J. Catal.* **35** (1974) 256.
40. Kim, T.J.; Ahm, W.S.; Hong, S.B., *Microporous Materials*. **7** (1996) 35.
41. Plank, C.J., Rosinski, E.J., and Rubin, M.K., US Pat. 4 016 245 (1977).
42. Borade, R.B., and Clearfield, A., *Zeolites.* **14** (1994) 458.
43. Ahedi, R. K., Manna, A. and Kotasthane, A.N., *Bull. Of the Catalysis Society of India*. **9** (1999) 148.
44. Guo, G. -q., Sun, Y. -j., and Long, Y. -c., Chem. Comm. **19** (2000) 1893.
45. Fjellvag, H., Lillerud, K.P., Norby, P., and Sorby, K., *Zeolites.* **9** (1989) 152.

46. Jacobs, P.A., and Martens, J.A., "*Synthesis of high silica aluminisilicate zeolites."* (Elsevier, Amstterdom), **33** (1987) 218.
47. Jacobs, P.A., Bayer, H.K., and Valyon, J., *Zeolites.* **1** (1981) 161.
48. Flanigen, E.M., Khatami, H., and Szymanski, H., *Adv. Chem. Ser.* **101** (1971) 161.
49. Ahedi, R.K. and Kotasthane, A.N., Journal of Porous Materials. **4** (1997) 171.
50. Ahedi, R.K. in "Ferrierite (FER) a Medium Pore Zeolite: Synthesis, Characterisation and Catalysis", thesis work, Pune University, (1999) 55.
51. Kuperman, A.; Nadimi, S.; Oliver, S.; Ozin, G. A.; Graces, G. M.; Olken, M. M. *Nature,* **365** (1993) 239.
52. Topsoe, N.; Pederson, K.; Derouance, E. G. *Nature*, **70** (1981) 41.
53. Corma, A.; Garcia, H. J. Primo, *Zeolites* (1991) 11.
54. Holderich, W. F.; Roseler, J.; Heitmann, G.; Liebens, A.T.; *Catal. Today* **37** (1997) 353.
55. Roseler, J.; Heitmann, G.; Holderich, W.F. *Appl. Catal. A* **144** (1996) 319.
56. Albert, P.; Seibold, K.; Haas, T.; Prescher, G.; Holdrich, W.F. *J. Catal.* **176** (1998) 249.
57. Singh, P.S.; Bandyopadhyay, R.; Hegde, S.G.; Rao, B.S. *Appl. Catal. A: General* **136** (1996) 249.
58. Sato, H.; Hirose, K.; Kitamura, M.; Nakamura, Y. *Stud. Surf. Sci. Catal.* **49** (1989) 1213.
59. Ushikubo, T.; Wada, K. *J. Catal.* **148** (1994) 138.
60. Reddy, J.S.; Ravishankar, R.; Sivasankar, S. and Ratnasamy, P. *Catal. Lett.,* **17** (1993) 139.
61. Roseler, J.; Heitmann, G.; Holderich, W.F. *Appl. Catal. A* **144** (1996) 319.
62. Komatsu, T.; Maeda, T.; Yashima, T. *Microporous Mesoporous Mater*., **35-36** (2000), 173.

Table 4.10: Influence of different ferrierite catalysts on the conversion of catechol and selectivity of *C*/*O*-alkylated products.

Temp 350°C Catalyst	Conversion (%) 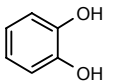	Selectivity (%)							
		LB	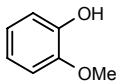	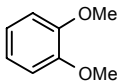	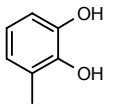	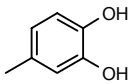	Poly-methylated products	Total O-alkylation Selectivity	Total C-alkylation Selectivity
Na-FER	30.8	1.2	65.2	31.3	0.3	1.8	0.2	96.5	2.1
Na-H-FER[#] (1.1)	36.4	3.3	52.2	25.8	3.5	12.1	3.1	78	15.6
Na-H-FER[#] (1.3)	40.9	2.8	43	22.6	6.4	20.8	4.4	65.6	27.2
H-FER[*] (34)	51.5	2.2	33.2	21.4	10.5	25.5	7.2	54.6	36
H-FER[*] (20)	64.2	4	26.5	19.5	15.9	23.2	10.9	46	39.1
H-FER[*] (50)	39.1	1.6	38.4	25.6	8.9	20.3	5.2	64	29.2
H-FER-TE[*] (34)	55.2	4.6	27.2	16.8	12.1	31.6	7.7	44	43.7
H-FER-TT[*] (34)	52.8	5.9	31.5	13.2	14.4	28.3	6.7	44.7	42.7

Reaction Conditions: WHSV= 1, catechol: methanol (mole) (1:3), TOS = 2h, Pressure = 1 atm., Catalyst = 3g.

[#] The value in the parentheses represents the Na weight percent by EDX.

[*] The value in the parentheses represents the SiO_2/Al_2O_3 ratio by XRF.

Table 4.11a: Influence of different temperature on the conversion of catechol and selectivity of *C*/*O*-alkylated products over H-FER-TE catalyst.

FER-TE Temp °C	Conversion (%) 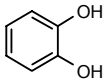	Selectivity (%)						Total O-alkylation Selectivity	Total C-alkylation Selectivity
		Low Boiling	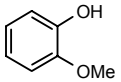	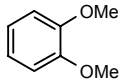	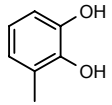	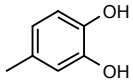	Poly-methylated products		
275	33.2	1.1	58.6	23.6	3.5	12.1	1.1	82.2	15.6
300	39.6	1.3	49.4	24.5	5.3	15.2	4.3	73.9	20.5
325	47.3	3.2	35.3	18.4	11.2	25.7	6.2	53.7	36.9
350	55.2	4.6	27.2	16.8	12.1	31.6	7.7	44	43.7
375	67.8	4.7	24.3	12.7	12.8	35.8	9.7	37	48.6
400	74.9	6.5	23.6	10.3	13.5	35.6	10.5	33.9	49.1
425	68.3	7.6	13.1	9.5	14.9	42.1	12.8	22.6	57

Reaction Conditions: WHSV= 1, Catechol: methanol (mole) (1:3), TOS = 2h, Pressure = 1 atm., Catalyst = 3g.

Table 4.11b: Influence of different temperature on the conversion of catechol and selectivity of *C*/*O*-alkylated products over H-FER-TT catalyst.

FER-TT Temp °C	Conversion (%) 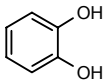	Selectivity (%)							
		Low Boiling	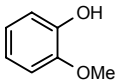	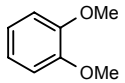	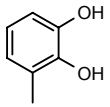	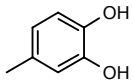	Poly-methylated products	Total O-alkylation Selectivity	Total C-alkylation Selectivity
275	20.7	2.8	56.1	21.9	2.2	13.2	3.8	78	15.4
300	35.4	3.2	49.3	20.5	5.1	17.4	4.5	69.8	22.5
325	44.6	4.3	40.5	15.8	11.5	22.8	5.1	56.3	34.3
350	52.8	5.9	31.5	13.2	14.4	28.3	6.7	44.7	42.7
375	63.4	6.6	24.5	10.5	15.5	34.6	7.3	35	51.1
400	70.5	7	22.7	9.4	14.3	38.5	8.1	32.1	52.8
425	71.5	8.6	22.9	4.4	21.5	31.1	11.5	27.3	52.6

Reaction Conditions: WHSV= 1, catechol: methanol (mole) (1:3), TOS =2h, Pressure = 1 atm., Catalyst = 3g.

Table 4.11c: Influence of different temperature on the conversion of catechol and selectivity of *C*/*O*-alkylated products over H-FER catalyst.

H-FER Temp °C	Conversion (%) 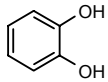	Selectivity (%)							
		Low Boiling	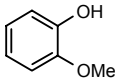	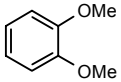	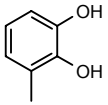	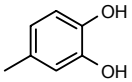	Poly-methylated products	Total O-alkylation Selectivity	Total C-alkylation Selectivity
275	29.8	0.8	55.1	23.3	2.9	13.1	4.8	78.4	16
300	34.1	1.4	53.5	19.8	3.9	15.5	5.9	73.3	19.4
325	42.8	1.5	40.7	20.8	7.9	22.7	6.4	61.5	30.6
350	51.5	2.2	33.2	21.4	10.5	25.5	7.2	54.6	36
375	57.7	3.5	20	22.5	14.9	30.2	8.9	42.5	45.1
400	64.4	4.4	17.9	21.8	17.5	28.4	10	39.7	45.9
425	57.5	6.5	13.1	17.7	24.1	27	11.6	30.8	51.1

Reaction Conditions: WHSV= 1, catechol: methanol (mole) (1:3), TOS = 2h, Pressure = 1 atm., Catalyst = 3g.

CHAPTER 5

SUMMARY AND CONCLUSIONS

The work reported in the present thesis covers various investigations carried out under micellar / microemulsion conditions. More specifically it includes the studies on some industrially important organic reactions, preparation of thiol- capped nanoparticles and molecular sieves synthesis.

Chapter 1 of the thesis gives a brief introduction and background literature on micelles and microemulsions, along with their technological applications to cover chemical reactions, nanoparticles and molecular sieves synthesis in the presence of surfactants.

Chapter 2 reports on two industrially important reactions in micellar / microemulsion media:

Part I reports the industrially important epoxidation of 1-octene in reverse microemulsions. Epoxidation reactions are important because of the ease with which they can convert olefins to oxygenated molecules. Epoxides and their derivatives are widely used in a variety of applications including cosmetics, food flavorings, fragrances, and curing agents. The work reported here uses a co-solvent free method where an anionic surfactant (AOT) overcomes the limitation of homogenization.

Part II reports hydroxylation of phenol to catechol and hydroquinone using anionic surfactant.

The hydroxylation of phenol to catechol and hydroquinone was successfully carried out in micellar media over titanium silicalite-1.

Catechol is an important chemical intermediate product with wide ranging uses. It can be used as rubber hardenidant, electroplate additive, skin preservative as well bactericide, dye hair, photographic developer, color photographic anti-oxidant, furcoloring agent, paint and varnish anti-shrivel. Furthermore, catechol is an important material of synthetic resin, tannic acid, agricultural chemical furantion, medical rhizome of chinese goldthread, perfume vanillin, pepper aldehyde and so on. Hydroquinone is an important chemical, which is mainly used in anthraquinone, azobenzene dye, synthetic ammonia flux, rubber antioxidant, paint and stabilizer as well as antioxidant of essense. The presence of surfactant gives high selectivity towards o-isomer rather than p-isomer.

Chapter 3 reports on the synthesis and characterization of different nanoparticles in micellar / microemulsion media.

Metal nanoparticles have received much attention during recent years because of their potential applications in microelectronics, photocatalyses, magnetic devices, chemisorption, aerosols, and powder metallurgies. These applications are strongly dependent on the size, shape (or morphology) and impurities of the metal nanoparticles. Small, monodisperse particles of semiconductors have received impressive attention in recent years because of the expectation of novel physical properties (optics and electronics) related to the use of such new materials. This increasing interest has led to a wide range of preparative approaches to nanostructures. The key point to any synthetic investigation must be a careful control of semiconductors' size and, even more important, their size-distribution. Amongst the several investigations, the use of microemulsions to obtain ultrafine particles represents an effective pathway.

The study includes:

Part I: This part reports the use of Winsor II microemulsion for the synthesis of thiol-capped CdS nanoparticles in Winsor II microemulsion of diethylether / AOT / water. The dual role of anionic surfactant viz. the formation of microemulsion and facilitating the extraction of oppositely charged ions from aqueous to the organic reverse micellar phase has been successfully used for the synthesis of dodecanthiol-capped cadmium sulfide (CdS) nanoparticles in a Winsor II type microemulsion.

Part II: This part reports the synthesis and characterization of gold nanoparticles stabilized by 3-mercaptopropyldimethoxysilyl end-blocked dimethyl silicone fluid. The stabilizing agent is low molecular weight polymer having terminal thiol groups. Mixing two reverse microemulsions, one containing gold-dithiol and the other containing sodium borohydride forms gold nanoparticles. The gold nanoparticles have been characterized by UV-visible spectroscopy, transmission electron microscopy, fourier-transform infra-red spectroscopy and X-ray photoelectron spectroscopy.

Part III: The synthesis and characterization of dodecanthiol-capped gold nanoparticles in a novel Winsor II type microemulsion of diethyl ether/DDAB / water is reported here. Again the dual role of cationic surfactant(s) viz. the formation of microemulsion as well as

extraction of oppositely charged tetrachloroaurate ions from aqueous to the organic reverse micellar phase has been profitably used. The gold nanoparticles characterized by FT-IR, XPS, TEM and UV-visible spectroscopy.

Chapter 4 reports on the synthesis and characterization of molecular sieves in micellar / microemulsion media. The study includes:

Part I: The hydrothermal synthesis of ferrierite type zeolites in the presence of nonionic surfactants containing catalytic amount of template, has been carried out systematically. Ferrierite exhibits excellent selectivity for the skeletal isomerization of 1-butene. In addition, cobalt-exchanged ferrierite is reported to be active for the selective reduction of NOx, which remains a serious environmental problem. The use of nonionic surfactant offers the following advantages: Drastically reduces the requirement of hazardous template (pyrrolidine) and ferrierite of uniform size can be crystallized in good yield and without impurity of any other phase.

The effect of varying the concentration of nonionic surfactant for the gel having same input SiO_2/Al_2O_3 molar ratio can change a) the output SiO_2/Al_2O_3 molar ratio of ferrierite product, b) particle size of ferrierite crystallites and c) surface area of the ferrierite product.

The ferrierite catalyst prepared by this method was used for vapor-phase Beckmann rearrangement of cyclohexanone oxime to caprolactam and catechol methylation to *O/C*-alkylated products.

Part II: This part reports the synthesis and characterization of titanium silicalite-1 in micellar media containing nonionic surfactant. Catalytic amount of template is used for the synthesis of TS-1. The surfactant used was the Tween 20. The procedure gives highly pure nanometer sized homogeneous crystalline product and higher rate of crystallization. The results are compared with the TS-1 sample prepared without surfactant. Characterization of TS-1 has been carried out by using XRD, FT-IR, SEM and UV-visible spectroscopy. Catalytic activity of TS-1 sample was also confirmed for octene epoxidation.

List of Publications and Patents

A. Publications

1. **R. B. Khomane**, B. D. Kulkarni and R. K. Ahedi, "Synthesis and characterization of ferrierite type zeolites in the presence of nonionic surfactants."

   ***J. Colloid and Interface Sci*. 2001, 236(2), 208-213.**

2. **R. B. Khomane,** B.D. Kulkarni, A. Parasker and S. R. Sainker "Synthesis and characterization of titanium silicalte-1 in micellar media."

   ***Materials Chemistry and Physics,* 2002, 76(1), 99-103.**

3. R.Anand**, R.B.Khomane**, B.S.Rao and B.D. Kulkarni, "Vapor-phase Beckmann rearrangement of cyclohexanone oxime to caprolactam over different ferrierites."

   ***Catal. Lett.* 2002, 78(1-4), 189-194.**

4. **R.B.Khomane,** A.B.Mandale and B. D. Kulkarni "Synthesis and characterization of dodecanthiol-capped CdS nanoparticles in Winsor II type microemulsions of diethylether/AOT/water."

   ***Langmuir*, 2002, 18(21), 8237-8240.**

5. **R.B.Khomane**, R.Anand, B.S.Rao, K.V.R.Chary and B.D. Kulkarni, "Vapor-phase catechol methylation over different ferrierite type zeolites."

   (communicated).

6. **R.B.Khomane** and B. D. Kulkarni, " Epoxidation of alkenes under microemulsion conditions." (**under preparation**).

7. **R.B.Khomane** and B.D.Kulkarni, "Synthesis and characterization of dithiol-passivated gold nanoparticles in reverse microemulsion" (**under preparation**).

B. Patents filed

1. "Enantioselective resolution process for arylpropionic acid drugs from the racemic mixture"

   N. K. Yadav, B. D. Kulkarni, **R. B. Khomane**, **US 6093830 A**, 25 Jul 2000.

2. "An improved process for the preparation of catechol or hydroquinone or a

mixture of catechol and hydroquinone in micellar/microemulsion media"
N. K. Yadav, B. D. Kulkarni, **R. B. Khomane** (**US Patent appl.)**.

3. "An improved process for the preparation of titanium silicalite-1"
B. D. Kulkarni, **R. B. Khomane**, S. Sivasanker (**Indian Patent**).